NTNU – Trondheim
Norwegian University of
Science and Technology

Effect of Copper and Zinc on Corrosion Behaviour and Mechanical Properties in 6082-Alloys

Marie Stoknes

Chemical Engineering and Biotechnology
Submission date: June 2015
Supervisor: Trond Furu, IMTE
Co-supervisor: Otto Lunder, IMT

Norwegian University of Science and Technology
Department of Materials Science and Engineering

Preface

This master thesis entitled *"Effect of Copper and Zinc on Corrosion Behaviour and Mechanical Properties in 6082-Alloys"* has been performed as a collaboration between the Norwegian University of Science and Technology (NTNU) and Hydro Aluminium. It has been conducted at the Department of Materials Science and Engineering during spring 2015 in the final semester of the 5-year master program Chemical Engineering and Biotechnology. Issues of this thesis build on the specialisation project written in the autumn 2014 concerning corrosion behaviour in extruded Al-Mg-Si alloys influenced by processing parameters. The focus in the present study is changed to concentrate on new influencing parameters. Various thesis related work have been conducted at the Department of Materials Science and Engineering at Bergbygget, NTNU, SINTEF press laboratory at NTNU and Hydro at Sunndalsøra.

Acknowledgments

My greatest acknowledgments are directed toward my supervisor Adjunct Professor Dr.-Ing. Trond Furu[1] and my co-supervisor Adjunct Professor Dr.-Ing. Otto Lunder[2] for appreciated guidance throughout this work. A special thanks goes to Martin Lefstad[2], Arne Gellein[2] and Regine Aagård for assisting with extrusion of aluminium profiles. Additional gratitudes are offered to Dr.-Ing. Trond Furu for his assistance with the Alstruc Homogenisation Model and for providing parameters related to processing of the test materials. Furthermore I am grateful for receiving aluminium alloys from Hydro Aluminium. Finally, Senior Engineer Trygve Lindahl Schanche[3] is acknowledged for demonstrating the use of instruments related to mechanical properties.

Trondheim, June 2015

Marie Stoknes

[1] Hydro Aluminium, Sunndalsøra
[2] SINTEF Materials and Chemistry, Trondheim
[3] NTNU Department of Materials Science and Engineering, Trondheim

Abstract

Extruded Al-Mg-Si alloys with Cu additions are frequently used in heavy loaded structures, offshore installations and the transportation industry. In contrast to the positive effect Cu has on mechanical properties, the resistance toward intergranular corrosion is found to descend by the introduction of potential differences in grain boundary regions. This type of corrosion is hard to spot on the material surface, is associated with increased risk for material failure and reduced ductility. Addition of Zn is believed to reduce the Cu-enhanced IGC susceptibility by making grain boundaries less cathodic. An accelerated IGC test was carried out on Cu-containing 6082-profiles with three levels of Zn, differed by rate of cooling after extrusion and ageing condition. The test was followed by optical light microscope examination of cross sectional areas with the aim of evaluating IGC resistance. Effects of adding Cu up to 0.3 wt% and Zn up to 0.6 wt% with variations in cooling rate and ageing time were also studied for mechanical properties and microstructure appearance by obtaining hardness measurements, electrical conductivity measurements and examination in optical light microscope. Furthermore, an Alstruc homogenisation model was applied for simulating the effect of increasing Cu content on precipitation behaviour during solidification and homogenisation.

Results from the IGC test revealed increased IGC frequency and weight loss due to corrosion with raised Zn content. IGC was also slightly promoted by overageing. Microstructure examination showed high influence of cooling rate on depth of recrystallised layers and Cu promoting recrystallisation in centre regions. Moreover, hardness and electrical conductivity were affected by all variables present in this study. Hardness was positively affected by Cu, water quenching and artificially ageing to T6 condition whilst air cooling and ageing raised electrical conductivity. Alstruc simulation indicated a dissolution of the Cu-containing Q-phase associated with IGC during homogenisation which gives reason to expect an absence of Q-phases after extrusion for 6082-profiles examined in this study.

Sammendrag

Ekstruderte Al-Mg-Si legeringer med kobbertilsats er mye brukt i tungt belastede strukturer, offshoreinstallasjoner og transportindustrien. I motsetning til den positive effekten kobber har på mekaniske egenskaper er det rapportert at kobber reduserer motstandsevnen mot intergranulær korrosjon som følge av introduksjon av potensialforskjeller i korngrenseområder. Denne typen korrosjon er vanskelig å observere på materialoverflater, øker risikoen for redusert levetid og reduserer duktiliteten. Som et tiltak for å øke resistansen mot intergranulær korrosjon i kobberholdige Al-Mg-Si legeringer har det blitt foreslått å tilsette sink for å gjøre korngrensene mindre katodiske. En aksellerert IGC test ble utført på kobberholdige 6082-profiler med tre sink-nivåer, variert med kjølehastighet etter ekstrudering og utherdingstilstand. Testen ble etterfulgt av studering av tverrsnittsområder i optisk lysmikroskop med mål om å evaluere motstandsevnen mot intergranulær korrosjon. Effekter av kobbertilsats opp til 0.3 vekt% og sink opp til 0.6 vekt% med variasjoner i kjølehastighet og utherdingstilstand ble også undersøkt for mekaniske egenskaper og mikrostruktur ved hjelp av målinger av hardhet, elektrisk ledningsevne og undersøkelse i optisk lysmikroskop. Videre ble en Alstruc homogeniseringsmodell brukt for å simulere effekten av økende kobbernivå på presipiteringsoppførsel under størkning og homogenisering.

Resultater fra IGC-testen ga økt forekomst av korrosjon langs korngrenser og vekttap relatert til korrosjon med økende sinktilsats. Intergranulær korrosjon ble også fremmet av utherding til overeldet tilstand. Mikrostrukturundersøkelse viste stor påvirkning av kjølehastighet på tykkelse av rekrystalliserte overflatesjikt, og kobber fremmet rekrystallisering i indre områder av materialet. Det ble fastslått at hardhet og elektrisk ledningsevne var påvirket av alle variablene som ble undersøkt i dette studiet. Hardhet ble positivt påvirket av kobbertilsats, vannkjøling og utherding til T6-tilstand samtidig som luftkjøling og utherdingstid økte elektrisk ledningsevne. Alstruc-simulering indikerte en oppløsning av den kobberholdige Q-fasen assosiert med intergranulær korrosjon under homogenisering, hvilket ga grunn til å forvente fravær av Q-faser etter ekstrudering for 6082-profilene undersøkt i dette studiet.

Table of Contents

Abbreviations

Abbreviation	Description
AC	Air cooling
WQ	Water quenching
SSSS	Supersaturated solid solution
GP zones	Guinier-Preston zones
PFZ	Particle-free zones
IGC	Intergranular corrosion
β''	Metastable precursor of β (Mg_5Si_6)
β'	Metastable precursor of β ($Mg_{1.8}Si$)
β	Equilibrium phase (Mg_2Si)
Q'	Metastable precursor of Q ($Al_4Mg_8Si_7Cu_2$)
Q	Equilibrium phase ($Al_4Mg_8Si_7Cu_2$)
AE	As-extruded
T6x	Underageing: 30 min at 185°C
T6	Peak-ageing: 5 h at 185°C
T7	Overageing: 24 h at 185°C
TEM	Transmission electron microscope
LM	Light microscope
AHM	Alstruc homogenisation model
OCP	Open circuit potential
GDOES	Glow discharge optical emission spectroscopy

1 Introduction

Efforts are directed toward achieving improved fuel efficiencies in vehicles, reduction of energy consumption and reduced air pollution in the automotive industry today [1]. Along follows the continuous drive for weight reduction and cost saving in construction materials not only in automotive, but also in offshore installations and heavy structures. High strength-to-weight ratio, good formability, remarkably high corrosion resistance, adequate surface quality and impressive recyclability are characteristics raising the popularity of heat-treatable Al-Mg-Si alloys for the replacement of heavier materials such as steel and copper in highly loaded constructions, outer panel bodies in transportation sectors and structures in harsh marine environments with high installation costs. [1-4].

By artificial ageing to peak strength subsequent to hot deformation, Al-Mg-Si alloys with excess Si relative to the stoichiometry of the Mg_2Si phase can obtain an extensively increase in mechanical strength. This is owing to the formation of various hardening metastable phases of the stable β-Mg_2Si precipitates [5, 6]. However, even with optimised thermomechanical history and artificial ageing, alloys in this aluminium series are still regarded as medium strength aluminium alloys whilst industrial demands for improved mechanical properties are increasing [7]. In order to further increase strength beyond the high age hardening response of Al-Mg-Si alloys, Cu is usually added to accelerate the age hardening process and raise peak hardness [8]. Unfortunately the addition of Cu is reported to reduce the resistance toward intergranular corrosion (IGC) by introducing the harmful grain boundary Q-phase [9, 10].

IGC attacks are hard to spot on the material surface and are characterised by rapid penetration along grain boundaries into the material by microgalvanic cell actions. This type of corrosion is associated with reduction of strength and ductility including an increased risk of material failure [11]. Due to the negative effect of Cu on IGC resistance, studies and reports have been made on improvement of IGC resistance in quaternary Al-Mg-Si(-Cu) alloys [9]. By increasing the Mg:Si ratio to achieve excess Mg, a reduction in IGC has been reported due to the formation of an anodic grain boundary film lowering the cathodic grain boundary potential imposed by Cu [7, 12]. Unfortunately, excess Mg is also associated with reduced hardening potential in Cu-containing Al-Mg-Si alloys [13]. In fabrication of Al-Mg-Si(-Cu)

extrusions for high strength applications in transportation, building and offshore industries it is of great importance to obtain both high IGC resistance and maximum peak strength [14]. Additional alloying of Zn which is an element normally present only in trace amounts has been suggested as a measure to reduce the driving force for IGC by reducing potential differences in a similar way as the anodic Mg-rich grain boundary film [9]. Yet, limited documented work exists on the effect of Zn addition on precipitation and IGC behaviour in Al-Mg-Si(-Cu) alloys and is the main interest in this study. Although Zn does not affect the extrudability of the alloy to a significant extent, the poor recyclability and limited surface quality of Zn encourage that Zn is not added in amounts higher than necessary [15].

The scope of this work is to find if adding Zn to a Cu-containing 6082-alloy can eliminate or reduce the susceptibility toward IGC and maintain satisfactory peak strength. In order to achieve this goal, three 6082-alloys with 0.3 wt% Cu and increasing Zn content, influenced by variations in cooling rate after extrusion and ageing time are subjected to an accelerated IGC test and further studied in optical microscope for IGC susceptibility. Microstructures are examined in order to address changes in microstrucural appearance influenced by processing variables and alloy composition to susceptible profiles. Hardness and electrical conductivity measurements are obtained from 96 profiles where increasing Cu content is included in order to relate changes in mechanical properties to the influence alloy chemistry and thermomechanical processing have on the extent of precipitation from the aluminium matrix. Finally, an Alstruc homogenisation model is performed with the aim of studying precipitation behaviour of Cu in various amounts.

2 Theory and documented work

2.1 Al-Mg-Si alloys

Al-Mg-Si alloys also referred to as the 6xxx aluminium series are used as medium strength structural alloys in industries such as construction, transportation and offshore where combinations of light weight, good weldability, sufficient mechanical properties and high corrosion resistance are required [3, 6, 8, 16]. Their high level of extrudability and machinability among other beneficial properties make this aluminium series commercial attractive for base material in extruded products. More than 90% of the total amount of aluminium extrusions in Western Europe is estimated to be dominated by the Al-Mg-Si alloy system [3].

Alloys in this series are designated as wrought alloys, indicating that they are cast as ingots or billets followed by a hot deformation process to achieve final shape. Together with Al-Cu-Mg alloys (2xxx-series) and Al-Zn-Mg alloys (7xxx-series), Al-Mg-Si alloys are also heat-treatable, giving them an impressive age hardening potential through the formation of strengthening metastable precipitates of the equilibrium Mg_2Si phase during heat treatment [5]. An overview of age hardenable and non-age hardenable wrought aluminium alloys is given in Figure 2.1. In addition to the main alloying elements Mg and Si with contributions of 0.5-1.3 wt% Mg and 0.4-1.4 wt% Si respectively [17], trace elements such as Mn, Fe, Cr, and Ti are usually added to commercial industrial 6xxx alloys in order to control grain size and prevent recrystallisation by forming dispersoids [18, 19]. Due to the high age hardening potential and extensive application prospects in automotive and offshore industries, 6xxx alloys have been widely studied for more than 50 years [16, 20]. Yield strength and tensile strength are found to have large variations of 190-360 MPa and 220-390 MPa respectively [17].

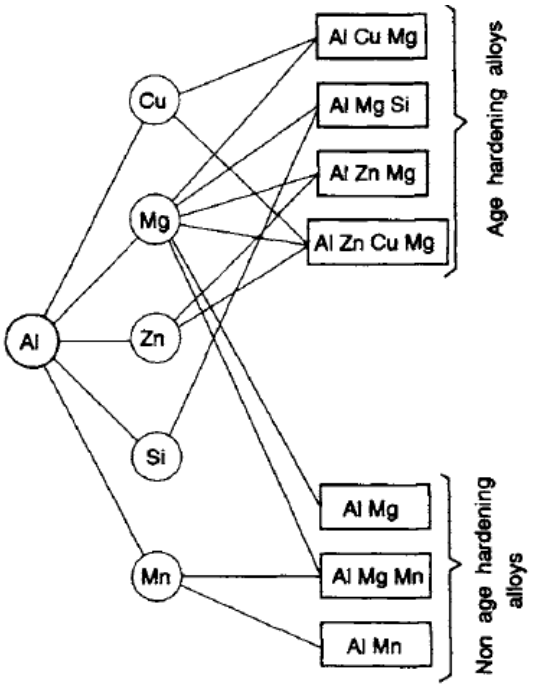

Figure 2.1 Heat treatable and non-heat treatable aluminium alloys [21].

In automotive applications, the 6xxx series is much used as a construction material for outer panels in vehicles. During the mid-late 19th century a gradual decrease in the use of steel and iron in vehicles has taken place due to the rising popularity of aluminium alloys, such as the 6xxx series [1].

2.1.1 AA6082

Within the 6xxx series, 6082 and 6061 alloys are ranked as the alloys being most suitable for medium-high strength applications due to their high contributions of strengthening Mg and Si atoms [3, 22]. In automotive industries these are readily applied in sections where tensile strength is required to reach 300 MPa. Europe prefers 6082 alloys whilst 6061 alloys dominate in North America [22]. This master thesis is focused on a version of the 6082 alloy with main alloying elements in levels of 0.62-0.70 wt% Mg and 0.95-1.05 wt% Si. In addition to trace elements of Fe, Mn and Ti, additional alloying of Cu and Zn is limited to maximum levels of 0.03 wt% Cu and 0.02 wt% Zn. In addition to applications in transportation industry, this specific Al-Mg-Si alloy is extensively used in scaffolding, bridges, cranes and heavy structures [23].

2.2 Casting of Al-Mg-Si alloys

The first step in producing extruded Al-Mg-Si alloys is to create a melt consisting of aluminium with appropriate and specified alloying additions in a suitable furnace. The constituents in the ingot are thorough mixed and filtered before casting. Al-Mg-Si ingots are normally direct-chill cast in a vertical or horizontal process with the aim of achieving a uniform ingot structure. The molten metal is poured into water-cooled moulds and solidified by contact with the chilled mould walls and spray cooling of the remainder of the ingot cross section [21]. An illustration showing the vertical direct-chill casting process is given in Figure 2.2.

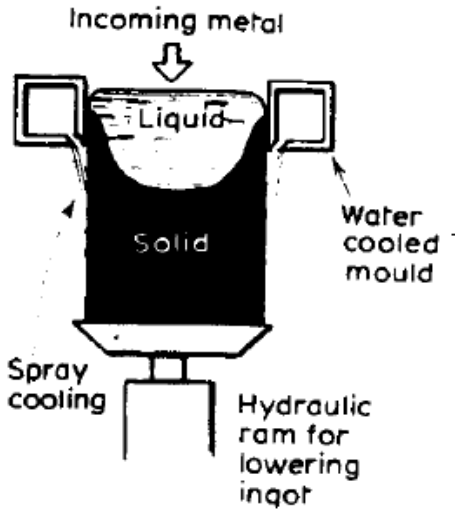

Figure 2.2 Vertical direct-chill cast process [21].

2.3 Homogenisation

Prior to the hot deformation process, wrought aluminium alloys such as the 6xxx series are usually given a three-step homogenisation heat treatment in order to improve extrudability and formability of the billet [24]. Homogenisation involves heating to a temperature in the range of 450-600°C, followed by a specified holding time normally in the range of 6 to 24 h and finally cooling to room temperature. Surface tearing during extrusion is prevented by dissolving detrimental β' (Mg_2Si) particles at the holding temperature formed in the interdentrite regions during solidification. Mg and Si atoms are forced to diffuse back to solid solution, and diffusion rates increase with increasing homogenisation temperature. Essential transformations of plate-like β-AlFeSi intermetallics into more spherical α-AlFeSi intermetallics for improving extrudability, formation of grain size controlling Fe- and Mn-

bearing dispersoids and uniform distribution of alloying elements are also desired from homogenisation [21, 24, 25].

2.3.1 Alstruc homogenisation model

A way to estimate nucleation and growth of primary particles containing Mg, Si, Cu, Fe and Mn during solidification accompanied by dissolution of primary particles and formation of secondary particles during homogenisation has been found through the Alstruc homogenisation model. Semi-quantitative estimates can be achieved from the later part of heating to the holding temperature in homogenisation and during the holding stage with temperatures above 400°C, while qualitative estimates can be obtained from the cooling step after homogenisation. For AA6082 alloys, the program is verified against Fe-bearing primary particles and density of Fe- and Mn-bearing dispersoids at the end of the holding period during homogenisation [24].

The homogenisation model builds on the solid solubility part of phase diagrams which gives fundamentals for applying growth and dissolution equations necessary to tell whether a particle should grow or dissolve. Accuracy of solubility limits is of high importance concerning qualitative prediction of phases present in an alloy after an isothermal heat treatment [24].

2.4 Microstructure in extruded 6xxx profiles

During the extrusion process, pre-heated Al-Mg-Si ingots are kept in a container in a hydraulic press and forced by a ram through a die opening as illustrated in Figure 2.3. The extrusion products possess elongated shapes or tubes [21]. Heat and severe mechanical deformation are generated in the metal during the extrusion process, increasing the dislocation density. The increased dislocation density tends to accelerate the precipitation process in the matrix, giving raise to increase in mechanical strength [26]. The amount of deformation is determined by the extrusion reduction ratio and extrusion speed and tends to be highly inhomogeneous during the extrusion process [27, 28]. The resulting deformed microstructure of as-extruded profiles has a significant effect on various properties such as hardness, yield stress and IGC resistance in terms of fraction of recrystallised material [28].

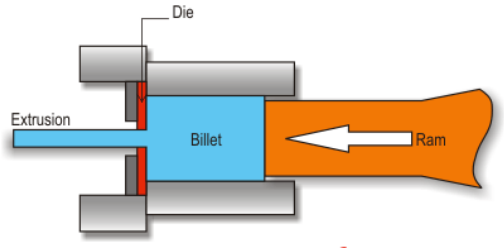

Figure 2.3 Schematic illustration of the extrusion process [29].

The microstructure is affected by the deformation path of the metal flow when being forced through the die. The result from varying levels of deformation is separable zones in the microstructure in terms of grain size, grain orientations and recrystallisation across the sample thickness [30]. High friction and heat are generated in the contact zone between the billet surface and extrusion tools, introducing shear deformation and accumulation of lattice defects in peripheral regions [31]. Severe plastic deformation acts as high driving force for recrystallisation, resulting in a thin recrystallised layer with extremely fine grains (~1 μm) along the periphery [27], which is hard to see with low magnification in LM. The region just below the outermost surface layer is affected by friction and heat to a slightly smaller extent, hence resulting in coarser and fewer grains. These are easier to spot with low magnification as displayed in Figure 2.4.

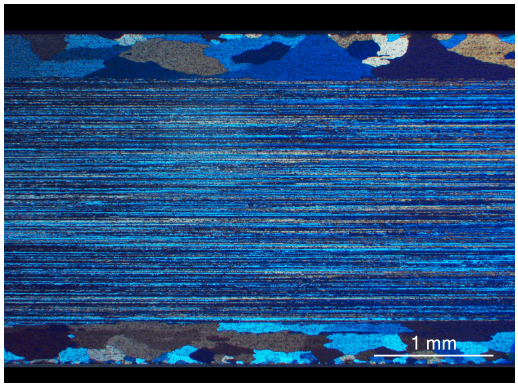

Figure 2.4 A characteristic deformed microstructure of a 6082-alloy after extrusion [32].

Grains in the centre regions appear more elongated and fibrous due to plane strain deformation, less heat generation and lower driving force for recrystallisation [31]. However, centre regions can also be partly recrystallised as a result of cooling rate and alloy chemistry [26].

2.5 Age hardening in Al-Mg-Si alloys

The age hardening phenomenon in aluminium alloys was first introduced by A. Wilm in 1911 as he noticed that hardness increased over time in Al-Mg alloys subsequent to quenching from elevated temperatures to room temperature. This discoverage was later followed up by e.g. the concept of dislocations and GP-zones in the 1930's [33]. Today it is widely known in the industry that a considerable increase in hardness can be achieved for extruded Al-Mg-Si alloys through artificial ageing. This beneficial property makes the 6xxx series highly important for various industrial applications where strength is regarded as crucial [5]. One of the reasons for the commercial popularity of the age hardening potential in 6xxx alloys together with 2xxx and 7xxx alloys is the "± effect", which contributes to enhanced strengthening and is based on the atomic radius differences the two major alloying elements each has to Al [34].

2.5.1 Precipitation from a supersaturated solid solution

The hardening process in Al-Mg-Si alloys operates through growth of various metastable versions of the equilibrium Mg_2Si precipitates nucleated from a supersaturated solid solution in the aluminium matrix [5, 19, 33, 35, 36]. Nucleation occurs in order to minimize the energy in the Al-Mg-Si system when the level of alloying elements is higher than their solubility in the aluminium matrix. The SSSS is presented by the two-phase field $\alpha + Mg_2Si$ in Figure 2.5, and is achieved upon quenching to room temperature as indicated by the red arrow from a temperature in the aluminium solid solution region α, located above the solvus temperature and below the melting temperature of the specific alloy [19].

Age hardening is divided into natural ageing, in which the alloy is left in room temperature for a prolonged period of time subsequent to quenching and artificial ageing, in which further heating to a higher temperature within the $\alpha + Mg_2Si$ region is conducted as indicated by the stipled red arrow in order to accelerate and enhance the precipitation process [19].

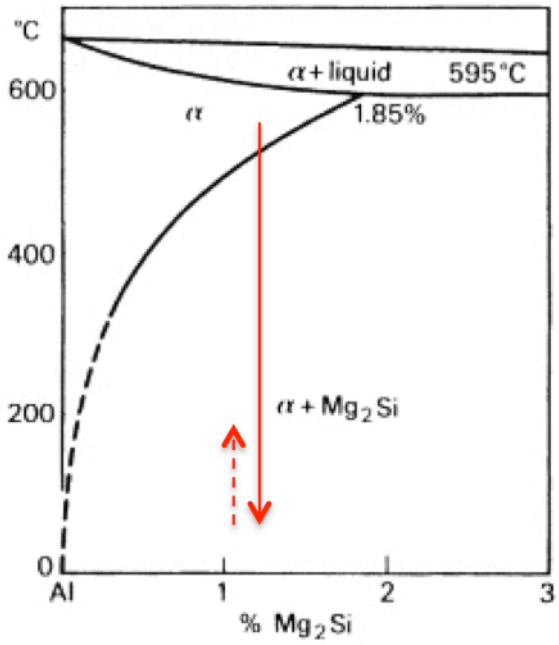

Figure 2.5 Pseudo-binary phase diagram for Al-Mg_2Si [21].

Precipitates strengthen the material to various degree, depending on their size, volume fraction, composition and how they interact with dislocations in the matrix. These properties can be affected by ageing time and temperature, composition of the alloy and how their crystal structure coincides with the crystal structure of the matrix [5, 33].

In automotive applications, age hardening is usually carried out during the paint bake cycle, which holds a temperature of 175°C to accelerate the hardening process. If the material is exposed to room temperature for an extensive period of time between quenching from solution treatment and heating to the ageing temperature, natural ageing also called ”pre-ageing” can occur. This usually has a detrimental effect on mechanical properties and formability after age hardening and is preferably avoided [2, 37].

2.5.2 Precipitation sequence

The total precipitation sequence in Al-Mg-Si alloys during age hardening is widely discussed in the literature. The generally accepted sequence is [2, 5, 20, 35, 37-39]:
SSSS → atomic clusters → GP zones → β´´ → β´ → β(stable) , where SSSS is the supersaturated solid solution achieved upon quenching from solid solution to room temperature after solution treatment or extrusion. Clustering of solute atoms is believed to form in the SSSS shortly after quenching caused by quenched-in vacancies. The clustering

process forms GP zones which include several metastable phases characterised by high coherency with the Al matrix, Si/Mg ratio > 1, size range of only 1-2 nm and nearly spherical shape. GP zones are found to contribute to very limited amount of hardening due to their shape and coherency. There are still uncertainties concerning their crystal structure in the literature [2, 35, 37]. Moreover, the GP zones have shown to be stabilised by the ”± effect” of Mg and Si, which further encourages the transition to successor precipitates [34].

The most effective hardening phase in the 6xxx alloys at the conventional ageing temperature has been found to be the needle-shaped, monoclinic β’’ phase aligned along the <100> direction in the Al matrix [2, 5, 35, 37, 38]. This phase is a successor of the GP zones and some authors suggest a composition of Mg_5Si_6 [5, 35]. A reason for the higher contribution to strength compared to the spherical GP zones is the non-spherical shape which is documented to have high influence on precipitation hardening [34]. There is agreement in the literature that the metastable β’ phase is a successor of β’’ in the ageing sequence. This phase has been confirmed to hold a hexagonal crystal structure and appears to be rod shaped. Like β’’, the β’ phase is also aligned in the $<100>_{Al}$ direction [2, 37, 38]. Its chemical composition is believed to be approximately $Mg_{1.8}Si$ [5]. The stable β phase with the composition Mg_2Si is the final phase to be formed in the precipitation sequence and usually carries a platelet shape. The crystal structure of β is documented to be FCC anti-fluorite and the phase lies in the $\{100\}_{Al}$ planes. This phase does not have a significant contribution to the hardness of the Al-Mg-Si alloy [2, 37].

2.5.3 Strengthening mechanisms during ageing

Underageing

Ageing is frequently defined as three states; underaged, peak-aged and overaged. In the early stages of precipitation in the undeaged regime, precipitates are small, coherent with the matrix, closely spaced and get sheared by moving dislocations as illustrated in Figure 2.6 [40, 41].

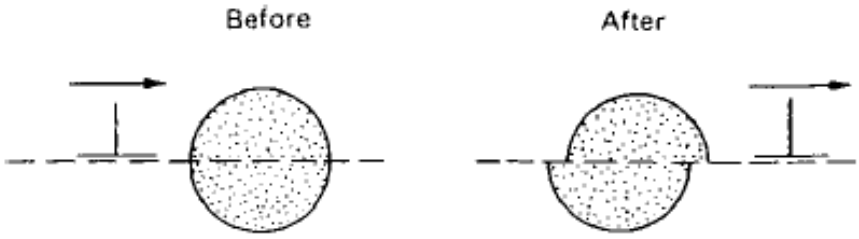

Figure 2.6 Illustration of dislocation shearing through coherent particles [41].

The contribution to hardness rises from chemical hardening and coherency strain hardening where dislocations interact with stress fields surrounding each precipitate [33, 40, 41]. As the ageing time proceeds but remains in the underaged state, precipitates gradually get depleted of aluminium and thereby reducing coherency with the Al matrix. They coarsen and get more widely spaced. The growth of particles with increased lattice mismatch with the matrix makes the particles stronger and harder and their coherency stress fields increase [41]. Dislocations will touch an increased amount of particles per unit length, and the interaction with increased coherency stress fields together with increased chemical hardening during particle penetration will hamper their movement through the precipitates, which is illustrated in Figure 2.7. Hence an increase in hardness is achieved [33, 35, 40, 41].

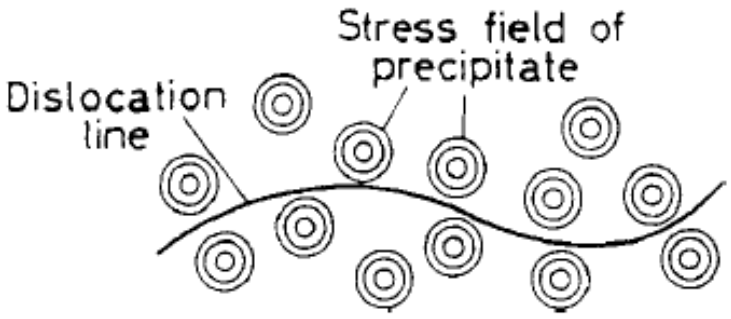

Figure 2.7 Interaction of dislocation with coherency stress fields [41].

GP zones and very short β'' precipitates (lengths of ~7 nm) are dominating the underaged regime in Al-Mg-Si alloys, depending on the ageing time whereas the presence of short β'' precipitates increases the hardness significantly compared to the GP zones [37].

Peak-ageing

In peak-aged condition a certain time is reached where precipitates have obtained a certain size, become semi-coherent and too widely spaced for dislocations to preferentially cut through the precipitates. Stress required for dislocations to circumvent them is now lower compared to shearing through them [40]. The strengthening effect now arise from the creation of Orowan-loops surrounding the particles as illustrated in Figure 2.8, named after Orowan who discovered this process in 1947. These loops introduce high work-hardening rates in the material in which enhanced dislocation interactions occur [33, 41].

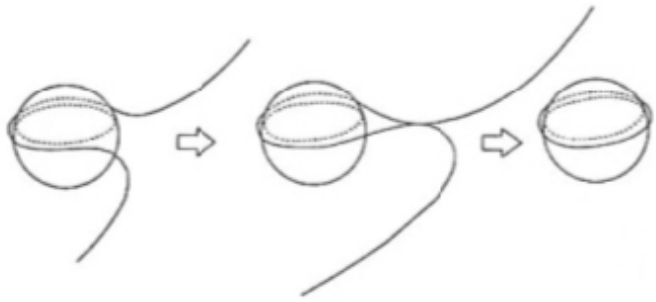

Figure 2.8 Dislocation bypassing a particle with Orowan looping [42].

The β'' phase is predominant in peak-aged condition when the ageing temperature is approximately 175°C [2, 5, 35, 37, 38]. β'' precipitates are often found to be accompanied by GP zones in Al-Mg-Si alloys [5], and have in peak-aged condition achieved a length of ~10 to 15 nm which makes β'' precipitates more strengthening in peak-aged state compared to the shorter β'' phases in underaged state [37].

Overageing

There is agreement in the literature that overageing results in lowered hardness [33, 37, 40, 41]. Totally incoherent precipitates are dominating this ageing condition and as the precipitates continue to grow in size, the particle spacing also increases. Increased particle spacing requires lower stress for dislocations to bypass the precipitates, and a corresponding loss in hardness occurs [40, 41]. Both β (Mg_2Si) and its precursor β' ($Mg_{1.8}Si$) can be formed during overageing, depending on the ageing time. Only in the final stage of overageing the equilibrium phase β (Mg_2Si) can occur.

2.6 Effect of additional elements on hardness

Alloying additions to the Al-Mg-Si system can significantly affect mechanical properties by influencing precipitate chemistry and precipitation kinetics. Some alloying elements tend to retard formation of clusters while others can accelerate the clustering formation process [43]. Electrical conductivity is widely used to study changes in mechanical properties during ageing by quantitatively investigate the extent of alloying elements leaving solid solution for precipitate formation [44]. In section 2.6.1, 2.6.2 and 2.6.3 the influence of Cu and Zn as additional alloying elements on mechanical properties in 6xxx-series with the alloy 6082 in particular will be highlighted.

2.6.1 Influence of Cu on precipitation kinetics

There are several documentations in the literature concerning the effect of Cu addition on the precipitation sequence in Al-Mg-Si alloys. Usually, Cu seems to enhance the kinetics of precipitation hardening, especially in the underaged regime [2, 6, 8, 20]. This behaviour originates from an increase in supersaturation of Mg and Si which further promotes driving force for precipitation at the given ageing temperature. As an effect of the accelerated age hardening rate from the very beginning of the precipitation sequence, increased Cu content in the alloy shortens the ageing time needed to achieve peak hardness. Jin et al. [6] found that with an ageing temperature of 170°C, a Cu-free AA6082 alloy needed 8 h to achieve peak strength whilst adding 0.3 wt% Cu reduced the necessary ageing time to 5 h. Further increasing the Cu content to 0.6 wt% resulted in only 4 h of ageing necessary to achieve peak strength. Another discoverage is that the value of peak hardness increases with Cu addition [8]. Hence, Cu is observed to enhance the material response to artificial ageing [2]. The reason was increased number density of the highly strengthening β'' phase [8]. The effect of Cu on increasing the age hardening potential is shown in Figure 2.9 where vickers hardness values are compared for Al-Mg-Si alloys with 0.4 wt% Cu and 0 wt% Cu as a function of ageing time.

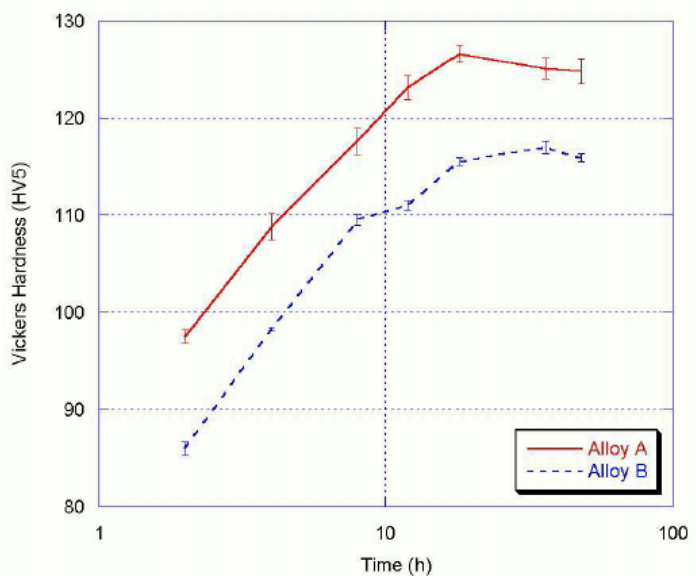

Figure 2.9 Comparison in Vickers Hardness of a 0 wt% Cu Al-Mg-Si alloy named Alloy B with a 0.4 wt% Cu Al-Mg-Si alloy named Alloy A [45].

2.6.2 Formation of Cu-bearing quaternary post-β'' phases

Moreover, adding Cu to ternary Al-Mg-Si alloys with excess Si strongly affects the post-β'' precipitates being formed in the precipitation sequence. Cu addition introduces a quaternary Q phase with precursor intermediate phases such as the lath-shaped Q' phase [38, 39]. Originally the Q' phase was discovered by Dumult et al. [46] and was believed to be a modified version of β' with orthorombic or hexagonal crystal structure and lath-shaped compared to the rod-shaped β'. The phase was then called B'. Chakrabarti et al. [39] later stated that this phase was a precursor of the equilibrium Q and named it Q' thereafter. Q' was found to be crystallographically identical to the hexagonal Q phase in addition to the similar lath-shape and chemical composition of $Al_4Mg_8Si_7Cu_2$ [6, 14, 39]. The only difference between Q' and Q is the level of coherency with the Al matrix and an increase in size for the equilibrium phase [6, 39].

A change in the precipitation sequence is observed when Cu is added in various amounts [2]. The original precipitation sequence in Al-Mg-Si without Cu is [35]: $SSSS \rightarrow GP\ zones \rightarrow \beta'' \rightarrow \beta' \rightarrow \beta$. It was observed that in a 6022 alloy, addition of only 0.07 wt% Cu was enough to change the precipitation sequence by introducing the intermediate Q' phase at peak age and/or during overageing [2, 39]: $SSSS \rightarrow GP\ zones \rightarrow \beta'' \rightarrow \beta' + Q' \rightarrow \beta + Si$. When the Cu content is 0.91 wt%, β' has completely been replaced by Q' and β by Q [2]: $SSSS \rightarrow GP\ zones \rightarrow \beta'' \rightarrow Q' \rightarrow Q + Si$. The amount of Q' is observed to increase with increasing

content of Cu and can be formed even at very low additions of Cu due to Q' being kinetically favoured over other phases [2].

Other reported effects of Cu are formation of a finer precipitate structure after the alloys have been artificially aged and reducing the harm from pre-ageing [2, 47]. Cu is also documented to reduce the grain size, hence increasing the total grain boundary area in the alloy which further has a positive influence on hardness and yield stress [26].

2.6.3 Hardness influence from addition of Zn

When added to most metals as alloying element, Zn has significantly low solid solubility in various metals, increasing the likelihood of producing intermetallics. However, when alloyed with Al the solid solubility can get as high as 80 wt% [48]. The high level of solubility is caused by the fairly weak interaction between Al and Zn atoms. Hence, aluminium intermetallics containing Zn are not preferably formed and the vast majority of Zn atoms will remain in solid solution [49]. In Al-Zn-Mg alloys (7xxx series) where Zn is applied as a main alloying element and the Si content is low, Zn and Mg combine to form the strengthening metastable η' and equilibrium η-$MgZn_2$ precipitates aligned along $\{111\}_{Al}$ planes. These phases are present within the solubility limits containing M (η-$MgZn_2$) in the section of the ternary Al-Zn-Mg phase diagram given in Figure 2.10 [50].

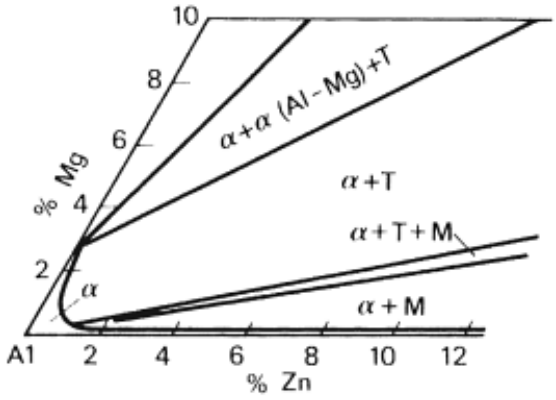

Figure 2.10 A section of the ternary Al-Zn-Mg phase diagram in which α=solid solution, M=$MgZn_2$, T=$Al_{32}(Mg,Zn)_{49}$ [21].

Compared to Al-Zn-Mg alloys, there is limited documented work on the influence of Zn on precipitation in Al-Mg-Si alloys when Zn is an additional alloying element to the ternary alloy system [19]. If added to the 6082 alloy focused on in this study, the fairly low Mg content of 0.62-0.70 wt% is according to the solubility limits of M (η-$MgZn_2$) in Figure 2.10

indicating that a quite high Zn level (above 1 wt%) is required in order to precipitate η-$MgZn_2$. Moreover, Saito et al. [15] found that by adding Zn in a level of 1 wt% to an Al-Mg-Si alloy, a slight increase in both hardness and conductivity occurred during ageing at 185°C which are presented in Figure 2.11 a) and b). The reason was however not the formation of η' and η precipitates as in Al-Zn-Mg alloys. The author claimed that increasing amount of Zn from 0.1 wt% to 1 wt% had a positive influence on hardness by both solid solution strengthening and by incorporation of Zn atoms into known Mg-Si constituent particles by replacement of other elements, promoting a slightly higher precipitate number density together with a finer precipitate structure. Zn was not found to alter the precipitation sequence, unlike the presence of Cu [15]. A lower conductivity as a result of increased addition of Zn was also observed, a result supporting the high solid solubility of Zn in the aluminium matrix [15, 49].

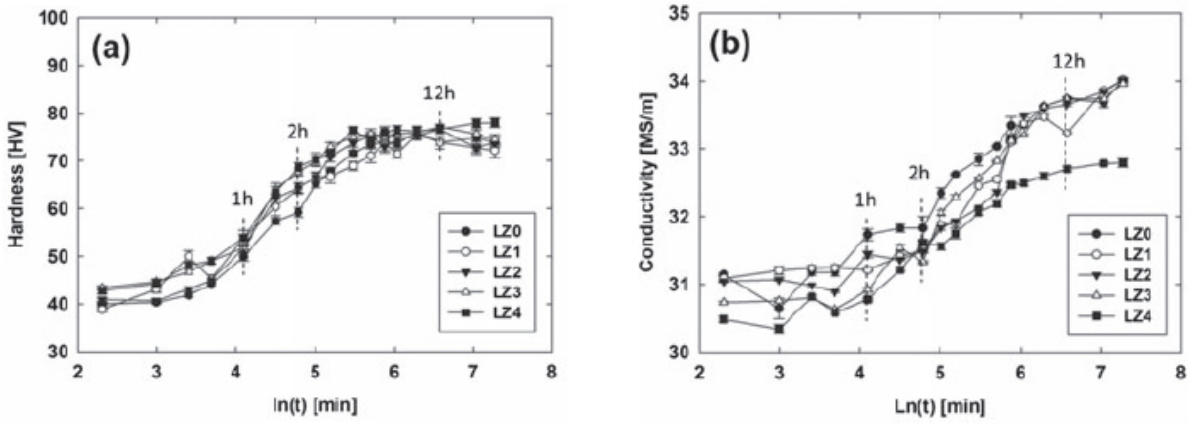

Figure 2.11 For various levels of Zn in the Al-Mg-Si alloy, increased ageing time resulted in increase in a) vickers hardness and b) electrical conductivity [15].

2.7 Hardness influence from cooling rate of extrudate

When billets exit the extrusion die, they generally have reached a temperature of approximately 500-600°C. Depending on the end product requirements, cooling rate to room temperature is specified and is usually proceeded through air cooling (AC) or water quenching (WQ) [28]. The difference in cooling rate between AC and WQ is observed to affect precipitation behaviour upon cooling with a resulting effect on the age hardening potential [14, 51].

Air cooling

A cooling rate below 75°C/min which can be assumed with non-forced AC allows time for segregation of solute elements like Si, Mg and Cu to grain boundaries [21, 28]. Si and Mg atoms are likely to be tied up in Mg-Si constituent particles, especially β' ($Mg_{1.8}Si$) precipitates at temperatures below 370°C which further reduce the supersaturation of Mg and Si atoms in solid solution. The reduced supersaturation leads to less quenched-in vacancies essential for clustering processes in the early stages of precipitation [51, 52]. Reduced strengthening potential coming with slow cooling in air indicates a drop in mechanical strength as seen in Figure 2.12 [28].

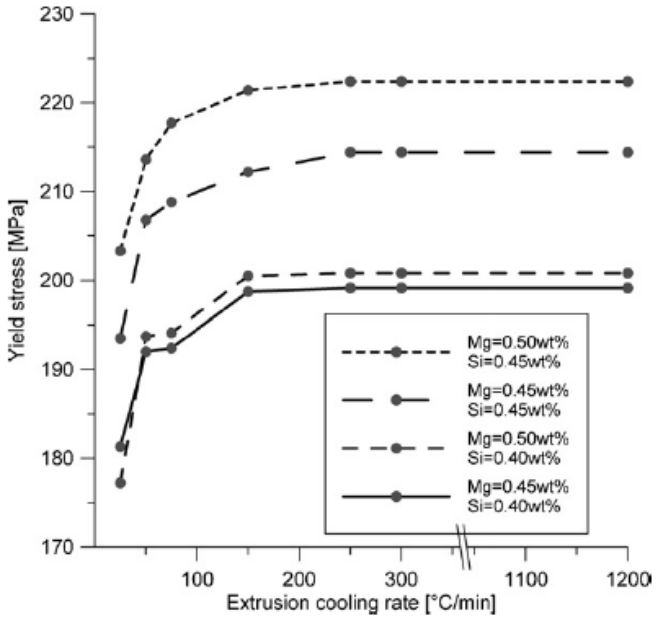

Figure 2.12 Yield stress as a function of extrusion cooling rate for various Mg/Si ratios [28].

The large drop in yield stress owing to slow cooling compared to a relatively stable level of yield stress showed with high quenching rates in Figure 2.12 may introduce larger hardness/yield stress variations among AC profiles as a consequence of lack in control of cooling rate. Billets of varying alloy composition may be left with different strengthening potential prior to ageing. With sufficient Cu present in the alloy, Mg and Si can also be tied up in the formation of Q-precipitates ($Al_4Mg_8Si_7Cu_2$) during cooling [14, 26]. AC is also observed to affect the microstructure by causing higher amount of recrystallisation throughout the sample thickness compared to water cooled samples [26]. This is believed to arise from sufficient time for post-extrusion static recrystallisation to take place [30]. A more

recrystallised microstructure is related to reduction in hardness in the extrusion direction [21, 31], hence AC is associated with a lowering in hardness.

Water quenching

Water quenching is assumed to have a cooling rate above the critical rate of 75°C/min and does not allow time for formation of Mg-Si constituent particles or Q-precipitates. The high quench rate ensure quenched-in vacancies necessary for further clustering and precipitation in addition to promoting a high and fine precipitate density [51]. Hence, WQ profiles have a higher artificial ageing potential compared to AC profiles [26, 28, 51]. By performing electrical conductivity measurements of as-extruded profiles, indications can be obtained concerning the extent of removal of solutes from solid solution due to precipitation [44].

2.8 IGC behaviour in Al-Mg-Si alloys with additional Cu and Zn

Al-Mg-Si alloys are generally considered to have high corrosion resistance compared to high strength Al-alloys rich in Cu or Zn (2xxx and 7xxx series) [7]. However, it is widely documented in the literature that adding Cu to ternary Al-Mg-Si alloys with excess Si in the stoichiometric Mg:Si ratio required to form Mg_2Si has a harmful effect on IGC susceptibility of this aluminium series [7, 9, 14]. Svenningsen et al. [14] found that thermal processing of the extrudate also has a significant effect on the IGC susceptibility, involving cooling rate and subsequently heat treatment.

This type of corrosion is galvanic on a microscopic scale which occurs when two dissimilar metals are brought into metallic contact when being exposed to a corrosive environment [53]. Solute metals located in the aluminium matrix close to grain boundaries tend to diffuse and segregate along the boundaries. This causes galvanic coupling between boundaries and the adjacent aluminium matrix depleted in solutes, given that grain boundary particles/grain boundary film and aluminium differ in corrosion potential. The particle free zone (PFZ) can act anodic and become preferentially dissolved if phases precipitating along grain boundaries together with precipitates and dispersoids embedded in the aluminium matrix in the grain bodies are made of more noble metals compared to aluminium in the galvanic corrosion series such as copper. If grain boundaries are enriched with metals being more active than aluminium such as zinc and magnesium, grain boundaries will act anodic and be corroded instead [9, 10, 54].

2.8.1 Electrochemical effect of Cu-containing phases

In both binary Al-Cu alloys and Al-Mg-Si-Cu alloys, Cu is highly noble compared to Al and the open circuit potential of the Cu-containing alloy is reported to change toward more noble values as more Cu is added. The effect of Cu on the open circuit potential of the aluminium alloy together with an opposite effect of Zn addition can be seen in Figure 2.13 [7, 55].

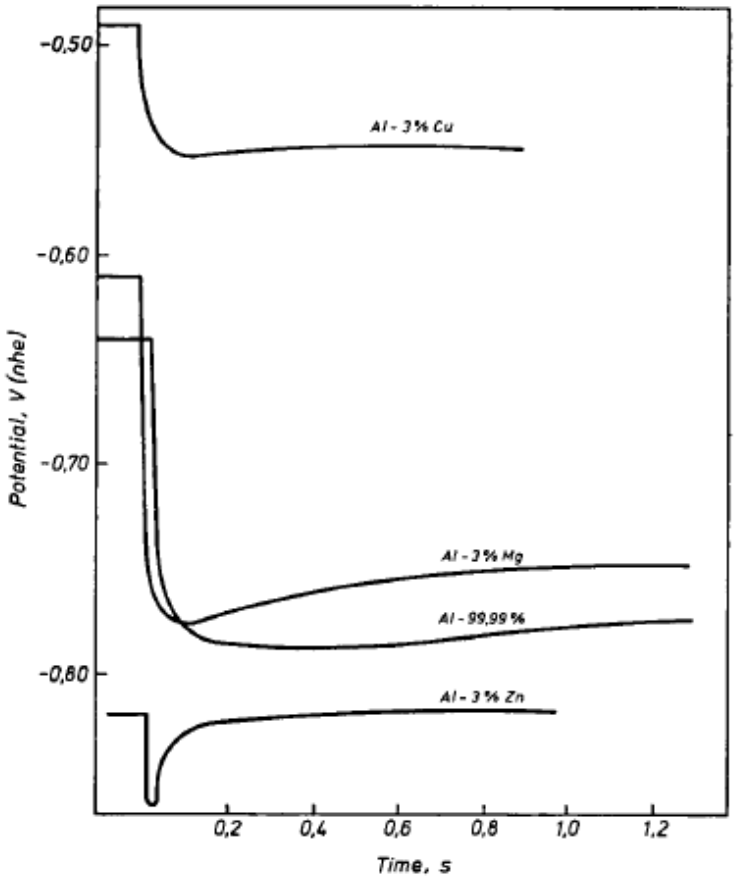

Figure 2.13 Effect of adding 3 wt% Cu, Mg and Zn respectively to a binary Al-alloy on the open circuit potential of the alloy [55].

In Al-Mg-Si alloys where Cu is added as alloying element, Cu is found to diffuse to grain boundaries together with Mg and Si, precipitating the Cu containing Q-phase ($Al_4Mg_8Si_7Cu_2$) together with a noble nanoscale Cu-rich grain boundary film of unknown composition. This film is believed to be a precursor of the Q-phase. The formation of the Q-phase and the Cu-film leave a narrow path of the aluminium matrix adjacent to grain boundaries depleted in Si and Cu, creating local anodes in the microgalvanic cells. The high potential difference caused by Cu concentrating at grain boundaries making them cathodic is believed to be a strong driving force for IGC [10, 56].

IGC is believed to propagate along the anodic PFZ while corroded grain walls and the continuous Cu-rich film is acting cathodic. Given that an agressive environment is present, Cu can dissolve from Q-precipitates and the film and redeposit on the grain walls which is illustrated in Figure 2.14 [10]. Anodic dissolution of the stable β-Mg_2Si along grain boundaries and precipitation of elemental Si at grain boundaries have also been proposed as a causes of IGC. However, Si precipitates are not effective cathodes as they tend to be covered by a protective layer of SiO_2 when exposed to water [10, 56].

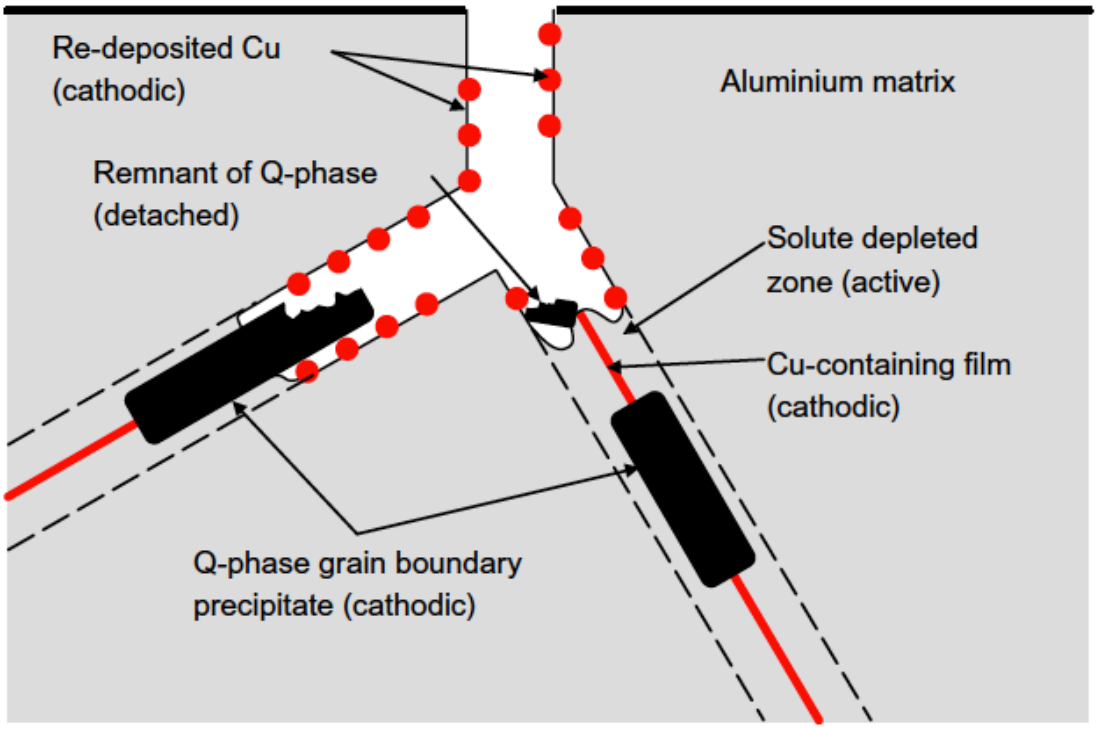

Figure 2.14 Redeposition of Cu from Q-phase and grain boundary film on grain walls in an aggressive environment [10].

Low Cu content

When the amount of Cu is less than 0.02 wt%, IGC has not been observed to occur [26]. Si-depleted zones adjacent to grain boundaries and formation of β-Mg_2Si grain boundary precipitates might still form, but these alone are not sufficient to cause IGC without a continuous grain boundary film enriched with Cu [26, 56].

2.8.2 Influence of Zn as additional alloying element

With excess amount of Mg in the Mg:Si ratio required to form Mg_2Si in an Al-Mg-Si-Cu alloy with ~0.4 wt% Cu, Holmestad et al. [12] discovered the presence of a continuous Mg-rich film along grain boundaries acting anodic compared to the adjacent aluminium matrix.

This film was observed together with the Cu-rich film having a cathodic behaviour. The occurrence of the film enriched with Mg was associated with reduced IGC susceptibility as a result of reduced driving force for IGC compared to Al-Mg-Si-Cu alloys with excess Si. The anodic behaviour of the Mg-rich film was found to counteract the cathodic behaviour imposed by the Cu-rich film, hence lowering the potential difference between the grain boundary and the PFZ. The positive effect of excess Mg on reducing IGC in Al-Mg-Si-Cu alloys was supported by Liang et al. [7].

In binary Al-Zn alloys the addition of Zn is found to change the open circuit potential of the aluminium alloy to a more active direction which is seen in Figure 2.13, increasing the uniform corrosion rate and is the opposite from the effect Cu has in Al-Cu alloys. The effect of Zn on IGC behaviour in Al-Mg-Si alloys is still limited in the literature [55, 57]. Saito [15] found when adding 1 wt% Zn to a Cu-free Al-Mg-Si alloy a continuous Zn-rich film along grain boundaries in peak-aged and overaged condition which was associated with increased frequency of IGC attacks. However, when Cu is present in the Al-Mg-Si alloy, adding Zn has been suggested as a measure to reduce IGC by lowering the corrosion potential [9]. In this master thesis there is a hypothesis considering that Zn can act in a similar way as Mg in the Mg-rich alloy mentioned above dealing with a coexistence of a Zn-rich film and a Cu-rich film in which the Zn-rich film might reduce the cathodic behaviour of the Cu-rich film. This might be the reason for the suggestion with Zn addition in the literature.

2.8.3 Microstructural impacts on IGC influenced by Cu and air cooling

The literature generally agrees on microstructure characteristics of extruded samples of Al-Mg-Si(-Cu) alloys which involve a thin recrystallised surface layer and a bulk region with more deformed and fibrous microstructure. The most important requirement for the microstructure to maintain resistance toward IGC is to have a high fraction of low-angle boundaries (misorientation angle < 5°) with highly elongated, unrecrystallised grains to impede IGC propagation perpendicular to extrusion direction [34]. Svenningsen et al. [14] reported that by increasing the Cu content in Al-Mg-Si(-Cu) alloys, recrystallisation is promoted in the bulk region as viewed in Figure 2.15 a) which otherwise appears fibrous as seen in Figure 2.15 b).

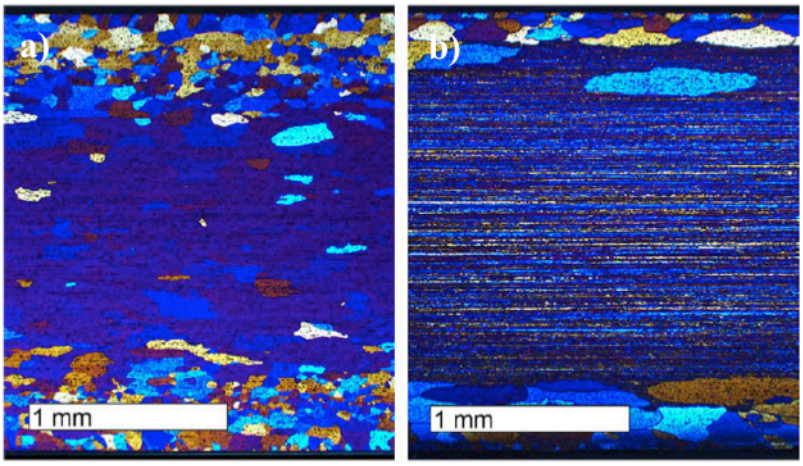

Figure 2.15 Comparison of amount of recrystallised material in the microstructures of extruded and water quenched Al-Mg-Si alloys with a) 0.12 wt% Cu and b) 0 wt% Cu [14].

AC is also observed to cause higher amount of recrystallisation throughout the sample thickness in addition to a thicker recrystallised surface layer, as seen in Figure 2.16 a) [26].

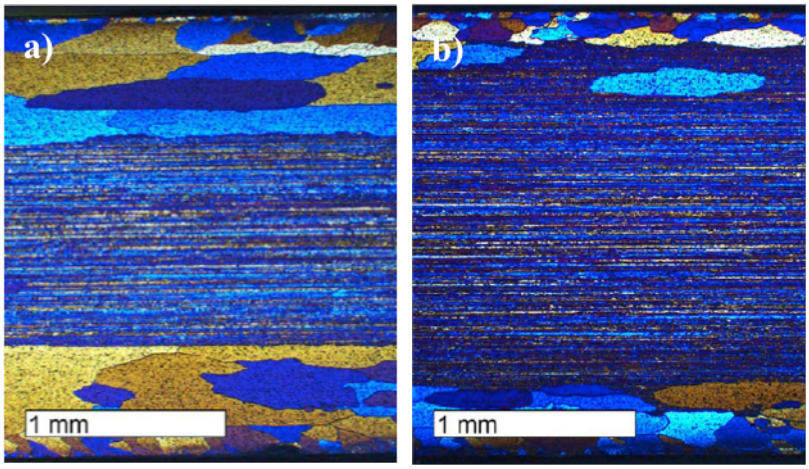

Figure 2.16 Comparison of thickness of recrystallised surface layer in extruded Al-Mg-Si alloys with 0 wt% Cu cooled with a) air and b) water [14].

Fraction of recrystallisation has shown to have significant influence on IGC appearance [26]. Minoda and Yoshida [9] found that recrystallised regions in the Al-Mg-Si-Cu alloy 6061 tempered to T6 were dominated by random high-angle grain boundaries (misorientation angle > 15°) while low-angle boundaries were predominant in more fibrous regions. Moreover, PFZs were found to be strongly affected by misorientation angle of grain boundaries. These readily occurred along high-angle boundaries compared to low-angle boundaries [9]. Taking into account that IGC propagates along PFZs [10], recrystallised regions with high-angle boundaries are more prone to IGC. Hence, by increasing recrystallisation encouraged by AC

and Cu addition, the total high-angle grain boundary area is raised and acts as driving force for IGC [34]. A thicker recrystallised surface layer commonly observed in air cooled profiles compared to water cooled profiles will allow for deeper IGC attacks as IGC is usually confined to recrystallised regions [26].

2.8.4 Effect of cooling rate on IGC-encouraging precipitates

According to Svenningsen et al. [14, 26], slow cooling in air makes Al-Mg-Si(-Cu) alloys more susceptible to IGC compared to water quenching due to the formation of large Q-precipitates ($Al_4Mg_8Si_7Cu_2$) and Mg-Si constituent particles along grain boundaries. However, the IGC susceptibility of air cooled profiles is observed to be positively affected by ageing [26].

Water cooling on the other hand does not allow time for the formation of grain boundary phases, resulting in a higher IGC resistance compared to air cooling. In contrast to the effect of ageing on air cooled profiles, the IGC resistance gets reduced by ageing in water cooled profiles [26].

2.8.5 Effect of heat treatment

Air cooling

Artificial ageing has in general been observed to have a positive effect on IGC susceptibility in air cooled Al-Mg-Si(-Cu) alloys. It has been suggested that grain boundary phases and the nanoscale Cu-rich film being formed upon cooling after extrusion are coarsening by ageing to T6 condition. This process results in disrupture of the noble grain boundary path which is illustrated in Figure 2.17, leaving patches of the film. The gaps between the patches have proved sufficient to impede IGC initiation and IGC arrest [10]. This leads to increased IGC resistance in which attacks are confined to few localised regions [26].

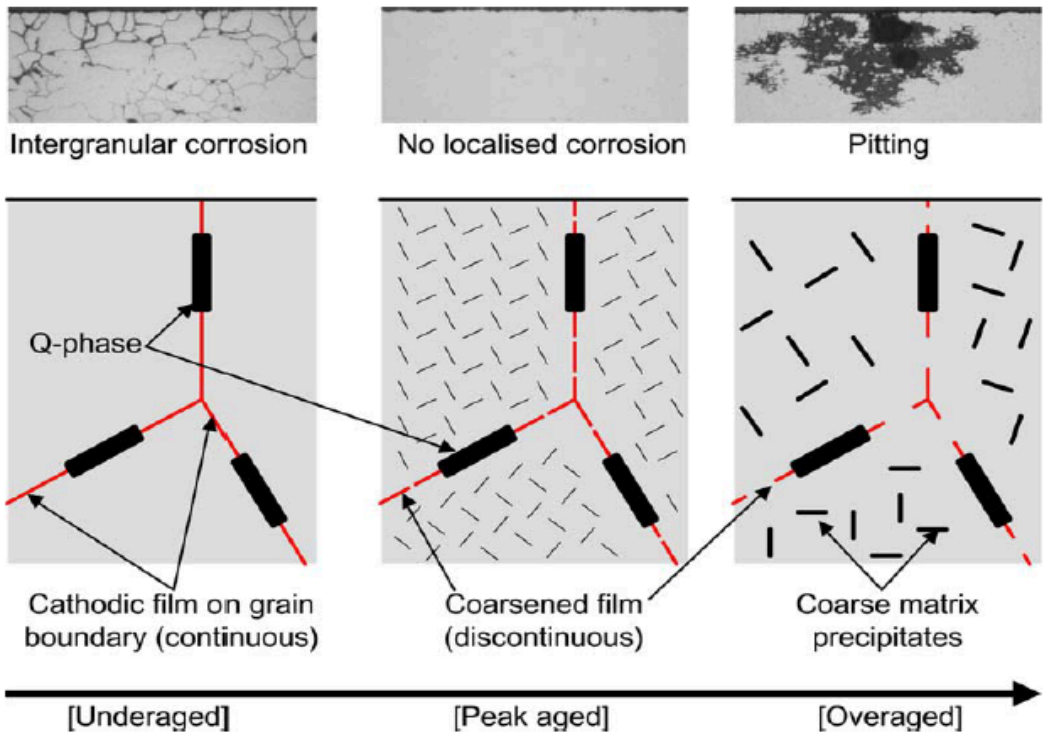

Figure 2.17 Schematic illustration of disrupture of nanoscale Cu-film by coarsening during ageing with resulting corrosion modes [10].

As-extruded samples are reported to suffer from uniform IGC. Natural ageing (T4) and underageing in general have not proved sufficient to reduce IGC susceptibility in air cooled profiles before 2500 s ageing time has passed [26]. IGC attacks generally appear uniform and knife-edged in underaged regime. Upon overageing however, pitting and localised IGC are introduced with coarser attacks compared to underageing and deeper attacks than in peak-aged condition, as viewed in Figure 2.18 [26]. Svenningsen et al. [10] and Larsen et al. [56] claim that the reason for pitting susceptibility in the overaged regime is extensive precipitation and coarsening of Q'-precipitates located in the matrix, reducing the electrochemical potential difference in the microgalvanic cell combining the PFZs and the aluminium matrix.

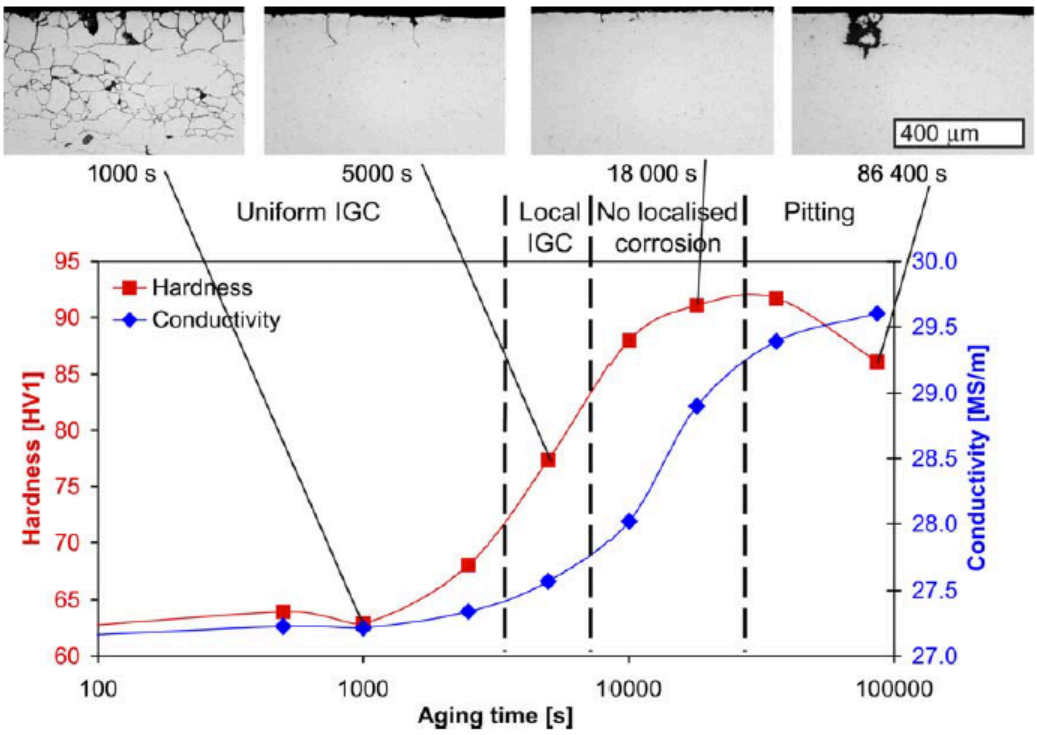

Figure 2.18 Corrosion modes of an Al-Mg-Si-Cu alloy with 0.13 wt% Cu influenced by ageing at 185°C [10].

Water quenching

As-extruded condition for water cooled profiles is documented to have high IGC resistance. Ageing of water quenched profiles to T6 condition has been observed to slightly introduce IGC susceptibility to the alloy by promoting formation of the nanoscale Cu-enriched film which is believed to be a precursor to the Q-phase together with precipitates of the Q-phase in the Cu containing alloys [10, 14, 26]. In Cu-free alloys, ageing to T6 promotes formation of β (Mg_2Si) precipitates. Overageing is dominated by coarser attacks compared to shorter ageing times, e.g. air cooled profiles suffering from pitting in the overaged regime [26].

3 Experimental

3.1 Materials as received

Twelve homogenised AA6082 bolts were received from Hydro Sunndalsøra with chemical compositions given in Table 3.1 in which Cu and Zn were added in increasing amounts. Levels of Mg, Si, Fe and Mn were kept relatively stable.

Table 3.1 Chemical compositions of examined 6082-profiles.

Profile	Mg	Si	Fe	Mn	Cu	Zn
1a	0.67	1.04	0.19	0.54	0.00	0.00
2a	0.68	1.07	0.20	0.55	0.10	0.00
3a	0.66	1.04	0.20	0.53	0.20	0.00
4a	0.66	1.04	0.20	0.53	0.30	0.00
1b	0.66	0.99	0.19	0.53	0.00	0.21
2b	0.66	0.99	0.20	0.53	0.10	0.21
3b	0.67	1.02	0.20	0.54	0.21	0.21
4b	0.66	1.02	0.20	0.55	0.31	0.21
1c	0.65	1.01	0.19	0.53	0.00	0.60
2c	0.65	1.02	0.19	0.53	0.11	0.60
3c	0.65	1.03	0.19	0.54	0.22	0.60
4c	0.65	1.02	0.19	0.54	0.31	0.60

As the first manufacturing step in producing extruded bars for further investigation, aluminium melts with chemical compositions presented in Table 3.1 were cast at 700°C into 95 mm bolts with respective lengths of ~1.2 m. Homogenisation was carried out according to industrial practice at Hydro Sunndalsøra for all chemical compositions by first heating each bolt to a holding temperature of 575°C with a heating rate of 100°C/h. Holding time was set to 2 hours + 15 min, followed by cooling to room temperature with a rate of 249°C/h.

3.2 Extrusion

Homogenised bolts were cut to lengths of 20 cm at Hydro Sunndalsøra followed by extrusion into flat bars with cross section 3 x 65 mm with the vertical SINTEF laboratory press at NTNU in Trondheim imaged in Figure 3.1.

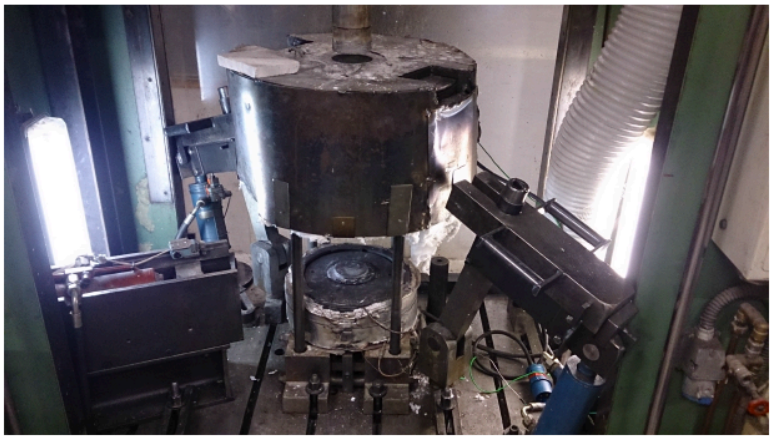

Figure 3.1 Image showing the extrusion press used at SINTEF press laboratory [32].

Graphical presentations showing the relation between press force required to maintain a stable ram speed of ~5.4 mm/s along the position of the extrudate were created for all 12 press bolts. Profile 1a with 0 wt% Cu, 0 wt% Zn is used as an example in Figure 3.2 in which the black line represents the ram speed being stabilised when the press bolt is forced through the die opening and the two peaks on the red line give maximum and minimum press force required.

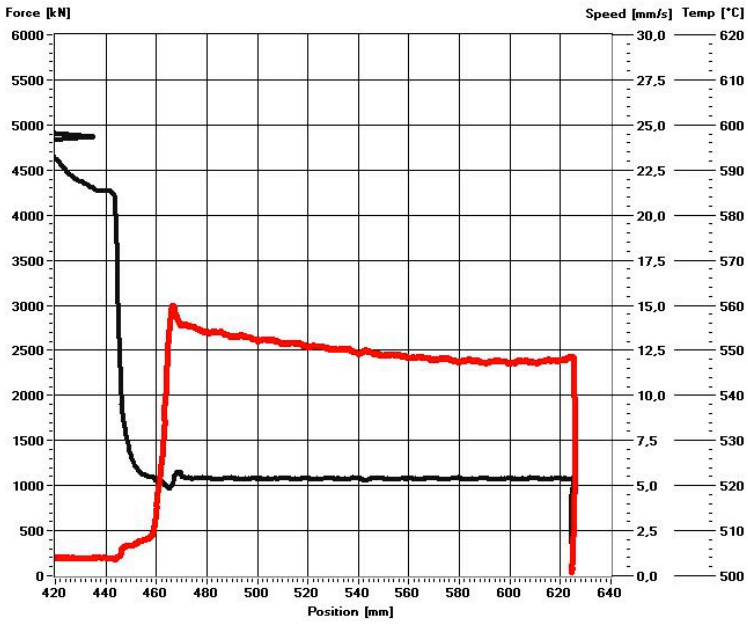

Figure 3.2 Relation between press force and position of press bolt from profile 1a.

The front half of each bolt was air cooled without forced convection by leaving the bar on the floor for 20-30 min prior to freezing storage while the rare half was water quenched by extruding the bars into a water filled pipe prior to freezing storage. Measured extrusion parameters are listed in Table 3.2.

Table 3.2 Measured extrusion parameters from extrusion of 12 profiles.

Profile	Avg ram speed [mm/s]	Temp front end [°C]	Temp rare end [°C]	Max press force [kN]	Min press force [kN]
1a	5.4	532	521	2990	2354
2a	”	533	522	2898	2234
3a	”	532	524	2941	2274
4a	”	533	522	2973	2232
1b	”	528	519	2927	2234
2b	”	530	521	2920	2234
3b	”	531	520	3046	2284
4b	”	532	521	2930	2288
1c	”	532	522	2845	2143
2c	”	532	520	2919	2219
3c	”	531	521	2916	2230
4c	”	530	520	2985	2273

3.3 Artificial ageing

Extruded bars were cut with a Discotom 2 cutting tool to different dimensions prior to artificial ageing depending on subsequent application. For measurements of mechanical properties and examination in LM, one sample from each profile in both air cooled and water quenched condition was cut with dimensions of 3 x 20 x 20 mm, illustrated in Figure 3.3 a). For the accelerated IGC test, profiles were cut to dimensions of 3 x 30 x 64 mm in Figure 3.3 b).

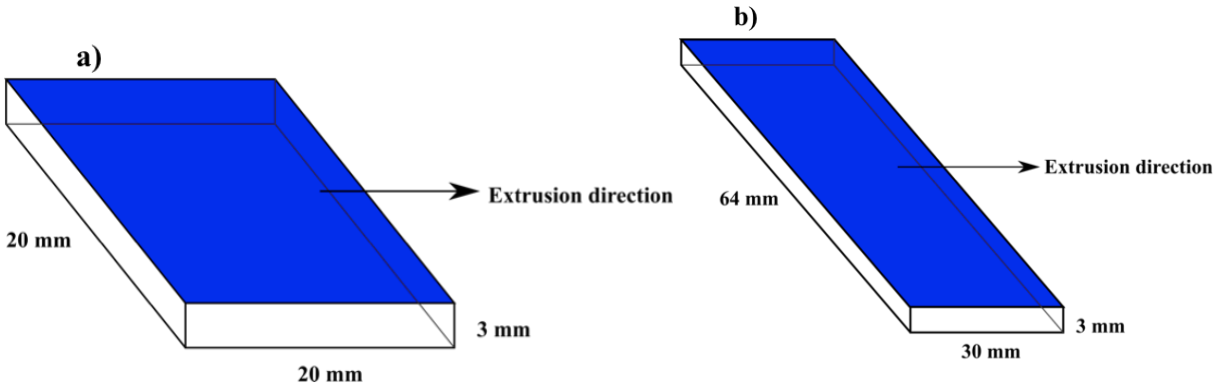

Figure 3.3 Dimensions for a) measurements of mechanical properties and b) IGC test.

All samples were artificially aged to 1800 s, 1800 s and 86400 s respectively in oil bath having a temperature of 185°C. One series of samples was left with as-extruded condition. An overview of ageing times used in this study is given in Table 3.3.

Table 3.3 Overview of ageing times in an oil bath holding 185°C.

Temp	Ageing time			
185°C	0 s	1800 s (30 min)	18000 s (5 h)	86400 s (24 h)

3.4 Mechanical properties

In order to find the influence of both Cu, Zn, cooling rate and temper condition on mechanical properties, 96 samples covering all mentioned variables were tested for vickers hardness and electrical conductivity. 12 chemical compositions were used for which each having 2 cooling rates and 4 ageing times (0 s, 30 s, 5 h and 24 h) within each cooling type.

3.4.1 Vickers hardness

Prior to hardness measurements, the extrusion plane indicated as the blue surface in Figure 3.4 was coarsely grinded with P500 SiC grinding paper for all samples. The hardness instruments Struers Duramin-A2500 and Matsuzawa DVK-1S were used to obtain five vickers hardness values from each of the 96 samples examined. Measurements were performed on the grinded surface with a spacing distance of approximately two diamond cone impressions between each measurement (1-2 mm). A load of 1 kg (HV1) was used for the measurements with a load time of 15 s in Matsuzawa DVK-1S.

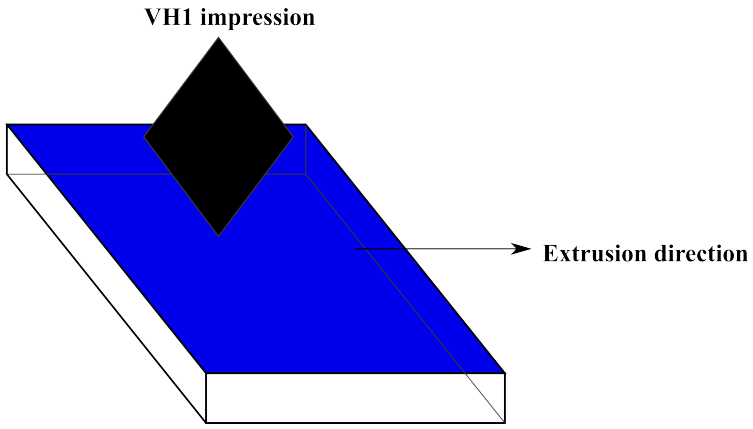

Figure 3.4 Illustration of vickers hardness (HV1) diamond cone impression perpendicular to extrusion direction on the extrusion plane.

3.4.2 Electrical conductivity

Electrical conductivity measurements are often carried out to quantitative examine the extent of precipitation of hardening phases occurring during heat treatment which indicates the extent of removal of minor constituents like Cu from solid solution [44]. Subsequent to hardness measurements, electrical conductivity was therefore measured for all 96 samples in order to find the effect of Cu and Zn additions, ageing time and cooling type by using a Foerster Sigmascope 2.069. The instrument was calibrated by calibration samples before use and three measurements were done for each sample on the extrusion plane.

3.5 Microstructure examination

All 12 AA6082-profiles with varying chemical composition were examined in LM in both air cooled and water quenched condition. Subsequent to vickers hardness and electrical conductivity measurements, 24 of the tested samples with dimensions 3 x 20 x 20 mm (12 AC and 12 WQ) were further prepared for microstructure examination in LM with view plane

parallel to extrusion direction as illustrated in Figure 3.5 and photos taken perpendicular to extrusion direction. Temper condition was not a variable for this examination. Hence, the purpose of studying microstructures in LM was to evaluate the influence of Cu and Zn as additional alloying elements and air cooling versus water quenching on fraction of recrystallised material and fiber texture.

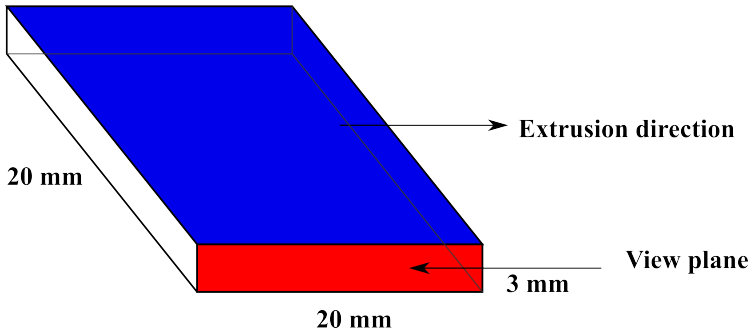

Figure 3.5 Illustration of view plane for microstructure examination in LM.

3.5.1 Sample preparation for LM

The 24 samples were mounted in ClaroCit resin and grinded by using a Stuers Rotopol31 with Rotoforce-4 modular rotating system. SiC grinding papers with increased fineness were used for grinding. Following grinding papers were used with 2-3 min grinding with each paper: P500 → P800 → P1200 → P2000 → P4000. Water was used as lubricant and samples were rinsed in soap water and ethanol between each grinding step. After grinding, samples were polished by the use of a Struers Tegrapol31 with Tegraforce-5 modular rotation system. Polishing discs of 3 μm MD Mol, 1 μm MD Nap and 1 μm OP-S suspension were used in ascending order with ~4 min polishing for each disc. A force of 20 N was used during grinding and samples were rinsed in soap water and ethanol between each polishing step.

When obtaining a sample surface free of defects, anodising was performed in order to examine the samples with polarised light. In the anodising step, samples were immersed in an electrolyte composing of 5% HBF_4 and 95% H_2O for 90 s. A current of 1 A and a potential of 20 V were applied to the electrolyte. Anodising was followed by rinsing samples in water and ethanol before air-drying.

3.5.2 Examination in LM

A Leica MEF4M optical light microscope with Jenoptik Laser Optic System camera was used to obtain optical micrographs perpendicular to extrusion direction and for studying the view plane of the anodised samples. A sub-parallel λ-plate and polarised light were applied for the examination. The software used to image the grain structures was ProgRes Capture v2.8.8.

3.6 Accelerated IGC test

The accelerated corrosion test British Standard BS-ISO 11846 method B [58] has been widely used since 1941 for evaluation of IGC susceptibility among various aluminium alloys when exposed to an aggressive environment. The test method has been found to accelerate corrosion mechanisms and to successfully distinguish between IGC resistant and IGC susceptible materials [10]. In this study, BS-11846 was applied in order to examine changes in corrosion behaviour and IGC susceptibility when varying the level of Zn, cooling rate and ageing time while the Cu level was constantly 0.3 wt%.

3.6.1 Sample preparation

24 samples cut to dimensions illustrated in Figure 3.3 b) having four different ageing conditions, three Zn levels and two cooling types were degreased in acetone and ethanol prior to alkaline etching. The etching media was a 7.5 wt% NaOH solution heated to 55-60°C. Samples were immersed in the solution for ~3 min followed by rinsing in water and dismutting by immersion in a 65 vol% HNO_3 for ~2 min in order to remove corrosion deposits. Gentle rinsing in water and air-drying were applied subsequent to dismutting. Weight was measured for all samples prior to the IGC test.

3.6.2 Test run-through

The electrolyte used for the IGC test was made acidic in order to maintain an aggressive environment with pH≈1. 3 wt% NaCl (30 g/l) and 1 vol% concentrated HCl (10 ml/l) were mixed to obtain desired test conditions and the solution was filled in glass vessels in volumes ensuring more than 5 cm^3/cm^2 exposed surface area. The samples were immersed in the acidified solution for 24 h followed by 2 min immersion in 64% HNO_3, rinsing in water and air-drying. Dry samples were weighed subsequent to the test in order to calculate the weight loss experienced by each sample due to corrosion.

3.6.3 Corrosion examination in LM

After the accelerated IGC test, surface areas were carefully studied for corrosion by visual inspection. One cross-sectional area parallel to extrusion direction from each sample was chosen for further investigation in LM. The cross sections were cut to dimensions illustrated in Figure 3.3 a) with the view plane illustrated in Figure 3.6.

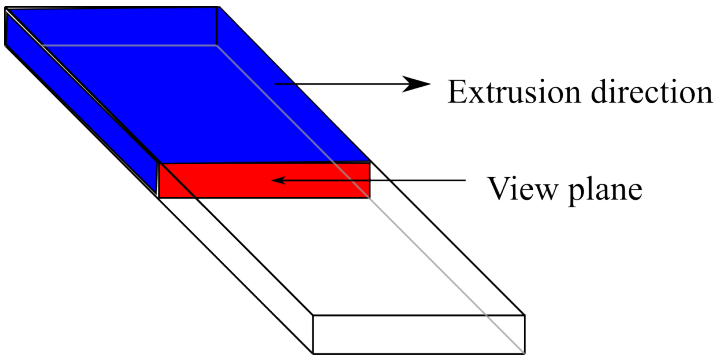

Figure 3.6 Illustration of view plane for examination in LM.

Selected cross sections were prepared for further investigation in LM by the procedures given in section 3.5.1 without performing anodising. Normal light was used instead of polarised as the purpose was to study corrosion along grain boundaries and not the grain structure. The periphery in each sample was examined in LM at various magnifications for IGC in addition to uniform corrosion, pitting corrosion and edge corrosion.

3.7 Alstruc homogenisation model

An Alstruc homogenisation model (ASM) was used to simulate volume fractions of certain precipitates and dispersoids containing Fe, Si, Mn, Mg and Cu and volume fractions of mentioned solutes in solid solution after casting and after homogenisation. The model provided information concerning precipitation changes during homogenisation and was used as an indication for precipitate structure evolving from extrusion. Hence, it was assumed that results gained with the ASM after homogenisation would give similar results after extrusion.

The simulation program was performed on a computer at Hydro Aluminium, Sunndalsøra. Inputs to the program were wt% of alloying elements. The purpose of this simulation was to investigate the effect of increasing content of Cu and Zn. The program for 6xxx alloys was however unable to include Zn as alloying element, and results were only obtained for the profiles with 0 wt% Zn and increasing level of Cu.

4 Results

4.1 Microstructure characterisation in LM

Variations in fraction of recrystallised material, texture and thickness of recrystallised layers have been observed by comparing optical micrographs showing post-extrusion microstructures for all 12 alloy compositions in both air cooled and water quenched condition. A magnification of x25 has been used when taking the LM photos perpendicular to extrusion direction. Obtained micrographs for the profiles with 0.2 wt% Zn and increasing wt% Cu are displayed in Figure 4.1 whilst micrographs with Zn levels of 0 wt% and 0.6 wt% are given in Figure A - 1 and Figure A - 2.

From studying microstructure appearance and measuring thickness of recrystallised surface layers in the optical micrographs in Figure 4.1, Figure A - 1 and Figure A - 2 it is seen that WQ profiles appear highly fibrous and textured in direction of extrusion in centre regions with recrystallised surface layers thinner than the surface layers in AC profiles of identical alloy composition. According to measurements of these layers in AC profiles in Table A – 1 and WQ profiles in Table A - 2 the layer thickness in WQ profiles is ranging from 248 μm to 515 μm with an average thickness of 379 μm . AC profiles have surface layers ranging from 360 μm to 753 μm with an average thickness of 540 μm. AC also tends to promote recrystallisation in the otherwise fibrous centre region in some of the profiles with 0.1 wt% Cu and 0.3 wt% Cu.

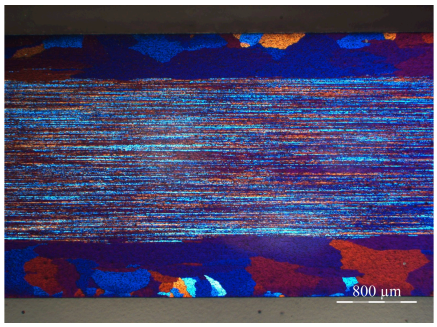

a) 0.2% Zn, 0% Cu, AC

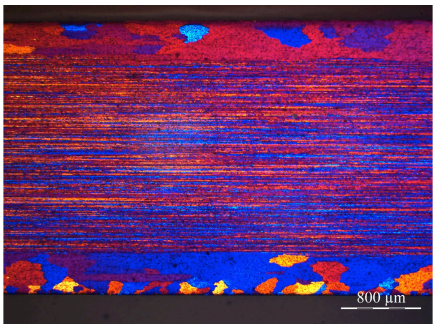

b) 0.2% Zn, 0% Cu, WQ

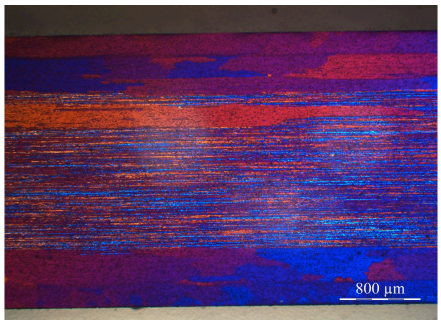

c) 0.2% Zn, 0.1% Cu, AC

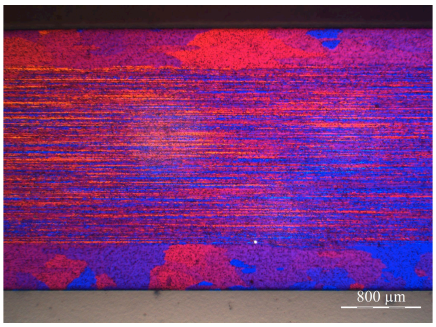

d) 0.2% Zn, 0.1% Cu, WQ

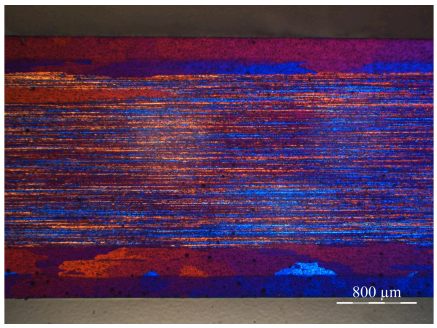

e) 0.2% Zn, 0.2% Cu, AC

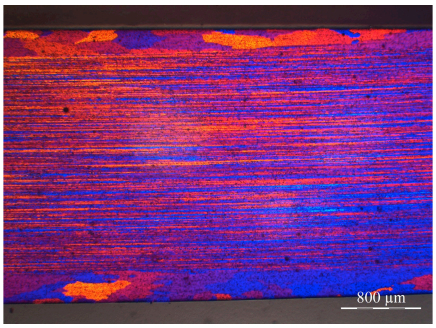

f) 0.2% Zn, 0.2% Cu, WQ

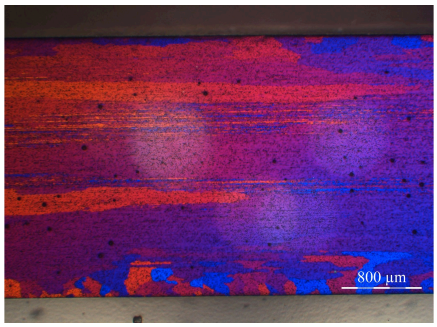

g) 0.2% Zn, 0.3% Cu, AC

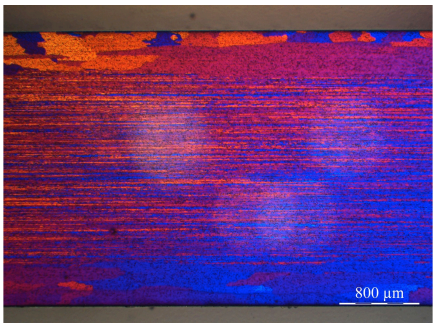

h) 0.2% Zn, 0.3% Cu, WQ

Figure 4.1 Optical micrographs showing grain structure parallel to extrusion direction for 0.2 wt% Zn with varying Cu addition and cooling type. AC = air cooling, WQ = water quenching.

4.2 Mechanical properties

4.2.1 Influence of alloying elements Cu and Zn

A quite distinct trend in vickers hardness (HV1) is observed for AC and WQ profiles respectively with three levels of Zn as a function of increasing amount of Cu from 0 wt% to 0.3 wt%. Graphical presentations of average vickers hardness measurements are given for all examined temper conditions in Figure B - 1. Average hardness used for the graphical presentations are given in Table E - 1, Table E - 2 and Table E - 3. In Figure 4.2 a) and b) profiles tempered to peak-aged condition are shown as examples for the observed overall trends with air cooled profiles in a) and water quenched in b).

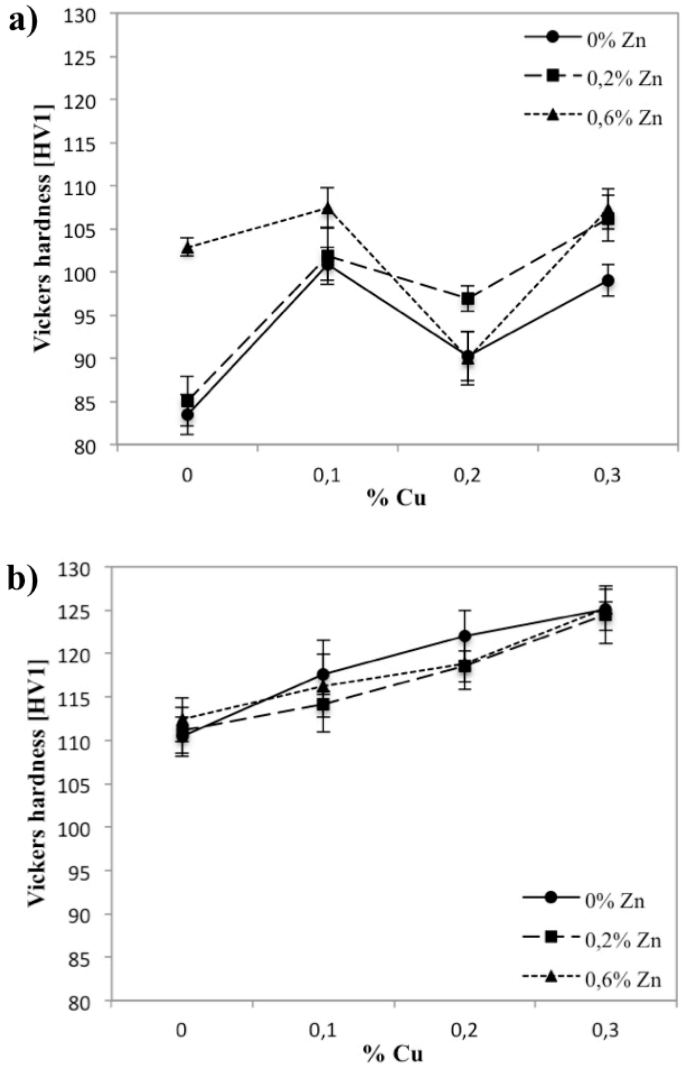

Figure 4.2 Vickers hardness measurements for profiles in T6 condition with three Zn levels for each level of Cu, a) air cooling, b) water quenching.

By comparing HV1 graphs for air cooled profiles in as-extruded, T6x, T6 and T7 condition shown in Figure B - 1 a), c), e) and g) it was observed that those profiles with no Cu present usually showed significantly higher HV1 for the profile variant containing 0.6 wt% Zn compared to the profiles with 0 wt% Zn and 0.2 wt% Zn. It was also observed that by adding Cu in levels of both 0.1 wt%, 0.2 wt% and 0.3 wt%, HV1 increased for all the heat treated profiles given that the level of Zn was kept at 0 wt% or 0.2 wt%. With 0.6 wt% Zn present, the profiles only experienced raised HV1 when Cu was added in amounts of 0.1 wt% and 0.3 wt%. From Figure 4.2 a) it can be seen that for AC profiles, highest HV1 was generally achieved with Cu additions of either 0.1 wt% or 0.3 wt%. Having Zn present in the alloy in amounts of 0.2 wt% and 0.6 wt% raised the hardness level compared to 0 wt% Zn in 11 out of 12 cases for all Cu levels and temper conditions.

The WQ profiles in T6 condition showed in Figure 4.2 b) represented a trend in the evolution of HV1 with increasing Cu addition obtained by HV1 measurements of as-extruded, T6x, T6 and T7 tempered profiles given in Figure B - 1 b), d), f) and h). Increased HV1 was achieved through addition of both 0.1 wt%, 0.2 wt% and 0.3 wt% Cu for all levels of Zn in all tempered profiles. Zn in water quenched profiles did not contribute to increase in hardness to the same degree as in air cooled profiles. Among WQ profiles, the vast majority with 10 out of 12 profiles showed highest level of HV1 when 0.3 wt% Cu was present in the alloy composition.

Electrical conductivity (EC) values were obtained for all 12 profiles with varying chemical composition in both AC and WQ condition in which each sample was examined in both as-extruded, underaged, peak-aged and overaged condition. The measurements revealed characteristic EC trends for AC and WQ profiles of identical alloy composition respectively with increasing Cu content. Graphical presentations of EC trends for each examined temper condition are shown in Figure C - 1 and EC average values are given in Table E - 1, Table E - 2 and Table E - 3. In Figure 4.3 a) and b), EC measurements for AC and WQ profiles respectively in T6 condition are presented as examples with three Zn levels for each level of Cu.

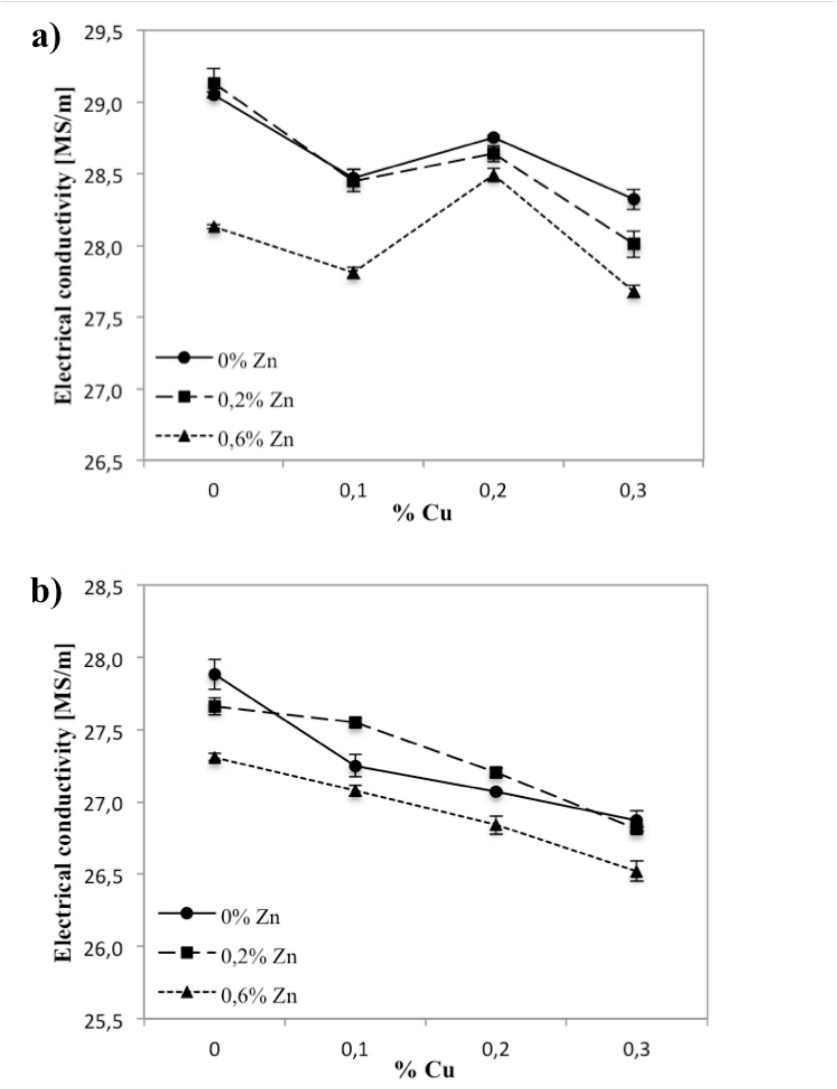

Figure 4.3 Electrical conductivity measurements for profiles in T6 condition with three Zn levels for each level of Cu, a) air cooling, b) water quenching.

Overall trends seen in Figure 4.3 have an appearance of nearly reciprocal correlation to corresponding HV1 measurements in Figure 4.2. By comparing EC graphs of varied Zn content for AC profiles in Figure 4.3 a) it is observed that in 10 out of 12 cases EC declined with a Zn content above 0 wt% independent of Cu levels and temper conditions. For profiles with 0 wt% Zn and 0.2 wt% Zn, highest level of EC was obtained when Cu was not present. However for profiles with 0.6 wt% Zn, maximum EC was achieved with 0.2 wt% Cu.

Unlike the general decline in EC for the air cooled profiles as the level of Zn increased at each level of Cu, WQ profiles only exhibited this trend when Cu was either absent or present in 0.3 wt% as seen in Figure 4.3 b). At 0.1 wt% Cu and 0.2 wt% Cu, EC was often higher for 0.2 wt% Zn compared to 0 wt% Zn. An observation made concerning the effect of Cu on the level of EC is that absence of Cu gave the highest EC for 11 out of 12 profiles. In 10 out of 12 of these profiles the increase in Cu content lead to a continuous decline in EC. Finally, the lowest EC for each Cu level and temper occurred in 11 out of 12 profiles when 0.6 wt% Zn was added to the alloy composition.

4.2.2 Influence of cooling rate and heat treatment

WQ profiles and AC profiles with identical chemical composition were compared in terms of HV1 and EC in as-extruded, T6x, T6 and T7 condition with ageing times of 0 s, 1800 s, 18000 s and 86400 s respectively in Figure D - 1, Figure D - 2 and Figure D - 3. In Figure 4.4 a) profiles with 0 wt% Zn and 0 wt% Cu are presented whilst Figure 4.4 b) contains the maximum amount of solutes with 0.6 wt% Zn and 0.3 wt% Cu.

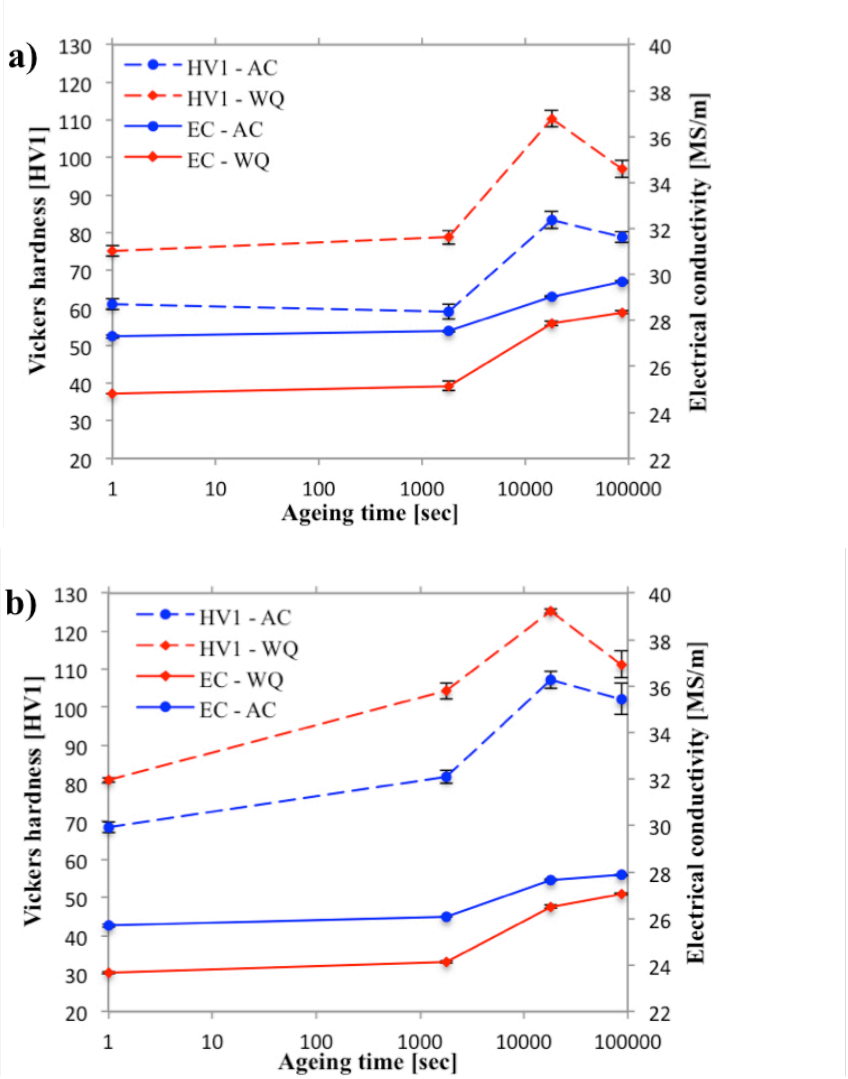

Figure 4.4 HV1 and EC as function of ageing time with as-extruded, T6x, T6 and T7 condition. Amount of Zn and Cu as alloying elements are minimum in a) 0 wt% Zn, 0 wt% Cu, and maximum in b) 0.6 wt% Zn, 0.3 wt% Cu.

Figure D - 1, Figure D - 2 and Figure D - 3 represented by the two examples in Figure 4.4 a) and b) the WQ profile showed higher hardness compared to the AC profile independent of applied heat treatment. When it comes to EC the AC profile showed higher values compared to the WQ profile in all examined temper conditions.

It was observed for the vast majority of the AA6082-profiles examined that hardness increased with ageing time until T6 condition (18000 s) was reached. A drop in hardness occurred when ageing beyond 18000 s. Observations of how ageing time affects the ability of AA6082 to conduct electric current revealed that EC increased as the profiles were tempered for a longer period of time at 185°C. Heat treatments carried out for 5 h (18000 s) and 24 h (86400 s) termed T6 and T7 respectively resulted in significantly higher EC compared to tempering for 30 min (1800 s) according to graphical presentations in Figure 4.4. Moreover, the difference in EC between AC and WQ profiles was significantly larger in as-extruded and underaged condition, followed by a smaller gap in peak-aged and overaged condition.

4.3 Accelerated IGC test

Profiles with constant Cu level of 0.3 wt% with varying Zn contribution, temper condition and cooling rate were exposed to an accelerated IGC test in an aggressive environment for 24 h followed by sample preparation and examination in optical LM. As only one region was chosen to be examined from each sample subsequent to the IGC test, micrographs obtained may therefore not necessarily be representative for the entire sample surface. Results from the examination in LM are presented in a way showing possible changes in corrosion appearance when increasing the content of Zn within each temper condition and cooling type. Obtained optical micrographs contain both an overview of the entire cross-sectional area, enlargement of one of the peripheral regions and an overview of edge corrosion propagating parallel to extrusion direction.

4.3.1 Effect of Zn on IGC in air cooled 6082-profiles

When focusing on AC profiles, the most severe IGC occurrence has definitely been observed for 0.6 wt% Zn in addition to significantly higher weight loss during the corrosion test. The amount of Zn appearing to give the best combinations of high hardness and satisfactory IGC resistance within each temper given that Cu was present in 0.3 wt% are listed in Table 4.1.

Table 4.1 Best combinations of Zn level and corresponding HV1 within each temper.

Temper condition	Zn level [wt%]	Vickers hardness [HV1]
As-extruded	0.2	64.82
T6x	0.2	94.84
T6	0.2	106.22
T7	0.2	103.33

As-extruded: no ageing

Optical micrographs of the three as-extruded AC profiles with increasing content of Zn and 0.3 wt% Cu are given in Figure 4.5 where a1-3), b1-3) and c1-3) represent Zn levels of 0 wt%, 0.2 wt% and 0.6 wt% respectively. No visible IGC occurred when the amount of Zn was kept absent or in 0.2 wt%. However in the case of 0.6 wt% Zn, uniform corrosion and severe IGC attacks became visible along the entire surface periphery as presented in Figure 4.5 c1).

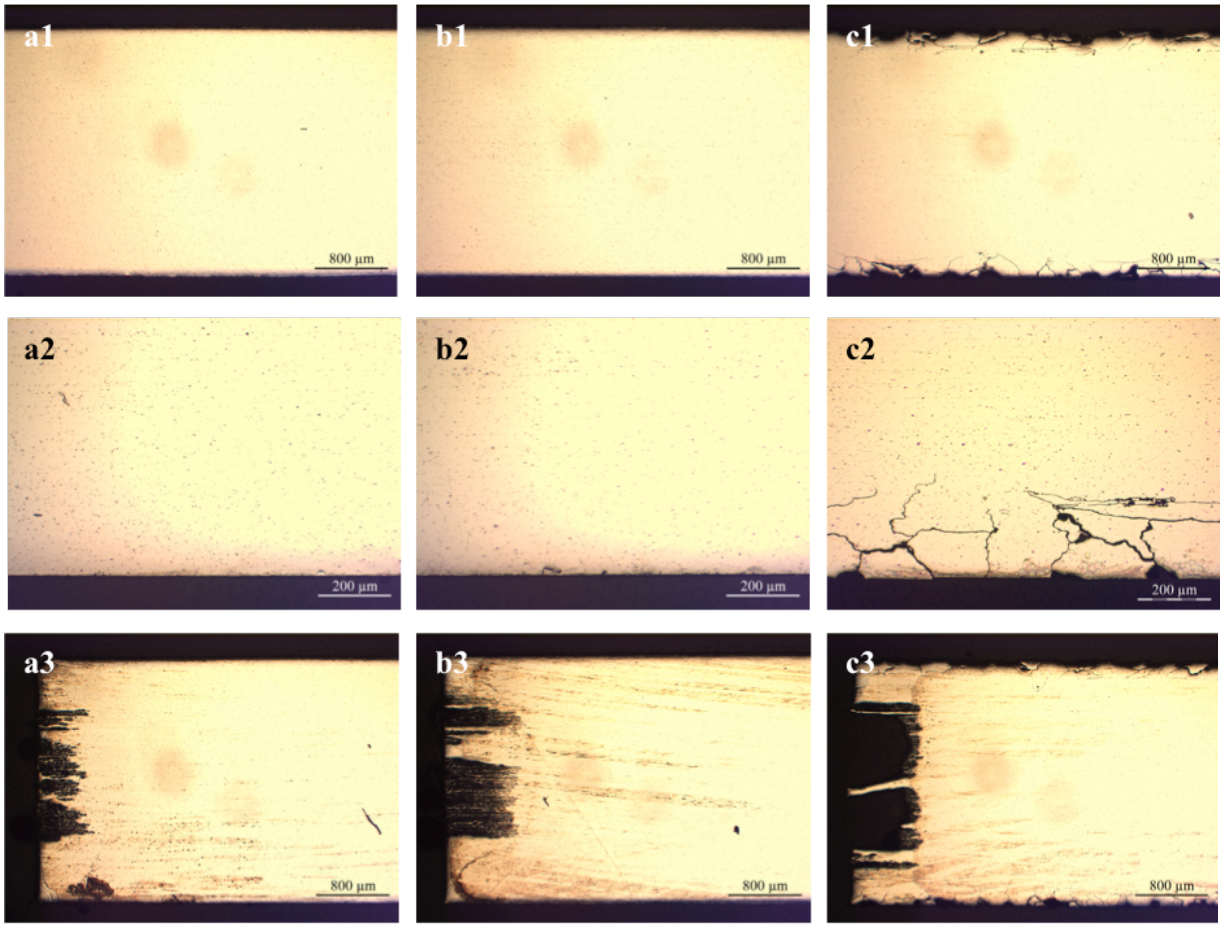

Figure 4.5 Optical micrographs with x25 mag in top row, bottom row and x100 mag in middle row showing AC profiles in as-extruded condition with 0.3 wt% Cu and with a1-3) 0 wt% Zn, b1-3) 0.2 wt% Zn and c1-3) 0.6 wt% Zn.

Increase in level of edge corrosion when increasing the Zn content was observed as showed when comparing a3, b3 and c3 in Figure 4.5. When present, a selection of IGC depths were measured in LM. Based on measurements, maximum and average IGC depths were found and are given in Table 4.2 for Zn levels of 0 wt%, 0.2 wt% and 0.6 wt%. In addition to IGC depths, weight loss was measured subsequent to the IGC test for each Zn level. With

relatively similar levels of weight loss for 0 wt% Zn and 0.2 wt% Zn as seen in Table 4.2, a large increase in weight loss is observed when adding 0.6 wt% Zn.

Table 4.2 Average IGC depths, maximum IGC depths and weight loss measurements for air cooled as-extruded profiles with increasing Zn content.

wt% Zn	Avg IGC depth [μm]	Max IGC depth [μm]	Weight loss [mg/cm^2]
0	0	0	1.82
0.2	0	0	2.70
0.6	271.50	284.90	10.69

T6x – ageing time: 30 min

In the case of profiles tempered for 30 min termed T6x, a similar trend was as for as-extruded profiles was observed. With a magnification of x25 no IGC attacks were spotted for 0 wt% Zn and 0.2 wt% Zn in Figure 4.6 a1) and b1) respectively. When increasing the magnification to x100, small and very localised IGC attacks appeared which are seen in Figure 4.6 a2) and b2), but in very limited amount. These appeared insignificant compared to the amount of IGC attacks along the entire periphery observed in Figure 4.6 c1-3) representing the profile containing 0.6 wt% Zn.

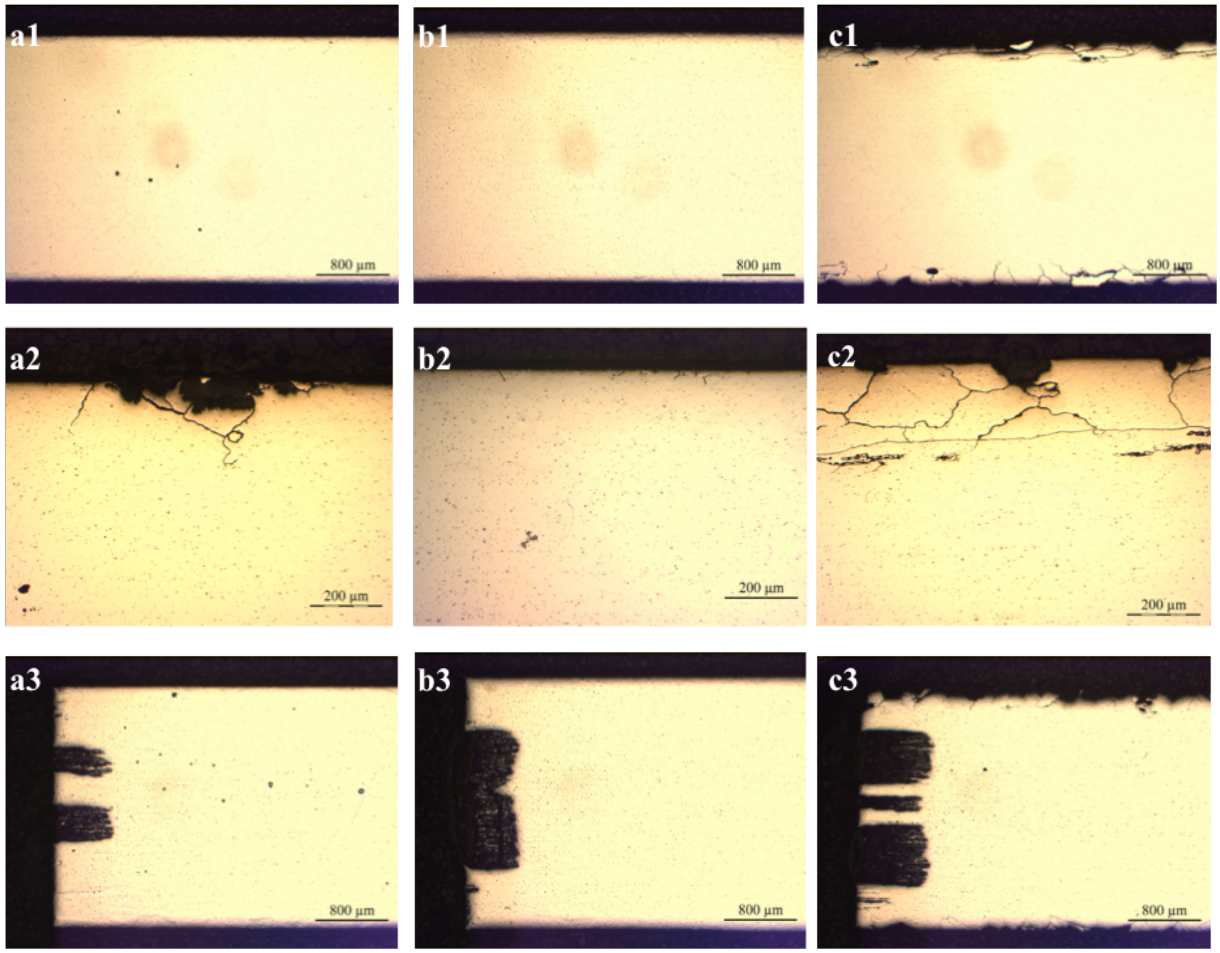

Figure 4.6 Optical micrographs with x25 mag in top row, bottom row and x100 mag in middle row showing AC profiles in T6x condition with 0.3 wt% Cu and with a) 0 wt% Zn, b) 0.2 wt% Zn and c) 0.6 wt% Zn.

A large increase in weight loss was observed when raising the Zn content from 0.2 wt% to 0.6 wt% and is showed in Table 4.3. Additionally, edge corrosion appeared more prominent as the Zn content increased in Figure 4.6 a3), b3) and c3). Maximum and average IGC depths

measured for air cooled profiles in T6x condition can be seen in Table 4.3 for Zn levels of 0 wt%, 0.2 wt% and 0.6 wt%.

Table 4.3 Average IGC depths, maximum IGC depths and weight loss measurements for air cooled T6x profiles with increasing Zn content.

wt% Zn	Avg IGC depth [μm]	Max IGC depth [μm]	Weight loss [mg/cm^2]
0	147.00	223.00	3.84
0.2	25.60	32.00	3.18
0.6	227.10	276.70	11.50

T6 – ageing time: 5 h

IGC was nearly absent in the T6 profiles with 0 wt% Zn and 0.2 wt% Zn as pictured in Figure 4.7 a1-3) and b1-3). Moreover, c1-3) shows that with a Zn level of 0.6 wt%, IGC attacks became prominent along the entire sample surface accompanied by obvious uniform corrosion.

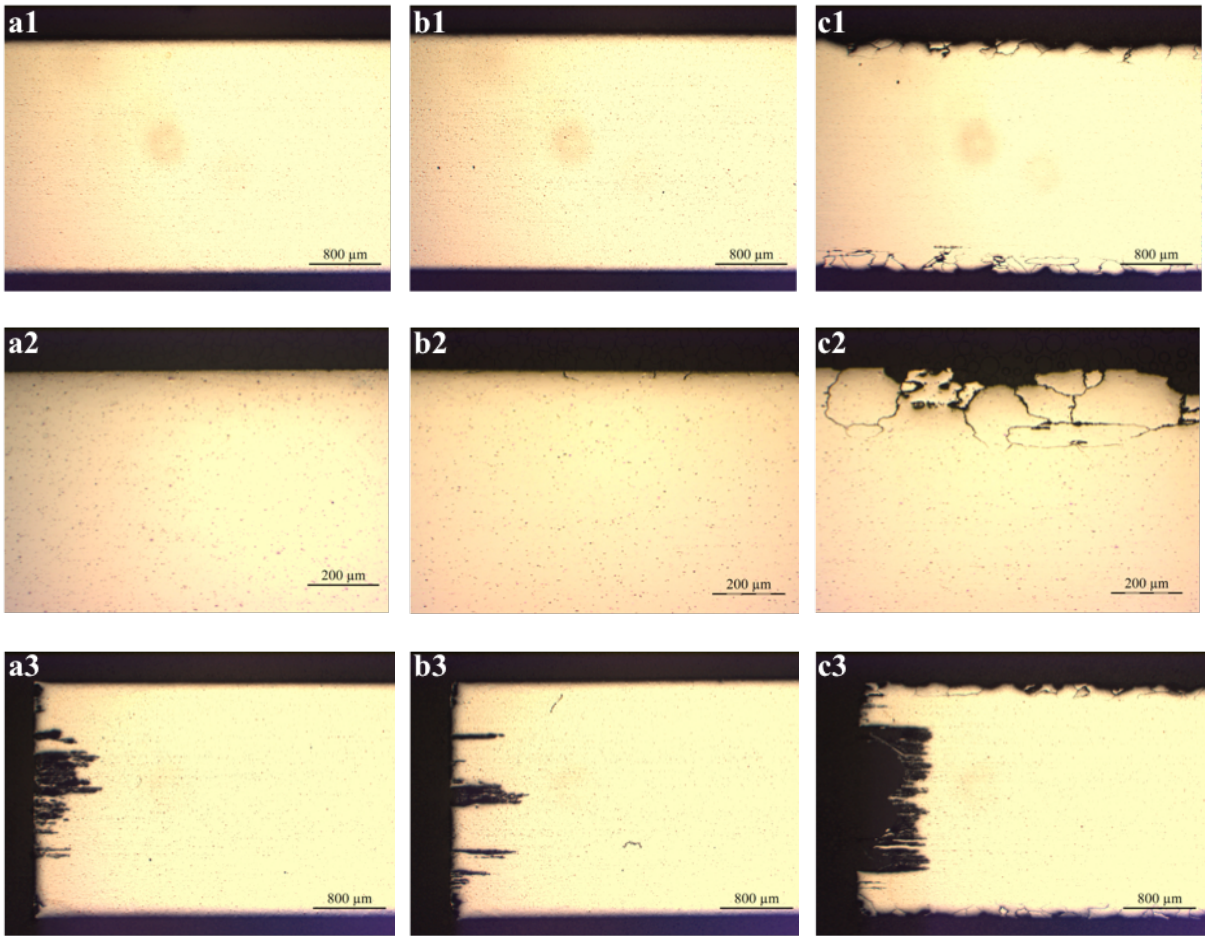

Figure 4.7 Optical micrographs with x25 mag in top row, bottom row and x100 mag in middle row showing AC profiles in T6 condition with 0.3 wt% Cu and with a) 0 wt% Zn, b) 0.2 wt% Zn and c) 0.6 wt% Zn.

Edge corrosion parallel to extrusion direction showed in Figure 4.7 a3), b3) and c3) appeared to be significantly higher for 0.6 wt% Zn in c3). Maximum and average IGC depths together with weight loss measurements are presented in Table 4.4 for increasing level of Zn.

Table 4.4 Average IGC depths, maximum IGC depths and weight loss measurements for air cooled T6 profiles with increasing Zn content.

wt% Zn	Avg IGC depth [μm]	Max IGC depth [μm]	Weight loss [mg/cm^2]
0	0	0	3.02
0.2	39.80	44.40	3.27
0.6	231.30	243.60	12.98

T7 – ageing time: 24 h

Among the T7 profiles tempered for 24 h, the 0.6 wt% Zn profile in Figure 4.8 c1-3) showed a much higher frequency of IGC attacks in addition to uniform surface corrosion compared to nearly IGC-free surfaces in the 0 wt% Zn profile showed in a1-3) and 0.2 wt% Zn profile in b1-3). Furthermore, the occurrence of localised coarse IGC in b2) with 0.2 wt% Zn was in contrast to IGC-free surface regions for air cooled 0.2 wt% Zn profiles in as-extruded, T6x and T6 condition.

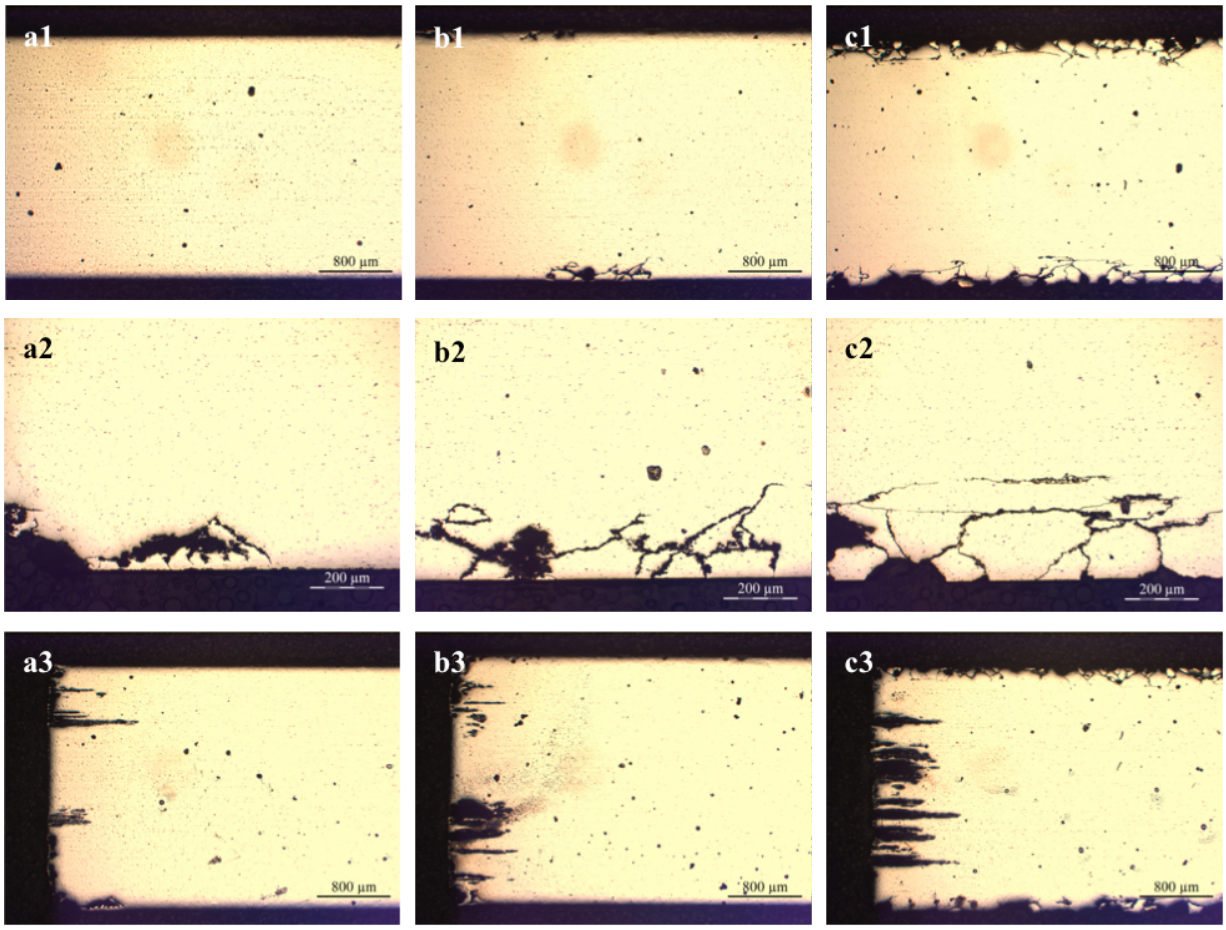

Figure 4.8 Optical micrographs with x25 mag in top row, bottom row and x100 mag in middle row showing AC profiles in T7 condition with 0.3 wt% Cu and with a) 0 wt% Zn, b) 0.2 wt% Zn and c) 0.6 wt% Zn.

A more widely spaced edge corrosion was found according to Figure 4.8 a3), b3) and c3) compared to lower ageing times. For Zn levels of 0 wt%, 0.2 wt% and 0.6 wt%, maximum and average IGC depths are given together with weight loss results in Table 4.5.

Table 4.5 Average IGC depths, maximum IGC depths and weight loss measurements for air cooled T7 profiles with increasing Zn content.

wt% Zn	Avg IGC depth [μm]	Max IGC depth [μm]	Weight loss [mg/cm^2]
0	172.40	191.00	2.28
0.2	173.20	253.90	2.28
0.6	265.30	308.70	10.33

4.3.2 Effect of Zn on IGC in water cooled 6082-profiles

Among the WQ profiles with 0.3 wt% Cu, profiles containing 0.6 wt% Zn appeared in all cases to suffer from deeper and more frequent IGC attacks compared to 0.2 wt% Zn and 0 wt% Zn. However, profiles with Zn level of 0.2 wt% were also observed to have some susceptibility toward IGC although not to the same degree as 0.6 wt% Zn. The amount of Zn appearing to give the best combinations of high hardness and satisfactory IGC resistance within each temper given that Cu was present in 0.3 wt% are listed in Table 4.6.

Table 4.6 Best combinations of Zn level and corresponding HV1 within each temper.

Temper condition	Zn level [%]	Vickers hardness [HV1]
As-extruded	0	82.56
T6x	0.2	103.98
T6	0.2	124.42
T7	0	102.20

As-extruded – no ageing

According to Figure 4.9 presenting the WQ profiles in as-extruded condition, no regions of the sample surface were observed to suffer from IGC regardless of the increase in level of Zn with 0 wt% in a1-3), 0.2 wt% in b1-3) and 0.6 wt% in c1-3). A few localised pitting attacks were present along the surface in the 0 wt% Zn profile as displayed in a1) in which one of the pits is enlarged in a2) with x100 mag. Pitting corrosion was however lowered when adding Zn in levels of 0.2 wt% and 0.6 wt%.

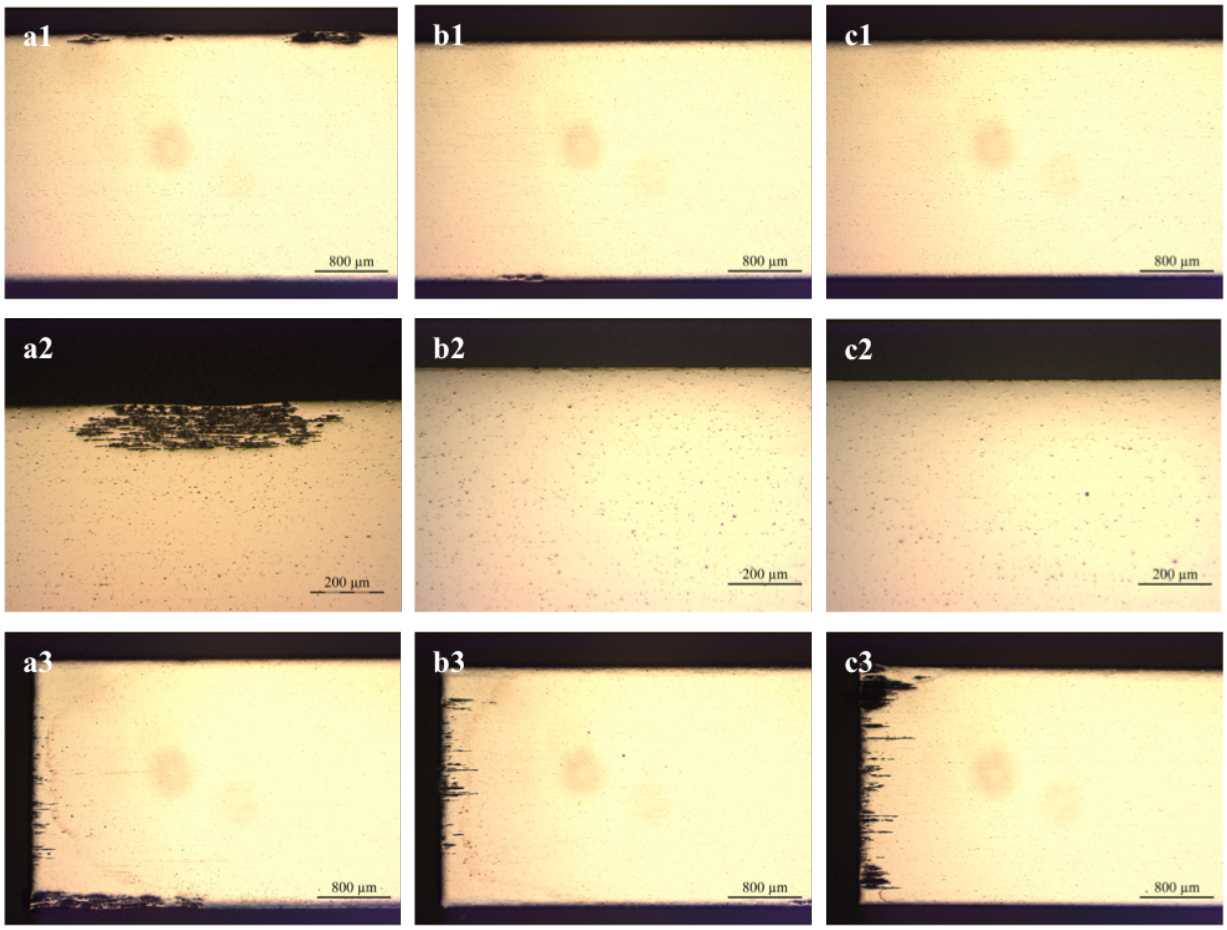

Figure 4.9 Optical micrographs with x25 mag in top row, bottom row and x100 mag in middle row showing WQ profiles in as-extruded condition with 0.3 wt% Cu and with a) 0 wt% Zn, b) 0.2 wt% Zn and c) 0.6 wt% Zn.

Edge corrosion appeared modest as seen in Figure 4.9 a3), b3) and c3) with widely spaced corrosion parallel to extrusion direction. Maximum and average IGC depths are together with weight loss measurements given in Table 4.7 for Zn levels of 0 wt%, 0.2 wt% and 0.6 wt%.

Table 4.7 Average IGC depths, maximum IGC depths and weight loss measurements for water quenched as-extruded profiles with increasing Zn content.

wt% Zn	Avg IGC depth [μm]	Max IGC depth [μm]	Weight loss [mg/cm^2]
0	120.30	127.00	1.76
0.2	70.20	71.20	1.59
0.6	0	0	1.99

T6x – ageing time: 30 min

For underaged WQ profiles with T6x condition tempered for 30 min, profiles with 0 wt% Zn and 0.2 wt% Zn were observed to have few localised IGC attacks with x100 mag as displayed in Figure 4.10 a2) and b2) respectively. In the situation where the level of Zn was raised to 0.6 wt%, IGC attacks became larger sized and more prominent along the sample periphery as can be observed in c2). Compared to corresponding air cooled profiles, uniform corrosion along the surface periphery was not as obvious in the water quenched profile with 0.6 wt% Zn in c1).

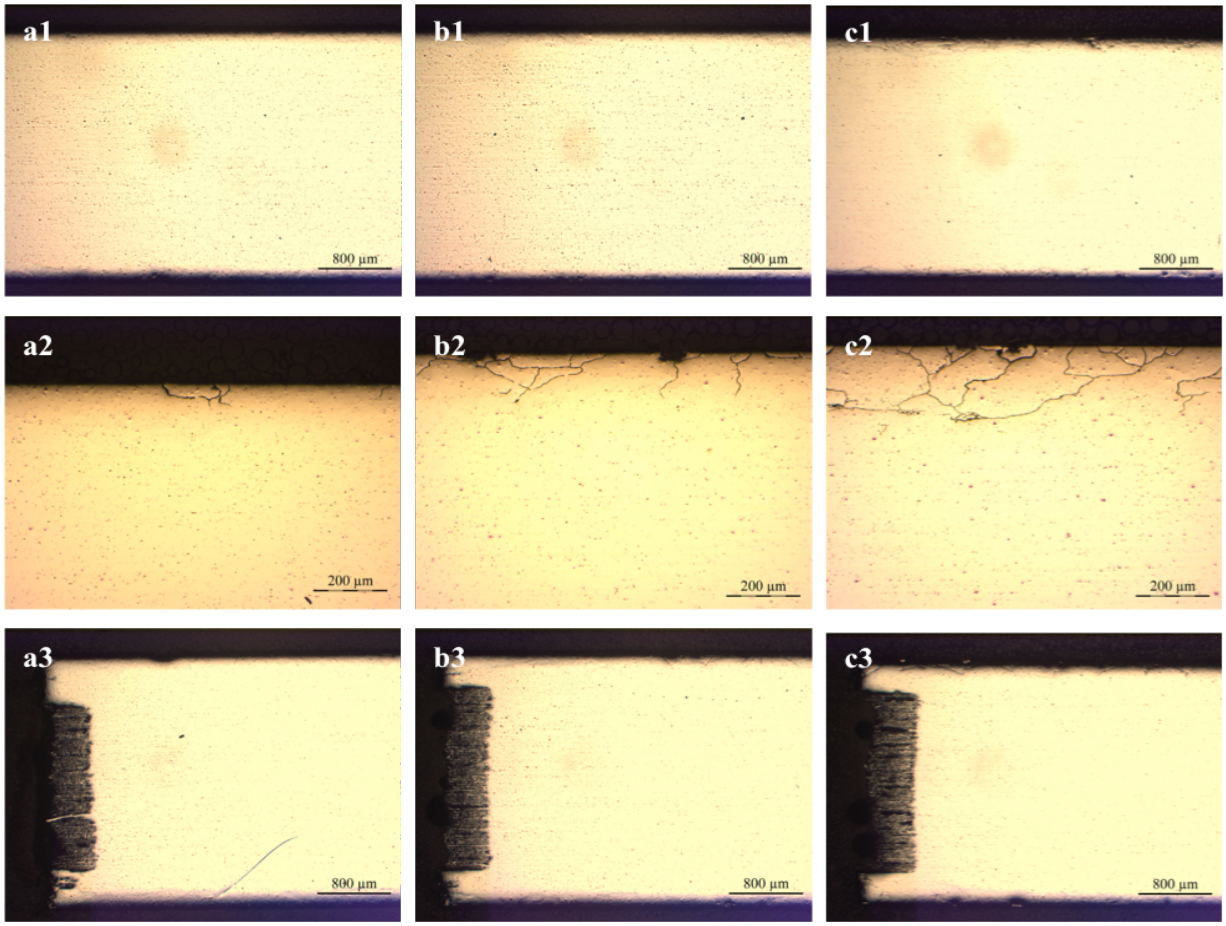

Figure 4.10 Optical micrographs with x25 mag in top row, bottom row and x100 mag in middle row showing WQ profiles in T6x condition with 0.3 wt% Cu and with a) 0 wt% Zn, b) 0.2 wt% Zn and c) 0.6 wt% Zn.

A quite homogeneous edge corrosion propagating parallel to extrusion direction was observed according to Figure 4.10 a3), b3) and c3) for increasing level of Zn. Maximum and average IGC depths are given in Table 4.8 accompanied by weight loss measurements for increasing Zn content.

Table 4.8 Average IGC depths, maximum IGC depths and weight loss measurements for water quenched T6x profiles with increasing Zn content.

wt% Zn	Avg IGC depth [μm]	Max IGC depth [μm]	Weight loss [mg/cm^2]
0	198.90	267.30	4.92
0.2	94.50	124.90	5.30
0.6	203.70	274.60	6.71

T6 – ageing time: 5 h

The T6 tempered profiles with 0 wt% Zn and 0.2 wt% Zn in Figure 4.11 a1) and b1) respectively showed a few localised IGC attacks with moderate size. By adding 0.6 wt% Zn to the alloy, IGC evolved more frequently along the surface of the sample. Some of these attacks can be seen in Figure 4.11 c2). Compared to the knife-edged shape of the IGC attacks in WQ profiles in T6x condition, IGC attacks appeared coarser in T6 condition. The depth of corrosion pits is higher for 0 wt% Zn in a2) compared to 0.2 wt% Zn in b2) and absent in 0.6 wt% Zn in c2).

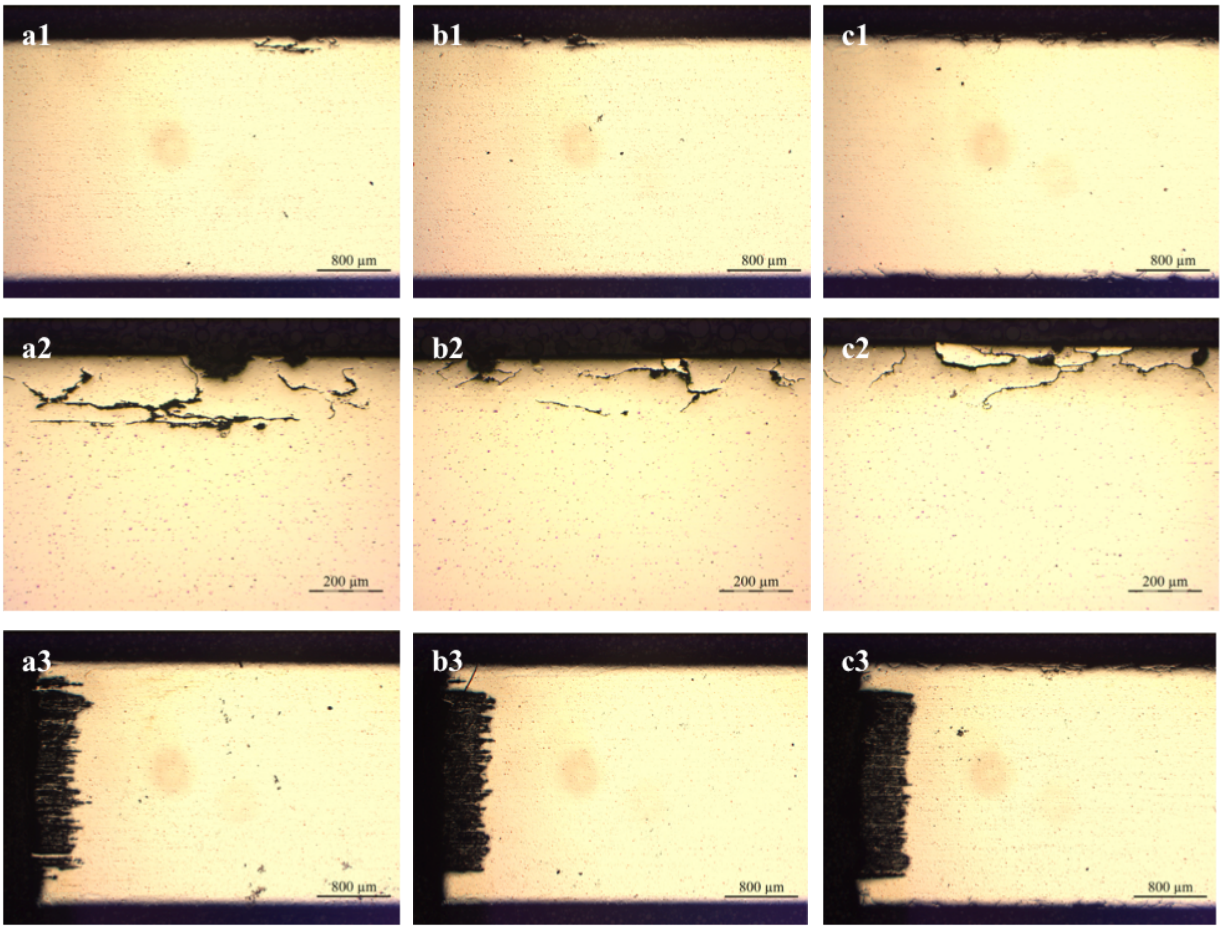

Figure 4.11 Optical micrographs with x25 mag in top row, bottom row and x100 mag in middle row showing WQ profiles in T6 condition with 0.3 wt% Cu and with a) 0 wt% Zn, b) 0.2 wt% Zn and c) 0.6 wt% Zn.

Amount of edge corrosion penetrating into the material in extrusion direction were relatively similar for 0 wt% Zn, 0.2 wt% Zn and 0.6 wt% Zn, showed in Figure 4.11 a3), b3) and c3) respectively. Weight loss measured subsequent after the corrosion test was somewhat higher for 0.6 wt% Zn compared to 0 wt% Zn and 0.2 wt% Zn as presented in Table 4.9 but not even

close to the weight loss experienced in air cooled profiles with 0.6 wt% Zn. Maximum and average IGC depths are also given in Table 4.9.

Table 4.9 Average IGC depths, maximum IGC depths and weight loss measurements for water quenched T6 profiles with increasing Zn content.

wt% Zn	Avg IGC depth [μm]	Max IGC depth [μm]	Weight loss [mg/cm^2]
0	216.30	248.80	5.07
0.2	153.50	168.30	4.89
0.6	159.70	171.40	7.26

T7 – ageing time: 24 h

In T7 condition the WQ profiles exhibited increased frequency of IGC as the level of Zn was raised from 0 wt% Zn to 0.2 wt% and 0.6 wt%. The optical micrograph of the WQ 0 wt% Zn profile showed in Figure 4.12 a1) hardly reveals any IGC attacks compared to the profiles with 0.2 wt% Zn and 0.6 wt% Zn presented in b1) and c1). In contrast to absent IGC in a1), corrosion pits were present in the alloy with 0 wt% Zn. The 0.2 wt% Zn profile showed IGC along one of the peripheries in b1) compared to the 0.6 wt% Zn profile which displayed IGC along both peripheries in c1). On average, deeper IGC attacks were observed for 0.6 wt% Zn than for 0.2 wt% Zn.

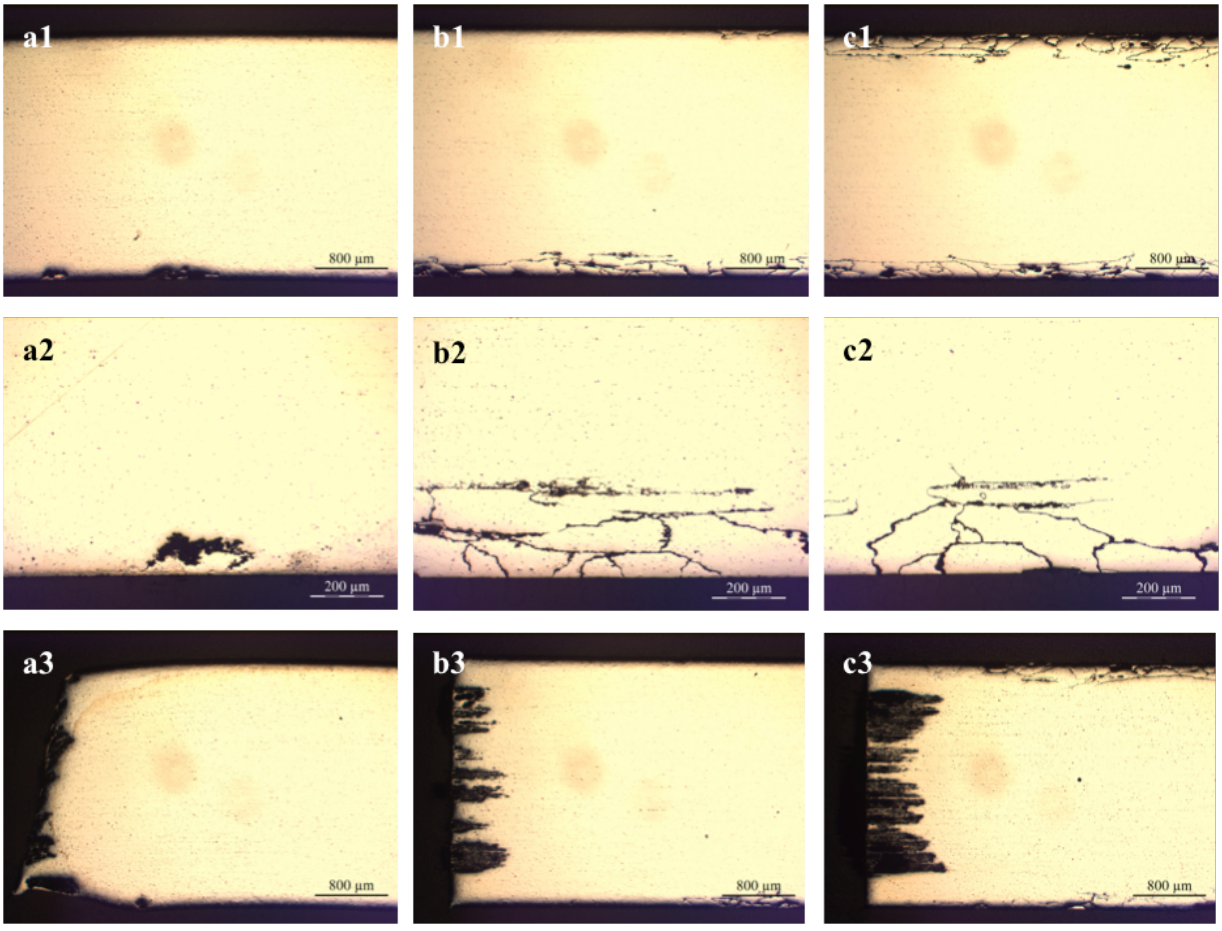

Figure 4.12 Optical micrographs with x25 mag in top row, bottom row and x100 mag in middle row showing WQ profiles in T7 condition with 0.3 wt% Cu and with a) 0 wt% Zn, b) 0.2 wt% Zn and c) 0.6 wt% Zn.

Maximum IGC depth and an average IGC depth are given in Table 4.10 for Zn levels of 0 wt%, 0.2 wt% and 0.6 wt%.

Table 4.10 Average IGC depths, maximum IGC depths and weight loss measurements for water quenched T7 profiles with increasing Zn content.

wt% Zn	Avg IGC depth [μm]	Max IGC depth [μm]	Weight loss [mg/cm^2]
0	116.70	118.70	2.60
0.2	224.90	276.70	2.69
0.6	293.90	325.20	6.54

4.4 Alstruc homogenisation model

Alstruc simulation of precipitation during solidification and changes occurring during homogenisation were conducted for profiles 1a, 2a, 3a and 4a with 0 wt% Zn and Cu levels of 0 wt%, 0.1 wt%, 0.2 wt% and 0.3 wt% respectively. Volume fractions of primary and secondary particles and elements in solid solution are given for all four profiles in Table G - 2, Table G - 4, Table G - 6 and Table G - 8. For Cu levels of 0 wt% and 0.1 wt% a β-AlFeSi primary phase was present after solidification accompanied by α-AlFeSi, Mg_2Si and Si primary particles. The effect of increasing the Cu content to 0.2 wt% and 0.3 wt% was replacement of β-AlFeSi with a AlCuMgSi-phase. The simulation revealed a fairly low contribution of Cu with ~1.1 to 1.4 vol% in α-AlFeSi and a significantly higher contribution of ~22 vol% in the AlCuMgSi-phase formed after solidification. The volume fraction of AlCuMgSi-phase was simulated to increase with raised Cu content in the alloy.

The homogenisation simulation claimed a dissolution of all primary particles except from α-AlFeSi. Additional secondary particles of α-AlFeSi and Mg_2Si were found to nucleate during the homogenisation step. For increased Cu content in the alloy, a smaller volume fraction of secondary α-AlFeSi particles was observed.

5 Discussion

5.1 Microstructure characterisation in optical microscope

Major differences in microstructure appearance of the deformed 6082 profiles after extrusion and subsequent cooling are related to level of recrystallisation compared to fibrousity throughout the sample thickness, depth of recrystallised surface layer, recrystallised grain orientations and size. With no variations in pre-extrusion thermomechanical history and extrusion speed, causes for the observed differences among the optical micrographs in Figure 4.1, Figure A - 1 and Figure A - 2 are partly based on the microstructural effects arising from varied contribution of additional alloying elements Cu and Zn.

In the extrusion parameters overview given in Table 3.2, increased Cu content was found to raise the press force required to maintain the given extrusion speed for 2 out of 3 Zn levels while increasing level of Zn did not seem to have a significant effect on press force. As higher required press force is associated with increased deformation resistance in the alloy, alloying elements giving high solid solution hardening effect are related to the level of press force. Even though Mg and Si have great contributions to solid solution hardening, these elements are held constant in the examined alloys. Zn has a significantly higher solid solubility in Al compared to Cu, but Cu has a greater strengthening potential in solid solution giving Cu a higher solid solution hardening potential in total [59]. Due to Cu and Zn being the only alloying elements to be varied in this study, the difference in solid solution hardening is a reasonable explanation for the increased press force exerted on profiles with increased Cu content. Results of higher force acting on the billet are higher mechanical deformation, dislocation density and thus increased driving force for recrystallisation [26]. This might be the reason for the occurrence of recrystallisated regions in the otherwise fibrous centre part in some of the air cooled profiles with 0.1 wt% Cu and 0.3 wt% Cu as presented when comparing optical micrographs of 0.2 wt% Zn with a) 0 wt% Cu and b) 0.3 wt% Cu in Figure 5.1.

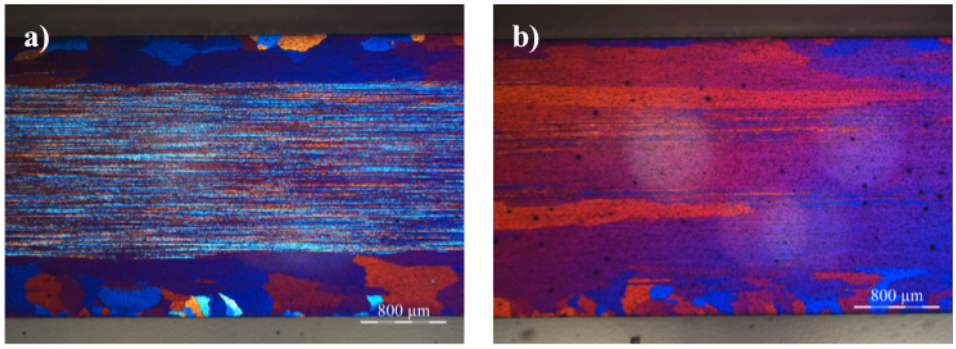

Figure 5.1 Optical micrographs with x25 mag of air cooled extruded profiles with 0 wt% Zn and a) 0 wt% Cu, b) 0.3 wt% Cu

Influences of extrusion air cooling and water quenching on microstructure when alloy composition is held constant have been found to give overall characteristics related to depth of recrystallised layer. As written in section 4.1, all of the examined profiles cooled by air showed averagely deeper recrystallised layers when comparing with the corresponding profiles cooled by water quenching. Some of the AC profiles in Figure 4.1 had additional recrystallisation in the centre region which always appeared fibrous for WQ profiles. An example of thicker recrystallised layer of the AC variant compared to the WQ variant can be seen in Figure 5.2 whereas the AC profile has an average recrystallisation depth of 495.3 µm and 388.4 µm for the WQ profile.

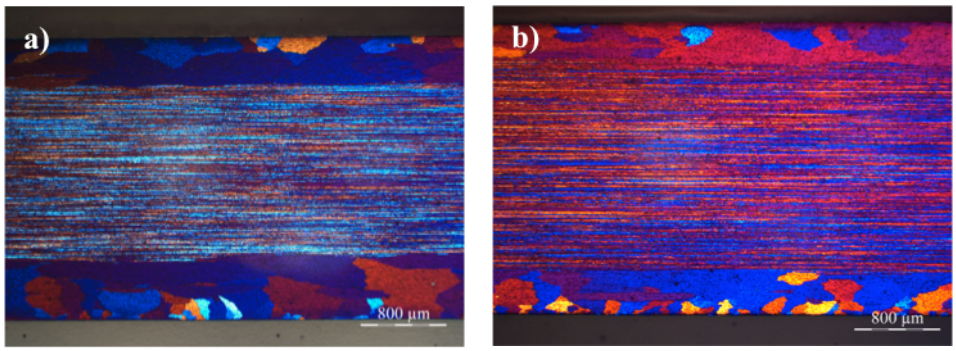

Figure 5.2 Optical micrographs with x25 mag comparing depths of recrystallised layer of profiles with 0.2 wt% Zn, 0 wt% Cu cooled by a) air, b) water

Thicker recrystallised layer and higher fraction of recrystallisation throughout the material thickness are believed to arise from sufficient time for post extrusion static recrystallisation when air cooling is applied [30].

5.2 Mechanical properties

5.2.1 Influence of Cu

In WQ profiles, hardness was found to have a continuous increase as a function of added Cu to the alloy in all tempers, e.g. in peak-aged condition showed in Figure 4.2 b). This behaviour corresponds to the strong influence Cu has on accelerating and enhancing the precipitation kinetics, enhancing the response to artificial ageing by raising the number density of the highly strengthening β'' precipitates and the promotion of reduced grain size [6, 8, 20, 60]. The higher minimum press force required to extrude billets with increased Cu levels as can be seen from the extrusion parameters in Table 3.2 is likely contributing to the observed increase in hardness by generation of more lattice defects and higher dislocation density [26, 28]. The drop in hardness experienced in the vast majority of AC profiles when 0.2 wt% Cu was added as visualised in Figure 4.2 a) may be related to the formation of Cu-containing phases with a hardening potential different from phases being formed with 0 wt% Cu and 0.1 wt% Cu present. Dissolution of precipitates encouraged by 0.2 wt% Cu compared to other levels of Cu contribution might also be an explanation. A third reason for the hardness drop may be caused by inhomogeneous cooling of the extrudate due to the fact that the bar was placed on the floor for slow cooling in air. Certain parts of the profile might have experienced higher cooling rates if touching the floor compared to the parts without direct floor contact.

During ageing in the underaged regime, the effect of increased level of Cu from 0 wt% to 0.3 wt% with both AC and WQ in Figure 5.3 a) and b) when Zn was absent clearly supports the theory concerning the effect of Cu on accelerating precipitation in the early stages of ageing, promoting earlier formation of the more strengthening β'' precipitates compared to the less strengthening GP zones already formed [8]. Stipled lines representing the change in hardness with ageing are steeper when ageing up to 30 min when Cu is present in 0.3 wt% in Figure 5.3 b) compared to no Cu present in Figure 5.3 a). The value in peak-aged condition after 18000 s is also seen to be higher for 0.3 wt% Cu which supports the theory of increased Cu giving higher value of peak hardness [8].

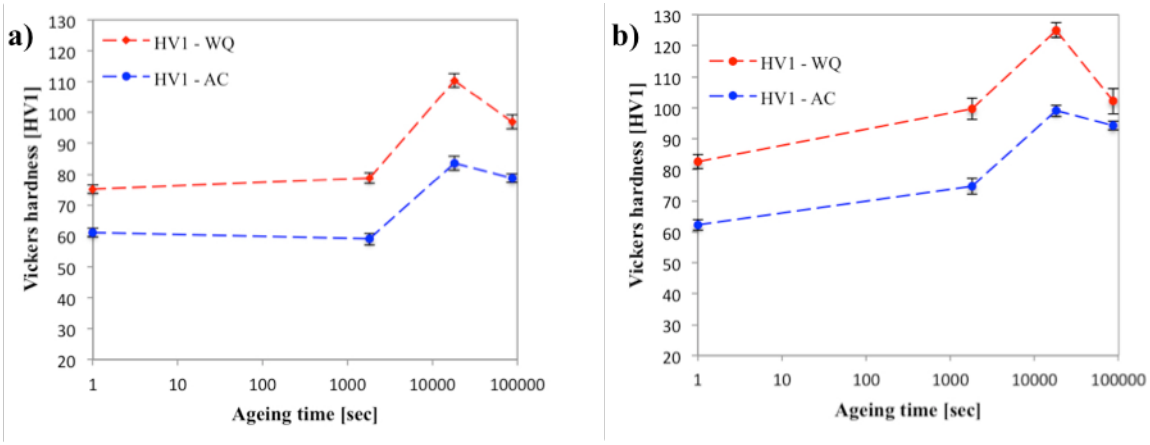

Figure 5.3 Vickers hardness measurements for air cooled and water quenched profiles with no Zn as a function of ageing time with 0 wt% Cu in a) and 0.3 wt% Cu in b).

The trend in electrical conductivity (EC) measurements for both AC and WQ profiles in Figure 5.4 is nearly reciprocal corresponding to the hardness trends seen in Figure 5.3 with identical temper condition. In WQ profiles a nearly stable decrease in EC with increasing amount of Cu is as expected due to the theory saying that addition of solute elements to the aluminium matrix is associated with decreased EC and elements in solid solution will to a greater extent depress conduction of electrons through the matrix [44]. By comparing profiles of minimum and maximum amount of alloying elements in this study in Figure 5.4 a) and b) for all temper conditions, the generally higher values of EC obtained for minimum amount of solutes support the recently mentioned documented effect of alloying elements on electrical conductivity.

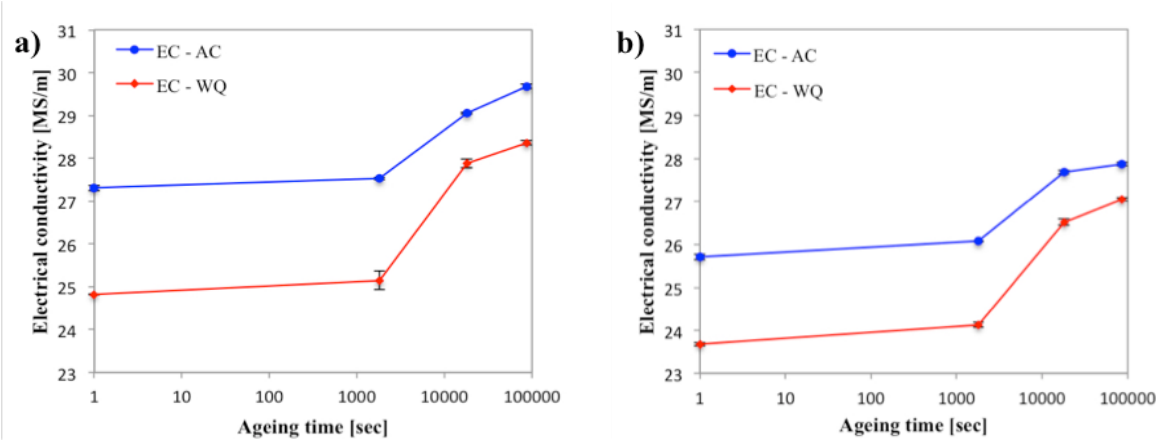

Figure 5.4 Electrical conductivity measurements for air cooled and water quenched profiles with 0 wt% Zn, 0 wt% Cu in a) and 0.6 wt% Zn, 0.3 wt% Cu in b).

With increasing amount of Cu it is assumed that a certain portion will remain in solid solution as Cu-containing precipitates have limits for contribution of Cu. In the AC profile in Figure

4.3 a) it seems that less Cu is in solid solution for 0.2 wt% Cu added compared to 0.1 wt% Cu. Otherwise the profile has more Cu in solid solution for increasing Cu level. A reason for 0.2 wt% Cu addition is deviating from the trend otherwise seen in both the AC and WQ profiles might possibly be the transition from the Q'-phase to the Q-phase with identical chemical composition, but a coarser Q-phase consuming more solute atoms.

5.2.2 Influence of Zn

As presented in section 4.2.1, AC profiles with the highest contribution of Zn (0.6 wt%) have shown to raise the hardness level significantly compared to profiles with low Zn content (0 wt% and 0.2 wt%) when Cu is not present in the alloy. Furthermore, independent of temper and Cu level, profiles with 0 wt% Zn have proved to possess lowest hardness levels. However in WQ profiles such as the example in Figure 4.2 b) the effect of 0.6 wt% Zn on hardness is not that prominent as in the AC version of the alloy in the same temper shown in Figure 4.2 a). This difference is most probably correlated to a decreased supersaturation of Mg and Si atoms caused by precipitation during air cooling, lowering the age hardening potential which further makes the AC alloy rely on other strengthening contributions. When Cu is not present, the increase in Zn might be the main contribution to raise the hardness. Due to the high solid solubility of Zn in Al [48], there is reason to believe that the strengthening from increased level of Zn can partly arise from the high amount of Zn in solid solution, impeding dislocation movements through the aluminium matrix [15]. Moreover, incorporation of Zn atoms in precipitates in small amounts making them disordered and thus promoting increased precipitate density has been suggested as a response to addition of Zn [15].

An addition of 0.6 wt% Zn clearly gives lower electrical conductivity in 7 out of 8 cases for examined alloys in Figure C - 1 when Cu is not present. This discoverage corresponds well to the results obtained by Saito et al. [15] when Zn was added to an Al-Mg-Si alloy and is associated with the high solid solubility of Zn in Al and the fact that any increase in solute elements in the alloy will contribute to lower EC. Even when increasing amount of Cu is added, the maximum contribution of 0.6 wt% Zn gives lower EC than 0 wt% Zn and 0.2 wt% Zn. This further highlights the effect of high Zn level on EC.

5.2.3 Influence of cooling rate

Characteristics were revealed when examining values of HV1 and EC at specific ageing times for AC and WQ profiles of identical alloy compositions given in Figure D - 1, Figure D - 2 and Figure D - 3. The general higher hardness achieved at all tempers and as-extruded condition for the WQ profile compared to the AC profile in the examples showed in Figure 5.3 a) and b) is very likely due to the quench sensitivity from air cooling where Mg-Si particles are tied up during the slow cooling. Reduced supersaturation of Mg and Si atoms will affect the alloy through subsequent heat treatment, reducing the age hardening potential [26, 28, 51].

The difference in electrical conductivity between the AC and WQ variant of alloys with identical alloy composition is observed to be opposite from the difference in hardness, as mentioned in section 4.2.2 and can be seen in Figure 5.4 a) and b). The reason why AC profiles hold a higher EC during all stages of ageing is the same reason why AC profiles give lower hardness. The formation of precipitates during AC has a purification effect on the aluminium matrix, suppressing conduction of electrons [44].

5.2.4 Influence of heat treatment

The overall slower increase in hardness when ageing for only 1800 s (30 min) compared to the more steep increase when approaching peak-ageing at 18000 s (5 h) observed in Figure 5.3 a) and b) reflects the difference in hardening effect from GP zones dominating the early ageing stages and β'' precipitates dominating during peak-ageing with main focus on shape, size and level of coherency of the precipitates. The slight increase in hardness achieved when ageing for 1800 s is mainly due to the internal stress created by growth of highly coherent GP zones in the aluminium matrix, enhancing their coherency strain fields and obstructing dislocation motion. Chemical hardening from the precipitates themselves also contribute to hardness, but to a smaller extent [44]. The level of increase in hardness in early stages of ageing has shown to be strongly dependent on level of Cu added to the alloy, as presented in the comparison of 0 wt% Zn, 0 wt% Cu in Figure 5.3 a) and 0 wt% Zn and 0.3 wt% Cu in Figure 5.3 b).

The significant increase in hardness arising during ageing from 30 min to 5 h as can easily be seen in Figure 5.3 a) is due to the stronger coherency strain fields surrounding β'' precipitates caused by larger mismatch with the lattice in addition to increased number density and fine

precipitate structure when peak-ageing is obtained. The drop in hardness observed after this point is theoretically caused by precipitates becoming incoherent with the matrix. Further growth of incoherent precipitates gives increased particle spacing, requiring lower stress for dislocation bypassing by Orowan looping [40, 41].

Electrical conductivity is increasing as a function of ageing time till 24 h for all tempers examined in this study as seen in Figure D - 1, Figure D - 2 and Figure D - 3. The overall trend of increasing EC can be seen as linear trendlines for the AC and WQ profiles of 0.6 wt% Zn and 0.3 wt% Cu in Figure 5.5 and is partly due to continuous growth of various metastable phases in the precipitation sequence during the entire ageing process.

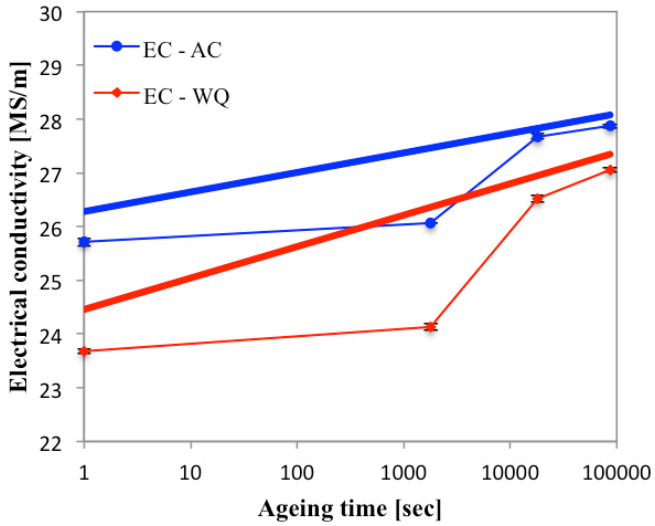

Figure 5.5 A graphical presentation of EC measurements for air cooled (AC) and water quenched (WQ) profiles with 0.6 wt% Zn and 0.3 wt% Cu with belonging linear trendlines as a function of ageing time.

When precipitates grow as ageing time passes, consumption of solutes in the alloy gives a purification effect in the aluminium matrix, encouraging an easier electron flow. However the level of increase in EC is varying during the ageing process as can be observed in the graphical presentations of AC and WQ profiles in Figure 5.5 and is probably related to the rate of growth, level of coherency and electron scattering effect of the different precipitates formed at different ageing times. The overall non-linear correlation between electrical conductivity and hardness as a function of ageing time seen in the examples with minimum alloying elements in Figure 4.4 a) and maximum alloying elements in b) is due to the difference in how well these material properties respond to age hardening. This makes it hard to predict one of these variables based on the result of the other [44].

Early stages of ageing for 1800 s to an underaged condition are characterised by relatively stable values of EC with a slight increase when higher amount of solutes are added. An increased number and size of GP zones are formed in this ageing region which is associated with a reduction in EC due to the prominent electron scattering effect. However, the diffusion of solutes from solid solution to GP zones is rising the ability to conduct electrons, thus lowering the electron scattering effect. The significant increase in EC obtained during ageing from 1800 s (30 min) to 18000 s (5 h) compared to the relatively stable and lower values obtained during early stages of ageing for 1800 s (30 min) is likely caused by the formation of less coherent and needle-shaped β'' precipitates in increasing number density and size with lower electron scattering ability [44]. EC is increasing to a smaller extent in the overaged region in Figure 5.4 a) and b), perhaps due to precipitates becoming less numerous. The significant low scattering effect from incoherent precipitates and the continuous consumption of solutes from the matrix still lead to a steady increase in EC [44].

Ageing time between 30 min and 5 h appears to reduce the difference in EC between the AC and WQ variant of identical alloy composition. When approaching peak-ageing after 5 h, the WQ profile has a higher rate of increase in EC which reduces the EC gap and is probably caused by the higher artificial ageing potential initiated from higher amount of quenched-in vacancies in the supersaturated solid solution. With higher ageing potential follows higher driving force for precipitation which purifies the aluminium matrix to a greater extent. In the early stages of the underaged regime AC and WQ profiles have a higher EC gap due to slower cooling rate provides more time for precipitation during cooling, causing a higher amount of precipitates prior to ageing [15, 26, 28].

5.3 Corrosion behaviour

Corrosion behaviour was examined for profiles with 0.3 wt% Cu and variation in Zn content, cooling rate after extrusion and ageing time at 185°C. The accelerated corrosion test mainly sought to find if the addition of certain Zn levels can possibly reduce the IGC susceptibility theoretically caused by the addition of Cu to an AA6082-alloy introducing an increased potential difference in grain boundary regions by making grain boundaries cathodic. The hypothetical reduction of IGC susceptibility by Zn addition is believed to arise from a reduction of potential differences by making grain boundaries less cathodic in a similar way as the addition of Mg to a Mg-rich alloy [12].

Contrary to previous studies by Svenningsen et al. [10] concerning the presence of a nanoscale Cu-rich film together with Q-precipitates along grain boundaries in Cu-containing Al-Mg-Si alloys causing visible IGC attacks in LM, none of the 6082-profiles with 0.3 wt% Cu and 0 wt% Zn examined in different temper conditions in the current study revealed any IGC attacks of significance in LM. This unanticipated finding might be due to lack of expected Q-phases after extrusion cooling and a Cu-film not sufficient to cause visible IGC alone in the profiles examined in LM. According to the obtained AHM results in Table G - 2, Table G - 4, Table G - 6 and Table G - 8, all Cu-bearing Q-precipitates were dissolved during homogenisation and rather tied up in secondary α-phases. A similar situation might have occurred during extrusion. It is hard to say with high level of certainty if a Cu-film has been formed at all and lowered the IGC resistance in the profiles with 0.3 wt% Cu without further investigation in TEM. Absent IGC attacks with 0.3 wt% Cu and 0 wt% Zn added make it difficult to decide whether the addition of Zn actually lowers the harmful effect of Cu on IGC susceptibility. The test can give indications of how Zn alone, together with cooling rate and temper condition affects IGC behaviour and rate of corrosion by studying changes in IGC appearance in LM and weight loss subsequent to the test.

Given the apparently high IGC resistance of the air cooled profile in as-extruded condition with 0.3 wt% Cu and 0 wt% Zn in Figure 5.6 a1-2) with a measured weight loss of 1.82 mg/cm^2 from the IGC test, increased amount of Zn added to the 6082-profile has without doubt increased the weight loss with a rise to 2.70 mg/cm^2 for 0.2 wt% Zn showed in Figure 5.6 b1-2) and finally a material loss of 10.69 mg/cm^2 for 0.6 wt% Zn in Figure 5.6 c1-2). An overview of corrosion rates for the different alloying compositions, cooling rate and temper conditions is given in Table F - 1. This finding correlates well with earlier studies [55, 61] claiming that addition of Zn to aluminium alloys lowers the open circuit potential of the alloy exposed to a chloride solution by changing the OCP toward a more active direction, promoting uniform corrosion and thereby increasing the weight loss of the material due to corrosion.

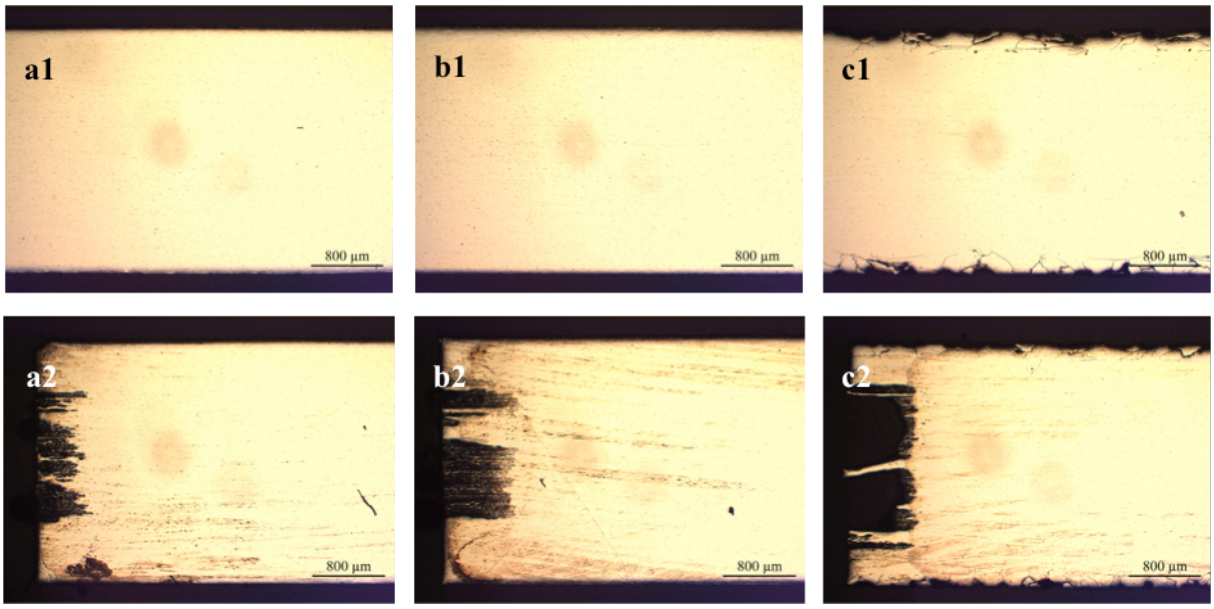

Figure 5.6 Increasing Zn level in air, as-extruded condition.

Occurrence of IGC attacks observed along the entire surface in the air cooled 0.6 wt% Zn profile in Figure 5.6 c1-2) and seen with higher magnification in Figure 4.5 c2) where the maximum IGC depth measured to 284.9 µm might be explained by sufficient time for diffusion of Zn atoms to grain boundaries, creating a Zn-rich film anodic to the adjacent aluminium matrix depleted of Zn. One such film was revealed in TEM by Saito et al. [15] in an Al-Mg-Si alloy with Mg slightly in excess which caused IGC in peak-aged and overaged condition. The study further reported that Zn was required in a level between 0.1 wt% and 1 wt% in order to cause IGC. This finding supports a possible Zn limit somewhere between 0.2 wt% and 0.6 wt%, explaining the high IGC resistance with 0.2 wt% Zn and high IGC susceptibility with 0.6 wt% Zn in the current study, seen when comparing Figure 5.6 b1) and c1). Results from the AHM in the current study indicated 100% of added Zn in solid solution which leaves high amount of Zn available to concentrate along grain boundaries.

Water cooled profiles with 0.3 wt% Cu in as-extruded condition with 0 wt% Zn and 0.2 wt% Zn presented in Figure 4.9 a3) and b3) showed similar but slightly lower loss of material compared to the corresponding air cooled variants in Figure 4.5 a3) and b3). However, a significantly smaller weight loss was observed for the water cooled 0.6 wt% Zn as showed in Figure 5.7 b) with 1.99 mg/cm^2 compared to 10.69 mg/cm^2 for air cooled 0.6 wt% Zn in Figure 5.7 a) in as-extruded condition in addition to non-existing IGC.

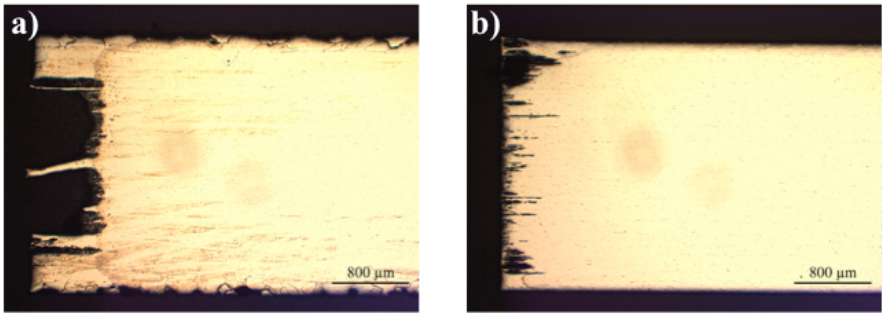

Figure 5.7 Edge corrosion in 0.3 wt% Cu, 0.6 wt% Zn in as-extruded condition with a) air cooling and b) water quenching.

The large difference in weight loss is an interesting finding due to nearly identical amount of Zn in solid solution. One possible explanation might be that air cooling provides sufficient time for Zn atoms to diffuse to surface regions, causing internal galvanic coupling between the Zn-enriched surface and regions just below the surface depleted of Zn, whereas selective dissolution of the more anodic Zn-rich regions occurs when the alloy is exposed to the highly acidic environment. A much more severe edge corrosion developing parallel to extrusion direction in Figure 5.7 a) in contrast to the losely spaced and modest edgde corrosion in Figure 5.7 b) is likely to highly contribute to the measured weight loss difference. The presence of IGC attacks in the air cooled 0.6 wt% Zn variant might be related to air cooling promoting higher fraction of high-angle grain boundaries and thicker recrystallised layer in which Zn atoms might diffuse toward to create microgalvanic cells [26]. By comparing Figure 5.8 a) and b) slightly more randomly oriented grains close to the surface can be observed for the air cooled variant, supporting this theory.

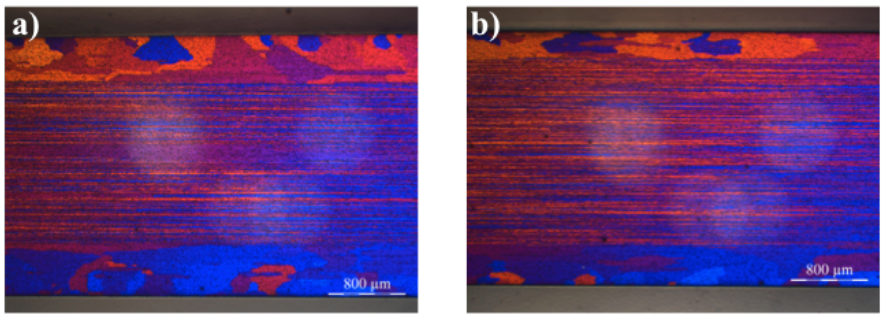

Figure 5.8 Recrystallised layers of 0.3 wt% Cu, 0.6 wt% Zn with a) air cooling and b) water quenching.

When comparing weight loss for the AC and WQ profiles with 0.2 wt% Zn in underaged, peak-aged and overaged condition in Figure 5.9, an overall effect of cooling rate and ageing time was found. Water quenched profiles showed approximately 2 mg/cm^2 higher weight loss

during the IGC test compared to the air cooled profiles in underaged and peak-aged condition, whereas the difference in weight loss and the weight loss itself were smaller for the overaged profiles. Similar observations were made when comparing air cooled and water quenched profiles with 0 wt% Zn.

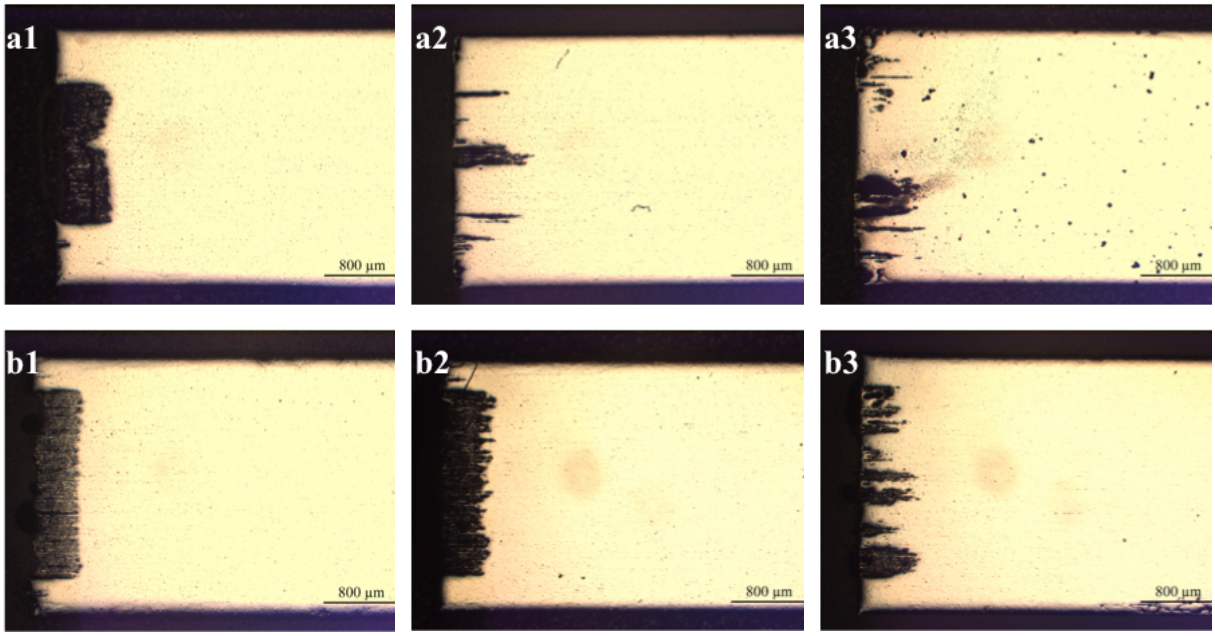

Figure 5.9 Overview of edge corrosion in 0.3 wt% Cu, 0.2 wt% Zn. Temper conditions are 1) T6x, 2) T6, 3) T7 and cooling type is a1-3) air cooling and b1-3) water quenching.

When studying optical micrographs for 0 wt% Zn and 0.2 wt% Zn profiles with no noteworthy IGC attacks or uniform corrosion perpendicular to extrusion direction, it is believed that measured weight loss subsequent to the IGC test is mainly due to corrosion observed parallel to extrusion direction along fibrous centre regions which are imaged in Figure 5.8. A reasonable explanation for both the wider corroded regions in thickness direction and the generally higher amount of corrosion in the centre edge regions for the water quenched profiles is the overall higher volume fraction of fiber texture associated with low angle grain boundaries which gives thinner recrystallised surface layers and less recrystallisation in centre regions *when seen perpendicular to extrusion direction*. When IGC initiates from the edge which is seen as corroded edge regions in Figure 5.9, the low angle grain boundaries posing the fiber texture observed perpendicular to extrusion direction become preferred high angle boundaries *parallel to extrusion direction* for IGC to easily propagate along. The extremely closely spaced grain boundaries at the edge surface leave

high angle grain boundaries highly available and easy accessable for microgalvanic corrosion and is the reason for IGC attacks being hard to separate in edge regions.

An interesting finding for 0.2 wt% Zn profiles in overaged condition seen in Figure 5.10 is the combination of a decline in weight loss combined with increased IGC occurrence compared to underaged and peak-aged condition with IGC depths in the range of 250-280 μm. One possible explanation for the higher frequency of IGC along the surface in overaged condition is the promotion of more prominent PFZs with overageing. As a PFZ is linked to diffusion of solutes to grain boundaries creating microgalvanic cells, higher occurrence of PFZs is directly related to increased IGC susceptibility [10].

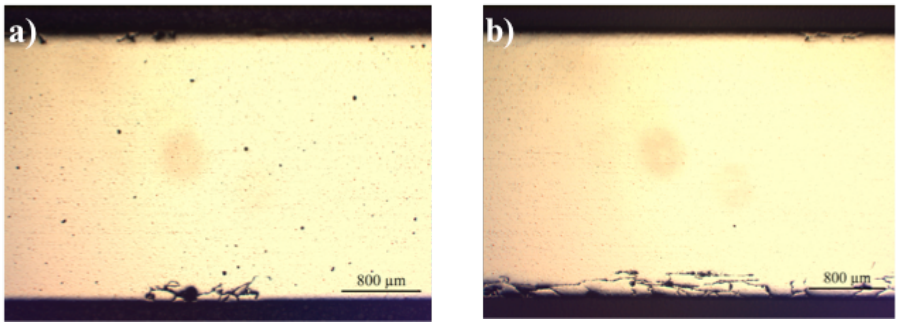

Figure 5.10 Optical micrographs taken perpendicular to extrusion direction showing IGC in surface regions in the 0.3 wt% Cu, 0.2 wt% Zn profile with a) air cooling and b) water quenching.

Air cooled profiles with 0.6 wt% Zn showed in Figure 5.11 a1-3) appear to be less affected by ageing time when comparing with corresponding water quenched profiles in b1-3) being significantly more prone to IGC in the overaged temper. The reduced visible effect of ageing on the air cooled profiles might partly be caused by the high initial level of corrosion of air cooled profiles prior to ageing. If a nanoscale Zn-rich film actually is present along grain boundaries, the film should theoretically be most prominent in peak-aged and overaged condition according to Saito et al. [15]. High concentration of Zn along grain boundaries in these tempers might be one possible reason for the high corrosion occurrence concerning the lowered effect from a possible Cu-film by coarsening and discontinuity during peak-ageing and overageing [10, 26]. Increased presence of IGC and deeper IGC attacks in the water cooled profile in overaged condition viewed in Figure 5.11 b3) are likely caused by the IGC-encouraging effect of overageing with respect to enhancement of PFZs as discussed for the 0.2 wt% Zn profiles above.

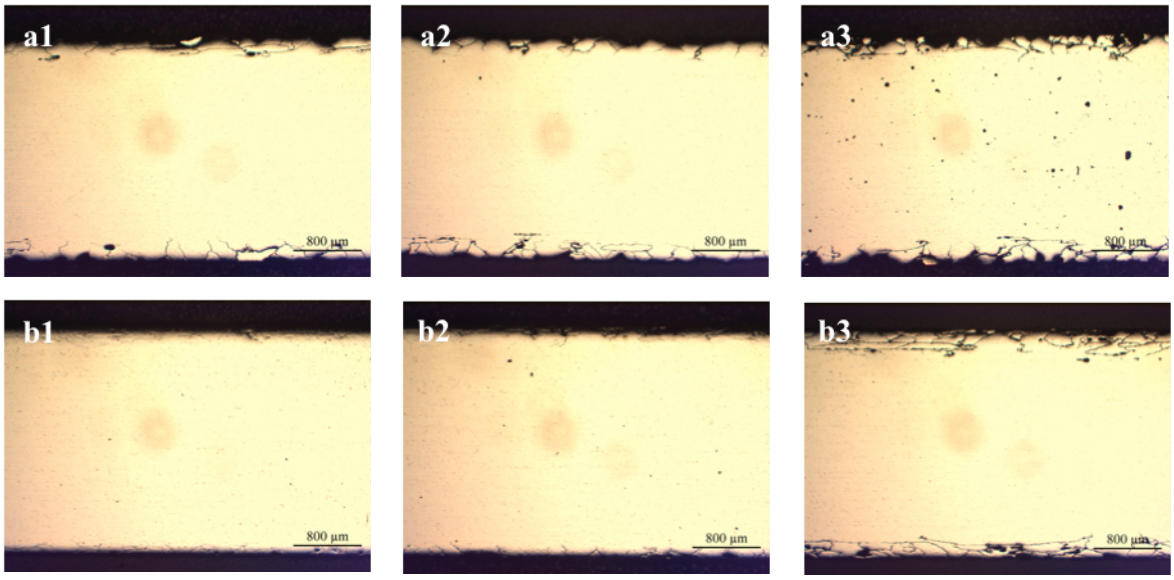

Figure 5.11 Increasing ageing time of profiles with 0.3 wt% Cu and 0.6 wt% Zn with temper conditions T6x in 1), T6 in 2) and T7 in 3). Profiles in a1-3) are air cooled and profiles in b1-3) are water quenched.

5.4 Alstruc homogenisation model

Increased contribution of Cu in the 6082-alloys investigated with the AHM with no Zn present has shown to give a negligible effect on formation of primary α-AlFeSi particles which might be due to the relatively low volume fraction of Cu in these particles. The higher influence of increased level of Cu on the volume fraction of AlCuMgSi-particles formed after solidification is believed to be caused by the high contribution of Cu in the AlCuMgSi-phase with ~22 vol%.

An observed lower volume fraction of secondary α-AlFeSi for 0.1 wt% Cu compared to 0 wt% Cu is likely caused by the reduced amount of β-AlFeSi observed to be present after solidification, hence causing less transformations of β-AlFeSi into α-AlFeSi during homogenisation. When introducing the AlCuMgSi-phase with 0.2 wt% Cu, the further drop in formation of secondary α-AlFeSi particles is assumed to be related to the lack of β-AlFeSi and only a dissolution of AlCuMgSi, not a direct transformation which was the case with β-AlFeSi particles. Moreover, the homogenisation simulation proclaimed that an addition of 0.1 wt% Cu will leave a slightly higher level of Si in solid solution subsequent to homogenisation accompanied by a lower volume fraction of secondary Mg_2Si in comparison to other

investigated Cu levels. These observations might further affect hardness properties as level of Si in solid solution is highly associated with age hardening potential.

5.5 Further work

Through this study, optical light microscope (LM) has been used to examine cross-sections of extruded profiles influenced by variations in level of alloying additions, cooling rate subsequent to extrusion and temper condition.

- Due to magnification limitations in LM, further investigation of grain boundaries on nano level in TEM would be of interest in order to qualitative and quantitative reveal possible grain boundary films when Cu and Zn are added in increasing amounts.
- Measurements of OCP would be helpful to explain differences in weight loss during the accelerated IGC test in addition to providing credible indications toward electrochemical effects of both Cu and Zn.
- By applying GDOES to surface regions of investigated profiles, one might find an explanation for the heavy uniform corrosion found in air cooled profiles with 0.6 wt% Zn by mapping concentration of atoms as a function of distance from the material surface.
- Examination with microprobe might give indications of homogeneous or heterogeneous distribution of chosen elements throughout the investigated profile. Possible segregations of e.g. Cu might be revealed.

6 Conclusion

The main objective of this study was to find if adding Zn to a Cu-containing 6082-alloy could eliminate or reduce the susceptibility toward IGC and maintain satisfactory peak strength. Results obtained from the work conducted on this topic show that adding Zn in 0.2 wt% does not affect corrosion behaviour to a large extent. When increasing the Zn content beyond this level, Zn has shown to negatively affect IGC resistance and weight loss due to corrosion, with weight loss enhanced by air cooling after extrusion and IGC enhanced by overageing. Based on these findings, addition of Zn above 0.2 wt% is not reducing IGC susceptibility in investigated 6082-alloys with Cu additions.

Based on results from hardness measurements obtained for increased alloying contribution of Cu and Zn with variations in cooling rate and ageing time it is concluded that water quenching, ageing to T6 condition and increased level of Cu give higher hardness. Zn did not contribute to raised hardness a large extent. Electrical conductivity measurements revealed lower values with increased addition of Zn whilst values increased with air cooling and artificial ageing time. With these results it can be concluded that mechanical properties are differently affected by influencing variables to various extent in examined 6082-alloys.

According to microstructure examinations, conclusions can be drawn toward averagely deeper recrystallised layers for air cooled profiles compared to water quenched profiles.

References

1. Miller, W., et al., *Recent development in aluminium alloys for the automotive industry.* Materials Science and Engineering: A, 2000. **280**(1): p. 37-49.
2. Miao, W. and D. Laughlin, *Effects of Cu content and preaging on precipitation characteristics in aluminum alloy 6022.* Metallurgical and Materials Transactions A, 2000. **31**(2): p. 361-371.
3. Reiso, O. *Extrusion of AlMgSi alloys*. in *Materials Forum*. 2004.
4. Tercelj, M., et al., *Influence of the chemical composition and process parameters on the mechanical properties of an extruded aluminium alloy for highly loaded structural parts.* Construction and Building Materials, 2013. **44**: p. 781-791.
5. Marioara, C., et al., *Post-β'' phases and their influence on microstructure and hardness in 6xxx Al-Mg-Si alloys.* Journal of materials science, 2006. **41**(2): p. 471-478.
6. Jin, M., J. Li, and G.J. Shao. *Study of Cu addition on precipitation behaviors and mechanical properties in AA6082 Al-Mg-Si alloy*. in *Materials science forum*. 2007. Trans Tech Publ.
7. Liang, W.J., et al., *General aspects related to the corrosion of 6xxx series aluminium alloys: Exploring the influence of Mg/Si ratio and Cu.* Corrosion Science, 2013. **76**: p. 119-128.
8. Murayama, M., et al., *The effect of Cu additions on the precipitation kinetics in an Al-Mg-Si alloy with excess Si.* Metallurgical and materials transactions A, 2001. **32**(2): p. 239-246.
9. Minoda, T. and H. Yoshida, *Effect of grain boundary characteristics on intergranular corrosion resistance of 6061 aluminum alloy extrusion.* Metallurgical and Materials Transactions A, 2002. **33**(9): p. 2891-2898.
10. Svenningsen, G., et al., *Effect of artificial aging on intergranular corrosion of extruded AlMgSi alloy with small Cu content.* Corrosion Science, 2006. **48**(6): p. 1528-1543.
11. Schweitzer, P.A., *Fundamentals of metallic corrosion: atmospheric and media corrosion of metals*. 2006: CRC press.
12. Holmestad, J.M., C. D.; Mathiesen, R. H.; Holmestad, Randi; Walmsley, J. C., *TEM studies of the effect of different Mg/Si-ratios on intergranular corrosion of Al-Mg-Si-Cu alloys.*
13. Marioara, C.D., et al., *Improving Thermal Stability in Cu-Containing Al-Mg-Si Alloys by Precipitate Optimization.* Metallurgical and Materials Transactions A, 2014. **45**(7): p. 2938-2949.
14. Svenningsen, G., et al., *Effect of low copper content and heat treatment on intergranular corrosion of model AlMgSi alloys.* Corrosion science, 2006. **48**(1): p. 226-242.
15. Saito, T., et al., *The effect of Zn on precipitation in Al–Mg–Si alloys.* Philosophical Magazine, 2014. **94**(21): p. 2410-2425.

16. Cayron, C. and P. Buffat, *Transmission electron microscopy study of the< i> β </i> ′ phase (Al–Mg–Si alloys) and QC phase (Al–Cu–Mg–Si alloys): ordering mechanism and crystallographic structure.* Acta Materialia, 2000. **48**(10): p. 2639-2653.
17. Solberg, J.K., *Teknologiske metaller og legeringer*. 2010, Institutt for Materialteknologi, NTNU.
18. Lodgaard, L. and N. Ryum, *Precipitation of dispersoids containing Mn and/or Cr in Al–Mg–Si alloys.* Materials Science and Engineering: A, 2000. **283**(1): p. 144-152.
19. Saito, T., *The Effect of Trace Elements on Precipitation in Al-Mg-Si alloys-A Transmission Electron Microscopy Study.* 2014.
20. Man, J., L. Jing, and S.G. Jie, *The effects of Cu addition on the microstructure and thermal stability of an Al–Mg–Si alloy.* Journal of alloys and Compounds, 2007. **437**(1): p. 146-150.
21. Polmear, I., *Light alloys: from traditional alloys to nanocrystals*. 2005: Butterworth-Heinemann.
22. Birol, Y., *The effect of processing and Mn content on the T5 and T6 properties of AA6082 profiles.* Journal of materials processing technology, 2006. **173**(1): p. 84-91.
23. Aluminium, H., *Extrusion ingot*, in *AlMgSi alloy 608250*. 1991.
24. Lise Dons, A., *The Alstruc homogenization model for industrial aluminum alloys.* Journal of Light Metals, 2001. **1**(2): p. 133-149.
25. Claves, S., D. Elias, and W.Z. Misiolek. *Analysis of the intermetallic phase transformation occurring during homogenization of 6xxx aluminum alloys*. in *Materials Science Forum*. 2002. Trans Tech Publ.
26. Svenningsen, G., et al., *Effect of thermomechanical history on intergranular corrosion of extruded AlMgSi (Cu) model alloy.* Corrosion science, 2006. **48**(12): p. 3969-3987.
27. Krumphals, F., et al., *Comparison of experimental and Finite Element Modelling of the extrusion of AA6082 on both tools and extrudate as a function of process parameters.* International Journal of Material Forming, 2008. **1**(1): p. 427-430.
28. Fjeldbo, S.K., et al., *Through-process sensitivity analysis on the effect of process variables on strength in extruded Al–Mg–Si alloys.* Journal of Materials Processing Technology, 2012. **212**(1): p. 171-180.
29. Amazon. *Aluminium and Aluminium alloys - extrusion*. [cited 2015 May 5th]; Available from: http://www.azom.com/article.aspx?ArticleID=1554.
30. Schikorra, M., et al., *Microstructure analysis of aluminum extrusion: grain size distribution in AA6060, AA6082 and AA7075 alloys.* Journal of mechanical science and technology, 2007. **21**(10): p. 1445-1451.
31. Furu, T., et al. *The influence of the extrusion speed on texture in the surface layer of aluminium profiles investigated by the EBSP technique*. in *Materials Science Forum*. 1994. Trans Tech Publ.
32. Bru, M., *The Effect of Mn and Homogenisation Procedure on Mechanical Properties and Grain Structure in Extruded AA6082*, in *Materials Science and Engineering*. 2014, Norwegian University of Science and Technology (NTNU): Trondheim. p. 83.
33. Nembach, E., *Particle strengthening of metals and alloys*. 1997: John Wiley & Sons, Inc.

34. Mukhopadhyay, A., *Microstructure and properties of high strength aluminium alloys for structural applications.* Transactions of the Indian Institute of Metals, 2009. **62**(2): p. 113-122.
35. Marioara, C., et al., *Atomic model for GP-zones in a 6082 Al–Mg–Si system.* Acta materialia, 2001. **49**(2): p. 321-328.
36. Myhr, O.R., Ø. Grong, and K.O. Pedersen, *A Combined Precipitation, Yield Strength, and Work Hardening Model for Al-Mg-Si Alloys.* Metallurgical and Materials Transactions A, 2010. **41**(9): p. 2276-2289.
37. Edwards, G., et al., *The precipitation sequence in Al–Mg–Si alloys.* Acta Materialia, 1998. **46**(11): p. 3893-3904.
38. Chakrabarti, D., Y. Peng, and D.E. Laughlin. *Precipitation in Al-Mg-Si alloys with Cu additions and the role of the Q'and related phases*. in *Materials Science Forum*. 2002. Citeseer.
39. Chakrabarti, D. and D.E. Laughlin, *Phase relations and precipitation in Al–Mg–Si alloys with Cu additions.* Progress in Materials Science, 2004. **49**(3): p. 389-410.
40. Shercliff, H. and M. Ashby, *A process model for age hardening of aluminium alloys—I. The model.* Acta Metallurgica et Materialia, 1990. **38**(10): p. 1789-1802.
41. Gladman, T., *Precipitation hardening in metals.* Materials Science and Technology, 1999. **15**(1): p. 30-36.
42. Mohamed, A. and F. Samuel, *A Review on the Heat Treatment of Al-Si-Cu/Mg Casting Alloys.* CONVENTIONAL AND NOVEL APPLICATIONS, 2012: p. 229.
43. Sato, T., et al., *Roles of microalloying elements on the cluster formation in the initial stage of phase decomposition of Al-based alloys.* Metallurgical and Materials Transactions A, 2003. **34**(12): p. 2745-2755.
44. Salazar-Guapuriche, M.A., et al. *Correlation of strength with hardness and electrical conductivity for aluminium alloy 7010*. in *Materials science forum*. 2006. Trans Tech Publ.
45. Holmestad, J., et al. *Investigation of grain boundaries in an Al-Mg-Si-Cu Alloy*. in *Materials Science Forum*. 2014. Trans Tech Publ.
46. Dumolt, S., D. Laughlin, and J. Williams, *Formation of a modified β' phase in aluminum alloy 6061.* Scripta metallurgica, 1984. **18**(12): p. 1347-1350.
47. Pashley, D., J. Rhodes, and A. Sendorek, *DELAYED AGEING IN ALUMINIUM-MAGNESIUM-SILICON ALLOYS--EFFECT ON STRUCTURE AND MECHANICAL PROPERTIES.* INST METALS J, 1966. **94**(2): p. 41-49.
48. Morgan, S.W.K., *Zinc and its alloys and compounds*. 1985: E. Horwood.
49. Skoko, Ž., S. Popović, and G. Štefanić, *Microstructure of Al-Zn and Zn-Al alloys.* Croat. Chem. Acta, 2009. **82**(2): p. 405-420.
50. Berg, L., et al., *GP-zones in Al–Zn–Mg alloys and their role in artificial aging.* Acta materialia, 2001. **49**(17): p. 3443-3451.
51. Strobel, K., et al. *The Effect of Natural Aging on Quench Sensitivity in Al‐Mg‐Si Alloys*. in *ICAA13: 13th International Conference on Aluminum Alloys*. Wiley Online Library.
52. Evancho, J. and J. Staley, *Kinetics of precipitation in aluminum alloys during continuous cooling.* Metallurgical Transactions, 1974. **5**(1): p. 43-47.
53. Oldfield, J.W., *Electrochemical theory of galvanic corrosion.* Galvanic Corrosion, 1988: p. 5-22.
54. Svenningsen, G., et al., *Effect of high temperature heat treatment on intergranular corrosion of AlMgSi(Cu) model alloy.* Corros. Sci., 2006. **48**(1): p. 258-272.

55. Muller, I.L. and J.R. Galvele, *Pitting potential of high purity binary aluminium alloys—II. Al Mg and Al Zn alloys.* Corrosion Science, 1977. **17**(12): p. 995-1007.
56. Larsen, M.H., et al., *Intergranular corrosion of copper-containing AA6xxx AlMgSi aluminum alloys.* Journal of the Electrochemical Society, 2008. **155**(11): p. C550-C556.
57. Holme, B.r., et al., *Preferential grain etching of AlMgSi (Zn) model alloys.* Journal of The Electrochemical Society, 2010. **157**(12): p. C424-C427.
58. Institution, B.S., *International Standard 11846*, in *Corrosion of metals and alloys - Determination of resistance to intergranular corrosion of solution heat-treatable aluminium alloys*. 1995.
59. Ma, D., et al., *Ab initio identified design principles of solid-solution strengthening in Al.* Science and Technology of Advanced Materials, 2013. **14**(2): p. 025001.
60. Meng, Q. and G. Frankel, *Effect of Cu content on corrosion behavior of 7xxx series aluminum alloys.* Journal of The Electrochemical Society, 2004. **151**(5): p. B271-B283.
61. Cramer, S.D., B.S. Covino Jr, and C. Moosbrugger, *ASM Handbook Volume 13b: Corrosion: Materials*. 2005: ASM International.

Appendix A) Microstructures in LM

A-1) 0 wt% Zn

Optical micrographs of profiles with 0 wt% Zn are given in Figure A - 1.

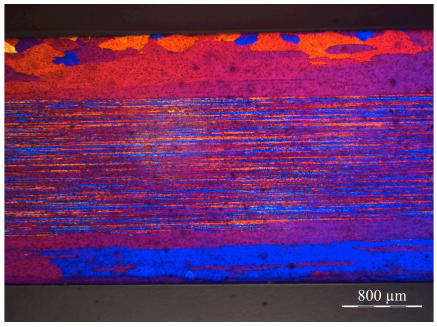

a) 0% Zn, 0% Cu, AC

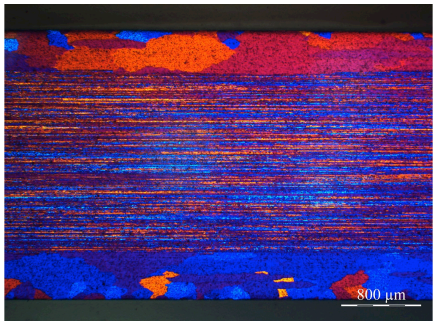

b) 0% Zn, 0% Cu, WQ

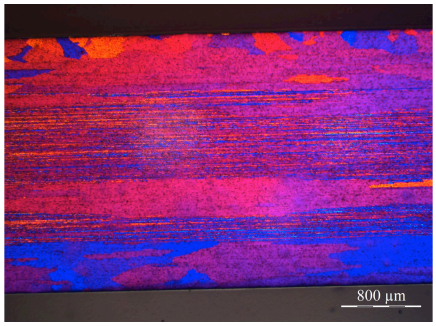

c) 0% Zn, 0.1% Cu, AC

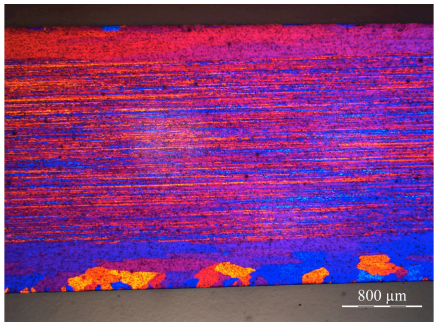

d) 0% Zn, 0.1% Cu, WQ

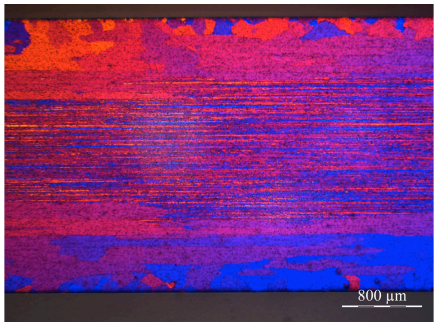

e) 0% Zn, 0.2% Cu, AC

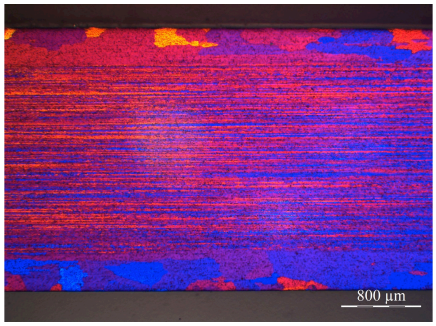

f) 0% Zn, 0.2% Cu, WQ

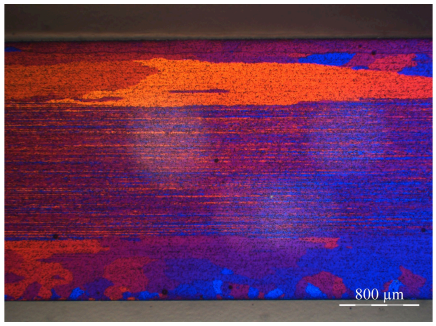

g) 0% Zn, 0.3% Cu, AC

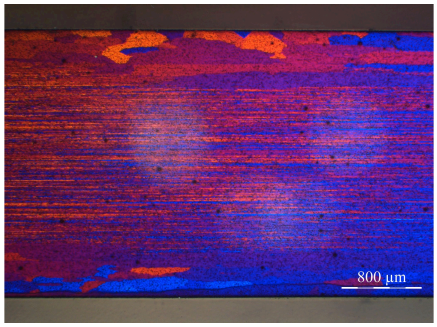

h) 0% Zn, 0.3% Cu, WQ

Figure A - 1 Optical micrographs showing profiles with 0 wt% Zn and increasing wt% Cu. AC = air cooling, WQ = water quenching.

A-2) 0.6 wt% Zn

Optical micrographs of profiles with 0.6 wt% Zn are given in Figure A - 2.

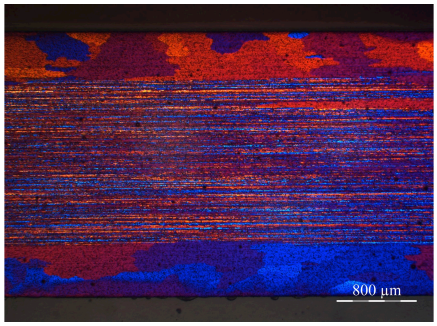

a) 0.6% Zn, 0% Cu, AC

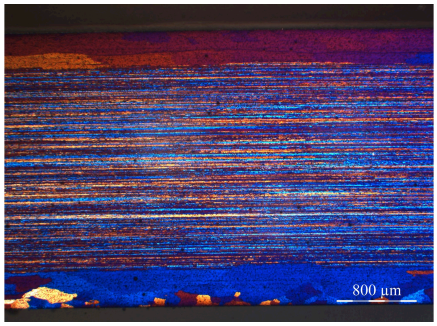

b) 0.6% Zn, 0% Cu, WQ

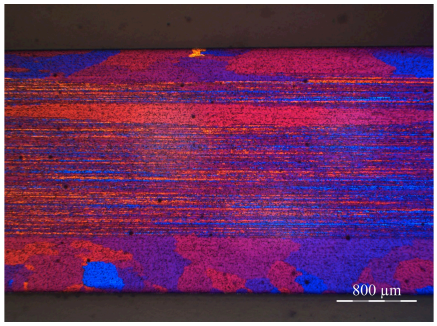

c) 0.6% Zn, 0.1% Cu, AC

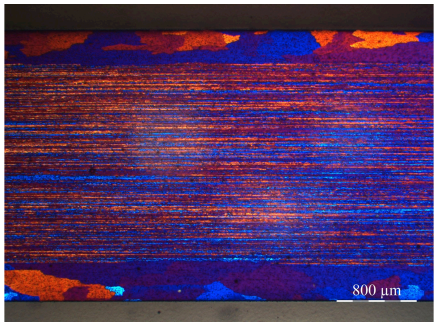

d) 0.6% Zn, 0.1% Cu, WQ

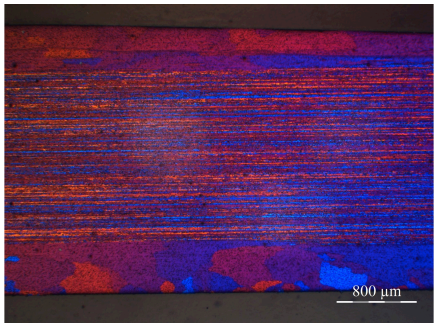

e) 0.6% Zn, 0.2% Cu, AC

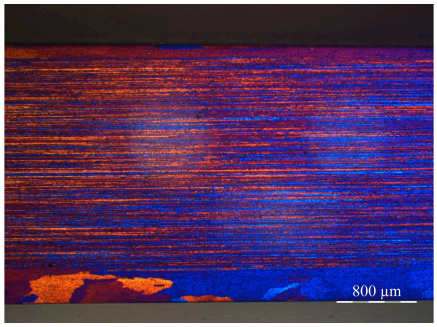

f) 0.6% Zn, 0.2% Cu, WQ

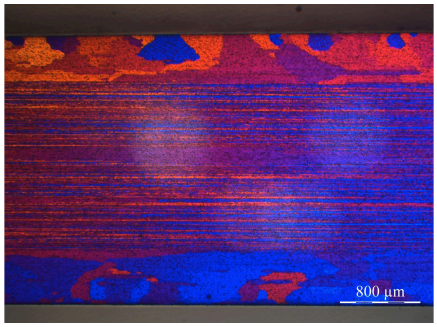

g) 0.6% Zn, 0.3% Cu, AC

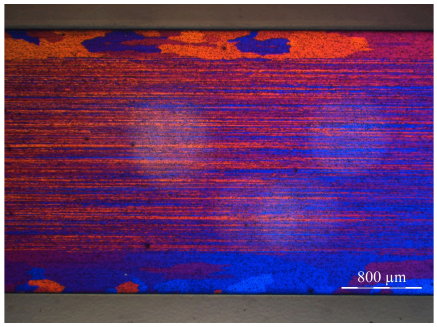

h) 0.6% Zn, 0.3% Cu, WQ

Figure A - 2 Optical micrographs showing profiles with 0.6 wt% Zn and increasing wt% Cu. AC = air cooling, WQ = water quenching.

A-3) Recrystallised surface layers

Depths of recrystallised surface layers were measured for all 24 profiles (12 AC and 12 WQ) when examined in LM. Measurements at random locations along the surface and calculated average depths are shown for air cooled profiles in Table A – 1 and for water quenched profiles in Table A - 2.

Table A – 1 Depths of recrystallised layers for air cooled profiles measured in LM.

	Measurements [μm]					Average [μm]
1a	607.2	619.7	656.9	397.9	489.1	554.2
2a	493.2	532.6	487.0	644.5	625.9	556.6
3a	607.2	590.6	729.5	696.3	775.1	679.7
4a	536.7	484.9	669.4	644.5	493.2	565.7
1b	503.6	538.8	460.1	462.1	511.9	495.3
2b	601.0	586.5	569.9	588.6	559.5	581.1
3b	455.9	433.1	329.5	294.4	288.1	360.2
4b	665.2	656.9	831.0	773.0	839.3	753.1
1c	462.1	563.7	433.1	505.7	524.3	497.8
2c	416.6	358.5	547.1	536.7	416.5	455.1
3c	476.7	474.6	470.4	520.2	493.2	487.0
4c	536.7	478.7	524.3	489.1	451.8	496.1

Table A - 2 Depths of recrystallised layers for water quenched profiles measured in LM.

	Measurements [μm]					Average [μm]
1a	404.1	393.8	478.7	472.5	420.7	434.0
2a	480.8	435.2	368.9	505.7	424.8	443.1
3a	447.6	412.4	422.8	381.3	368.9	406.6
4a	526.4	563.7	495.3	538.8	453.9	515.6
1b	418.6	383.4	352.3	379.2	408.3	388.4
2b	373.0	364.7	362.7	410.3	366.8	375.5
3b	263.2	259.1	240.4	232.1	248.7	248.7
4b	410.3	385.5	375.1	455.9	387.6	402.9
1c	395.8	368.9	362.7	337.8	377.2	368.5
2c	315.0	302.6	339.9	346.1	327.4	326.2
3c	321.2	364.8	362.7	364.7	346.1	351.9
4c	279.8	302.6	290.1	294.3	271.5	287.7

Appendix B) Vickers hardness

Vickers hardness measurements based on average values are graphically presented in Figure B - 1 with three Zn levels as a function of increasing Cu content for both air cooled (AC) and water quenched (WQ) cooling type in as-extruded, underaged, peak-aged and overaged condition.

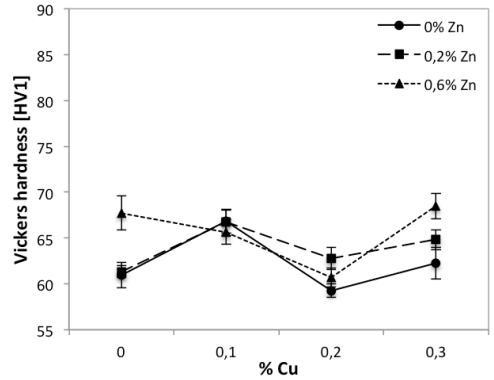

a) As-extruded, AC

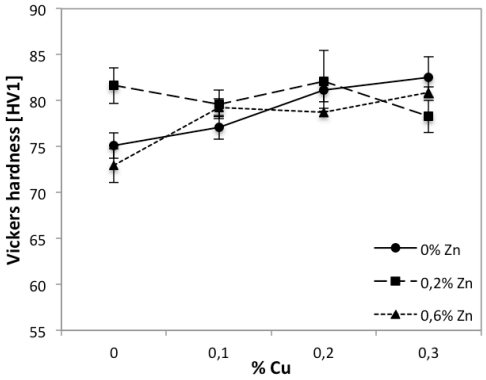

b) As-extruded, WQ

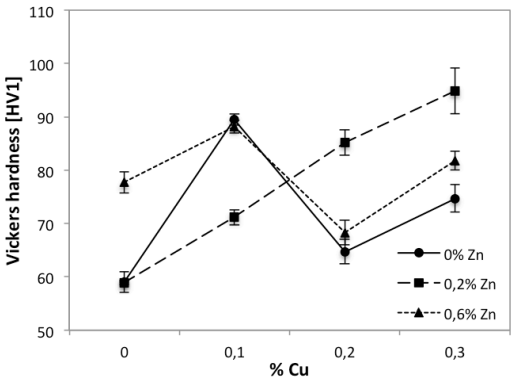

c) T6x, AC

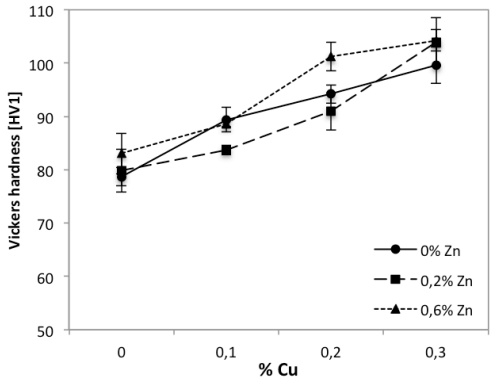

d) T6x, WQ

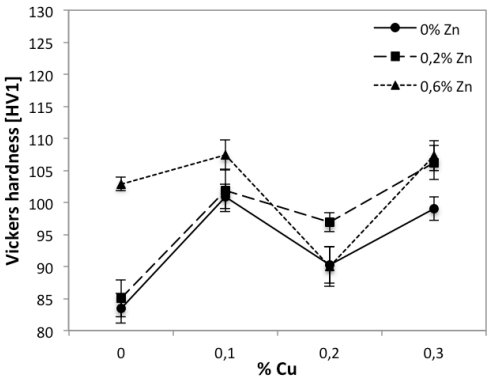

e) T6, AC

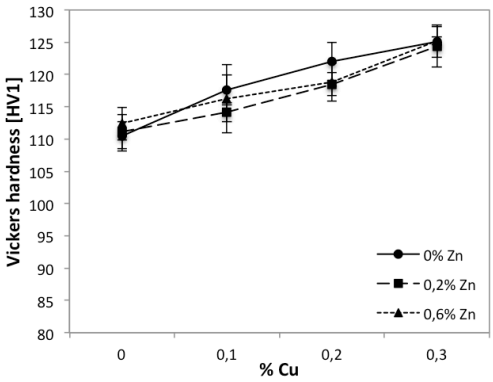

f) T6, WQ

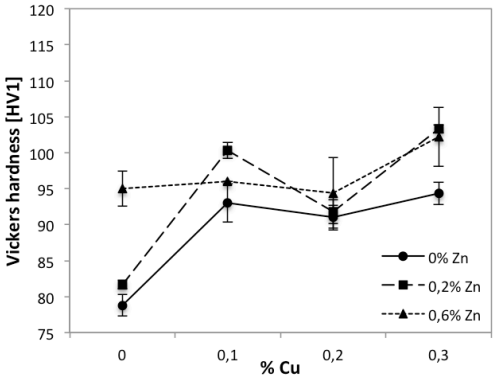

g) T7, AC

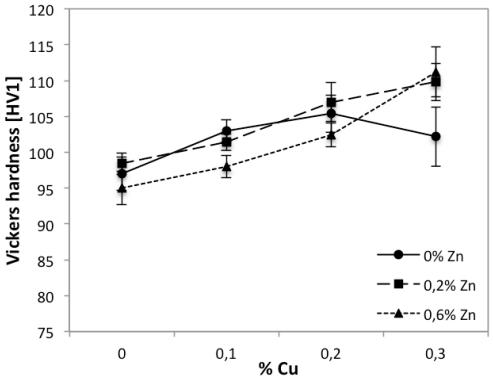

h) T7, WQ

Figure B - 1 Vickers hardness measurements for various alloy compositions and temper conditions.

Appendix C) Electrical conductivity

Electrical conductivity measurements based on average values are graphically presented in Figure C - 1 with three Zn levels as a function of increasing Cu content for both air cooled (AC) and water quenched (WQ) cooling type in as-extruded, underaged, peak-aged and overaged condition.

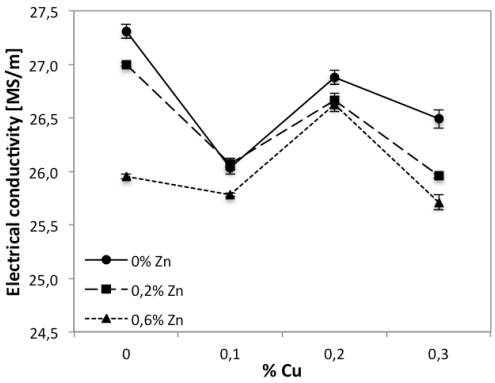

a) As-extruded, AC

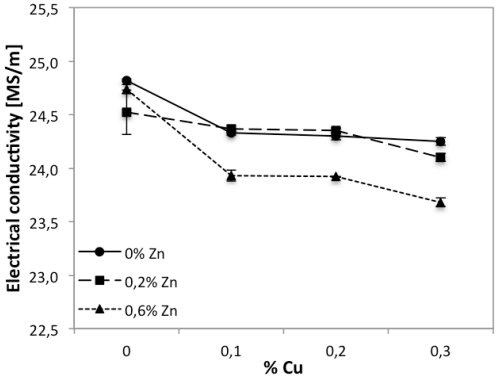

b) As-extruded, WQ

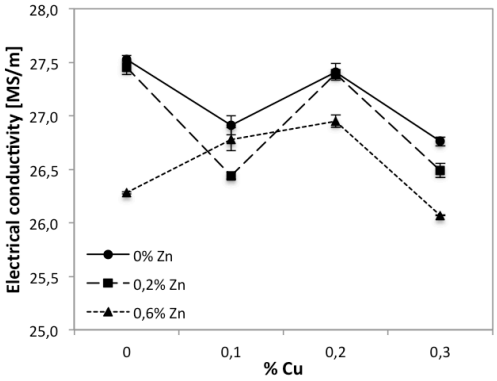

c) T6x, AC

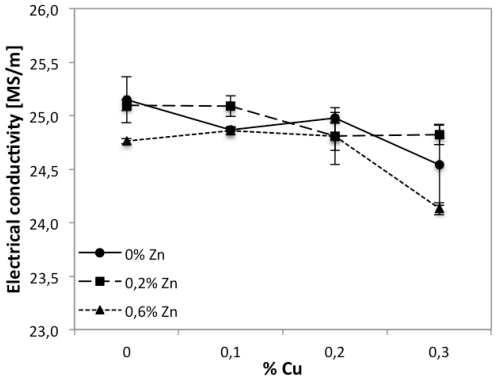

d) T6x, WQ

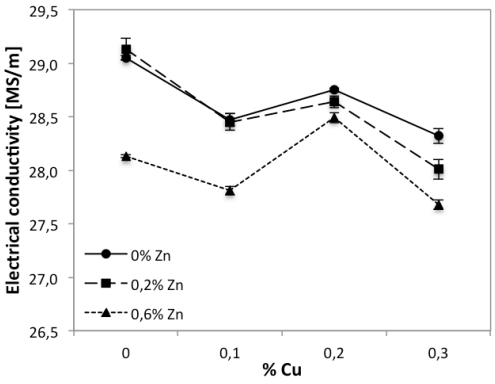

e) T6, AC

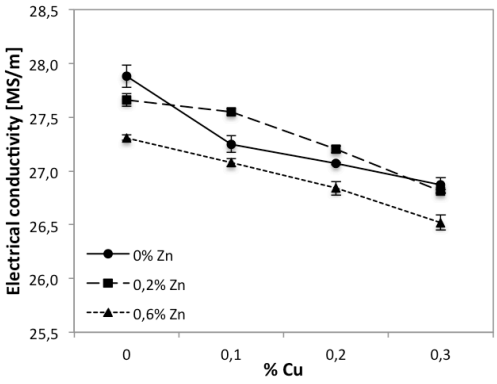

f) T6, WQ

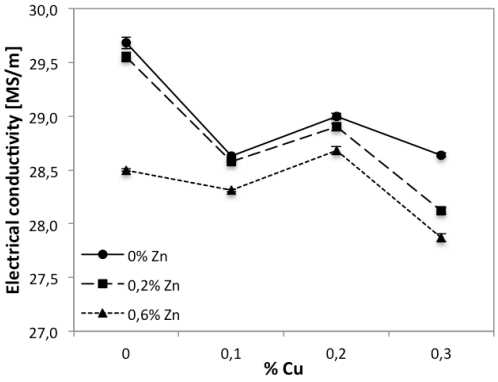

g) T7, AC

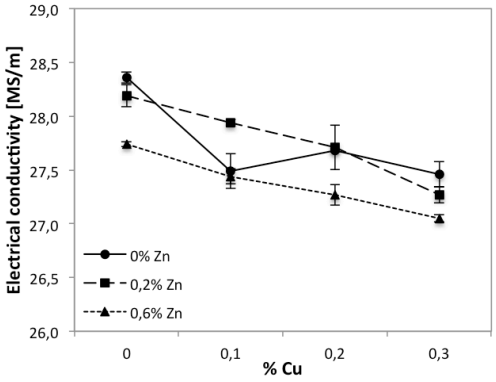

h) T7, WQ

Figure C - 1 Electrical conductivity measurements for various alloy compositions and temper conditions.

Appendix D) HV1 and EC combined as a function of ageing time

D-1) 0 wt% Zn

Vickers hardness and electrical conductivity measurements combined as a function of ageing time are showed in Figure D - 1 for both air cooled and water cooled profiles with 0 wt% Zn and increasing Cu level.

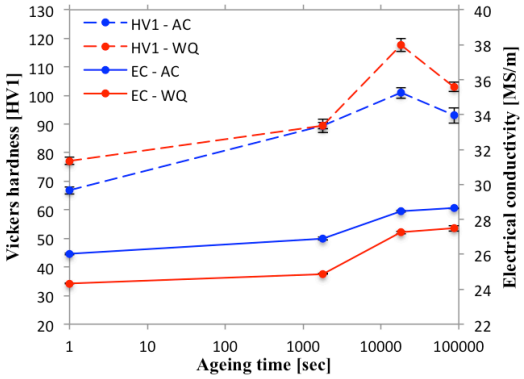

a) 0 wt% Zn, 0.1 wt% Cu

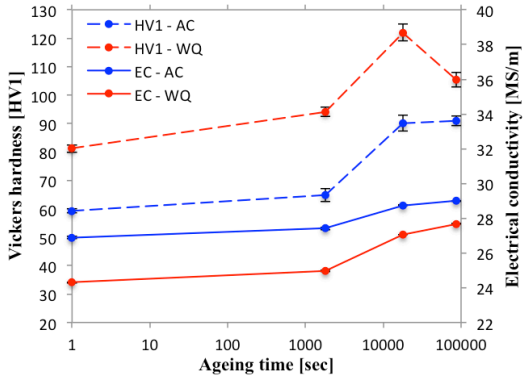

b) 0 wt% Zn, 0.2 wt% Cu

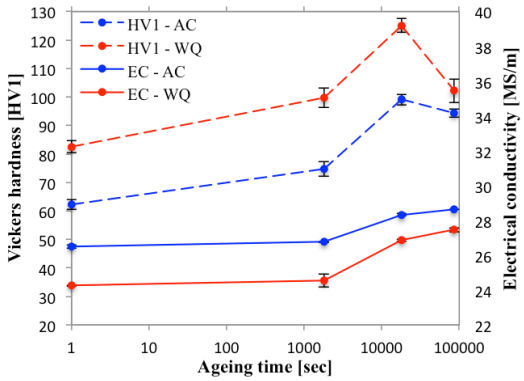

c) 0 wt% Zn, 0.3 wt% Cu

Figure D - 1 Difference in HV1 and EC for air cooled and water cooled profiles with 0 wt% Zn and increasing Cu content as a function of ageing time.

D-2) 0.2 wt% Zn

Vickers hardness and electrical conductivity measurements combined as a function of ageing time are showed in Figure D - 2 for both air cooled and water cooled profiles with 0.2 wt% Zn and increasing Cu level.

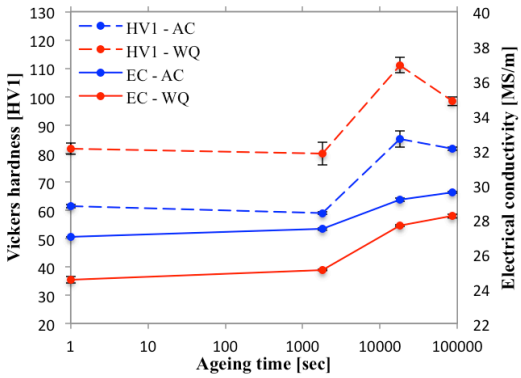

a) 0.2 wt% Zn, 0 wt% Cu

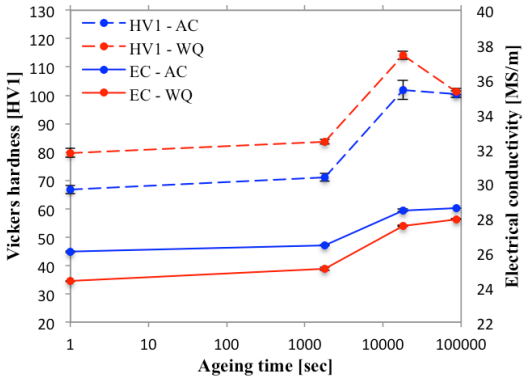

b) 0.2 wt% Zn, 0.1 wt% Cu

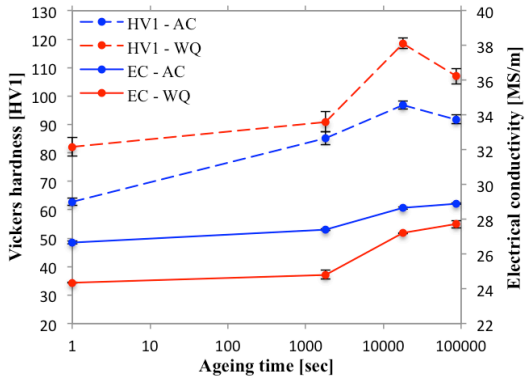

c) 0.2 wt% Zn, 0.2 wt% Cu

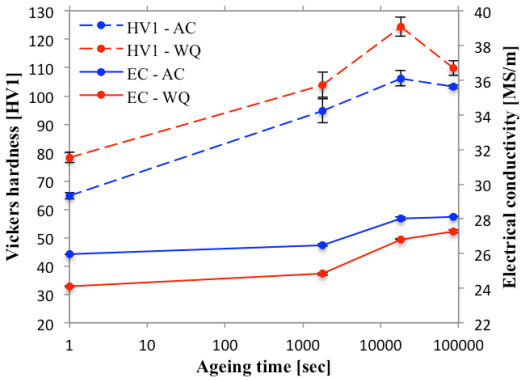

d) 0.2 wt% Zn, 0.3 wt% Cu

Figure D - 2 Difference in HV1 and EC for air cooled and water cooled profiles with 0.2 wt% Zn and increasing Cu content as a function of ageing time.

D-3) 0.6 wt% Zn

Vickers hardness and electrical conductivity measurements combined as a function of ageing time are showed in Figure D - 3 for both air cooled and water cooled profiles with 0.6 wt% Zn and increasing Cu level.

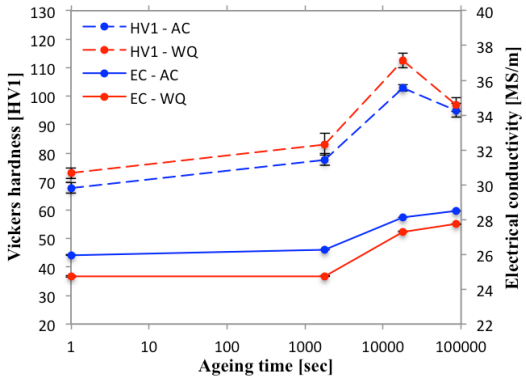

a) 0.6 wt% Zn, 0 wt% Cu

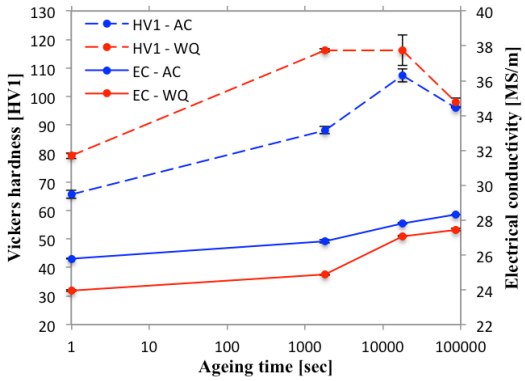

b) 0.6 wt% Zn, 0.1 wt% Cu

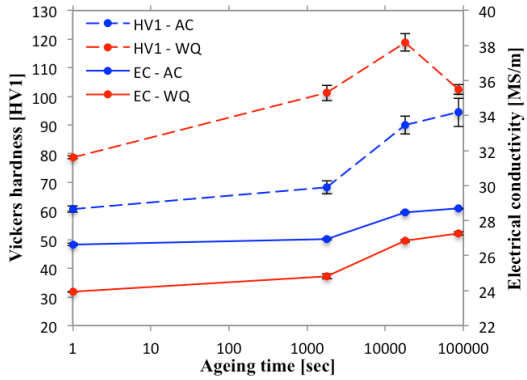

c) 0.6 wt% Zn, 0.2 wt% Cu

Figure D - 3 Difference in HV1 and EC for air cooled and water cooled profiles with 0.6 wt% Zn and increasing Cu content as a function of ageing time.

Appendix E) HV1 and EC values

E-1) 0 wt% Zn

Average values and standard deviations from vickers hardness and electrical conductivity measurements are listed in Table E - 1 for 0 wt% Zn and increasing Cu content. Each average value of HV1 is based on five measurements and three for EC average values.

Table E - 1 HV1 and EC average and standard deviation values for AC and WQ profiles with 0 wt% Zn and increasing Cu content.

		Vickers hardness [HV1]				Electrical conductivity [MS/m]			
		AC		WQ		AC		WQ	
		Avg	Stdev	Avg	Stdev	Avg	Stdev	Avg	Stdev
1a	AE	60.98	1.40	75.12	1.40	27.31	0.07	24.82	0.01
	T6x	58.98	1.95	78.72	1.76	27.53	0.03	25.15	0.22
	T6	83.46	2.29	110.42	2.27	29.05	0.02	27.88	0.10
	T7	78.80	1.48	97.00	2.35	29.68	0.05	28.36	0.05
2a	AE	66.82	1.27	77.12	1.31	26.03	0.06	24.33	0.02
	T6x	89.44	1.04	89.42	2.37	26.91	0.09	24.87	0.02
	T6	100.92	1.87	117.62	2.32	28.47	0.06	27.25	0.08
	T7	93.00	2.65	103.00	1.58	28.63	0.02	27.49	0.16
3a	AE	59.26	0.71	81.18	1.30	26.88	0.07	24.30	0.04
	T6x	64.72	2.27	94.20	1.70	27.41	0.08	24.98	0.05
	T6	90.20	2.83	122.02	2.94	28.75	0.02	27.07	0.01
	T7	91.00	1.73	105.40	2.61	29.00	0.03	27.68	0.02
4a	AE	62.26	1.72	82.56	2.25	26.49	0.09	24.25	0.04
	T6x	74.70	2.54	99.64	3.42	26.76	0.04	24.54	0.38
	T6	99.04	1.83	125.06	2.38	28.32	0.07	26.87	0.07
	T7	94.33	1.53	102.20	4.15	28.64	0.02	27.46	0.12

E-2) 0.2 wt% Zn

Average values and standard deviations from vickers hardness and electrical conductivity measurements are listed in Table E - 2 for 0.2 wt% Zn and increasing Cu content. Each average value of HV1 is based on five measurements and three for EC average values.

Table E - 2 HV1 and EC average and standard deviation values for AC and WQ profiles with 0.2 wt% Zn and increasing Cu content.

		Vickers hardness [HV1]				Electrical conductivity [MS/m]			
		AC		WQ		AC		WQ	
		Avg	Stdev	Avg	Stdev	Avg	Stdev	Avg	Stdev
1b	AE	61.34	0.67	81.64	1.93	27.00	0.02	24.52	0.21
	T6x	58.94	0.43	79.88	4.04	27.45	0.07	25.10	0.05
	T6	85.02	2.86	111.14	2.69	29.13	0.10	27.66	0.06
	T7	81.67	0.58	98.40	1.52	29.55	0.05	28.19	0.10
2b	AE	66.72	1.43	79.62	1.58	26.07	0.06	24.37	0.03
	T6x	71.16	1.42	83.70	0.85	26.44	0.04	25.09	0.10
	T6	101.88	3.31	114.14	1.51	28.45	0.08	27.55	0.03
	T7	100.33	1.15	101.40	1.14	28.58	0.01	27.94	0.03
3b	AE	62.80	1.23	82.14	3.29	26.66	0.07	24.35	0.03
	T6x	85.18	2.37	90.96	3.49	27.39	0.04	24.81	0.27
	T6	96.90	1.45	118.52	1.79	28.64	0.06	27.20	0.03
	T7	91.80	1.64	107.00	2.74	28.90	0.03	27.71	0.21
4b	AE	64.82	1.11	78.30	1.76	25.96	0.03	24.10	0.04
	T6x	94.84	4.26	103.98	4.52	26.49	0.07	24.82	0.09
	T6	106.22	2.68	124.42	3.31	28.01	0.09	26.81	0.02
	T7	103.33	0.58	109.80	2.59	28.12	0.03	27.27	0.08

E-3) 0.6 wt% Zn

Average values and standard deviations from vickers hardness and electrical conductivity measurements are listed in Table E - 3 for 0.6 wt% Zn and increasing Cu content. Each average value of HV1 is based on five measurements and three for EC average values.

Table E - 3 HV1 and EC average and standard deviation values for AC and WQ profiles with 0.6 wt% Zn and increasing Cu content.

		Vickers hardness [HV1]				Electrical conductivity [MS/m]			
		AC		WQ		AC		WQ	
		Avg	Stdev	Avg	Stdev	Avg	Stdev	Avg	Stdev
1c	AE	67.74	1.88	72.92	1.82	25.95	0.02	24.74	0.04
	T6x	77.74	2.01	83.04	3.80	26.28	0.01	24.76	0.02
	T6	102.90	1.09	112.40	2.54	28.13	0.01	27.31	0.02
	T7	95.00	2.45	97.00	2.35	28.50	0.01	27.74	0.02
2c	AE	65.64	1.34	79.22	0.96	25.78	0.02	23.93	0.05
	T6x	88.18	1.21	116.20	0.55	26.78	0.11	24.86	0.04
	T6	107.40	2.37	116.20	5.28	27.81	0.04	27.08	0.04
	T7	96.00	0.00	98.00	1.58	28.31	0.01	27.44	0.07
3c	AE	60.68	1.05	78.72	0.47	26.63	0.07	23.92	0.01
	T6x	68.32	2.31	101.24	2.69	26.95	0.06	24.81	0.13
	T6	89.98	3.10	118.84	2.99	28.49	0.05	26.84	0.06
	T7	94.40	4.88	102.40	1.67	28.68	0.04	27.27	0.10
4c	AE	68.50	1.41	80.92	0.58	25.71	0.07	23.68	0.04
	T6x	81.78	1.73	104.26	2.03	26.07	0.01	24.13	0.06
	T6	107.28	2.31	125.26	0.63	27.68	0.05	26.52	0.07
	T7	102.20	4.09	111.20	3.49	27.87	0.04	27.05	0.04

Appendix F) IGC test

Weight loss due to corrosion during the accelerated IGC test is given in Table F - 1 for investigated 6082-profiles with 0.3 wt% Cu and increasing level of Zn in both air cooled (WC) and water quenched (WQ) condition and in temper conditions AE (as-extruded), T6x, T6 and T7. Area of exposure for each profile was 40.44 cm^2. Weight loss is rather given as mg/cm^2 instead of $mg/40.44cm^2$.

Table F - 1 Weight loss per cm^2 exposed material during the accelerated IGC test.

	AE [mg/cm^2]	T6x [mg/cm^2]	T6 [mg/cm^2]	T7 [mg/cm^2]
0 wt% Zn, AC	1.82	3.84	3.02	2.28
0.2 wt% Zn, AC	2.70	3.18	3.27	2.28
0.6 wt% Zn, AC	10.69	11.50	12.98	10.33
0 wt% Zn, WQ	1.76	4.92	5.07	2.60
0.2 wt% Zn, WQ	1.59	5.30	4.89	2.69
0.6 wt% Zn, WQ	1.99	6.71	7.26	6.54

Appendix G) Alstruc homogenisation model

G-1) 0 wt% Cu

Initial levels of alloying elements relevant for Alstruc simulation for profile 1a with 0 wt% Cu, 0 wt% Zn are given in Table G - 1. Results from Alstruc simulation model are given in Table G - 2.

Table G - 1 Initial levels of alloying elements added to profile 1a relevant for Alstruc simulation.

Element	Fe	Si	Mn	Mg	Cu
wt%	0.19	1.04	0.54	0.67	0.00

Table G - 2 Vol% precipitates and dispersoids in addition to wt% of alloying elements in solid solution are simulated for the 6082-profile with 0 wt% Cu, 0 wt% Zn after solidification and after homogenisation.

After solidification, initial 0 wt% Cu

	Solid solution [wt%]	α-AlFeSi [vol%]	β-AlFeSi [vol%]	Mg_2Si [vol%]	Si [vol%]
Primary		0.830	0.007	0.359	0.372
Fe	0.010				
Si	0.550				
Mn	0.380				
Mg	0.510				
Cu	0.000				

After homogenisation

	Solid solution [wt%]	α-AlFeSi [vol%]	β-AlFeSi [vol%]	Mg_2Si [vol%]	Si [vol%]
Primary		0.840			
Secondary		0.610		0.006	
Fe	0.000				
Si	0.890				
Mn	0.140				
Mg	0.670				
Cu	0.000				

G-2) 0.1 wt% Cu

Initial levels of alloying elements relevant for Alstruc simulation for profile 2a with 0.1 wt% Cu, 0 wt% Zn are given in Table G - 3. Results from Alstruc simulation model for 0.2 wt% Cu, 0 wt% Zn are given in Table G - 4.

Table G - 3 Initial levels of alloying elements added to profile 2a relevant for Alstruc simulation.

Element	Fe	Si	Mn	Mg	Cu
wt%	0.20	1.07	0.55	0.68	0.10

Table G - 4 Vol% precipitates and dispersoids in addition to wt% of alloying elements in solid solution are simulated for the 6082-profile with 0.1 wt% Cu, 0 wt% Zn after solidification and after homogenisation.

After solidification, initial 0.1 wt% Cu

	Solid solution [wt%]	α-AlFeSi [vol%]	β-AlFeSi [vol%]	Mg_2Si [vol%]	Si [vol%]
Primary		0.889	0.002	0.394	0.408
Fe	0.010				
Si	0.540				
Mn	0.380				
Mg	0.500				
Cu	0.095	0.005			

After homogenisation

	Solid solution [wt%]	α-AlFeSi [vol%]	β-AlFeSi [vol%]	Mg_2Si [vol%]	Si [vol%]
Primary		0.890			
Secondary		0.606		0.002	
Fe	0.001				
Si	0.910				
Mn	0.140				
Mg	0.679				
Cu	0.095				

G-3) 0.2 wt% Cu

Initial levels of alloying elements relevant for Alstruc simulation for profile 3a with 0.2 wt% Cu, 0 wt% Zn are given in Table G - 5. Results from Alstruc simulation model for 0.2 wt% Cu, 0 wt% Zn are given in Table G - 6.

Table G - 5 Initial levels of alloying elements added to profile 3a relevant for Alstruc simulation.

Element	Fe	Si	Mn	Mg	Cu
wt%	0.20	1.04	0.53	0.66	0.20

Table G - 6 Vol% precipitates and dispersoids in addition to wt% of alloying elements in solid solution are simulated for the 6082-profile with 0.2 wt% Cu, 0 wt% Zn after solidification and after homogenisation.

After solidification, initial 0.2 wt% Cu

	Solid solution [wt%]	α-AlFeSi [vol%]	AlCuMgSi [vol%]	Mg_2Si [vol%]	Si [vol%]
Primary		0.873	0.056	0.357	0.397
Fe	0.010				
Si	0.510		0.018		
Mn	0.360				
Mg	0.480		0.019		
Cu	0.180	0.010	0.012		

After homogenisation

	Solid solution [wt%]	α-AlFeSi [vol%]	AlCuMgSi [vol%]	Mg_2Si [vol%]	Si [vol%]
Primary		0.873			
Secondary		0.566		0.005	
Fe	0.001				
Si	0.894				
Mn	0.143				
Mg	0.657				
Cu	0.190				

G-4) 0.3 wt% Cu

Initial levels of alloying elements relevant for Alstruc simulation for profile 4a with 0.3 wt% Cu, 0 wt% Zn are given in Table G - 7. Results from Alstruc simulation model for 0.3 wt% Cu, 0 wt% Zn are given in Table G - 8.

Table G - 7 Initial levels of alloying elements added to profile 4a relevant for Alstruc simulation.

Element	Fe	Si	Mn	Mg	Cu
wt%	0.20	1.04	0.53	0.66	0.30

Table G - 8 Vol% precipitates and dispersoids in addition to wt% of alloying elements in solid solution are simulated for the 6082-profile with 0.3 wt% Cu, 0 wt% Zn after solidification and after homogenisation.

After solidification, initial 0.3 wt% Cu

	Solid solution [wt%]	α-AlFeSi [vol%]	AlCuMgSi [vol%]	Mg_2Si [vol%]	Si [vol%]
Primary		0.883	0.117	0.333	0.402
Fe	0.010				
Si	0.490				
Mn	0.360				
Mg	0.470				
Cu	0.260	0.014	0.026		

After homogenisation

	Solid solution [wt%]	α-AlFeSi [vol%]	AlCuMgSi [vol%]	Mg_2Si [vol%]	Si [vol%]
Primary vol%		0.883			
Secondary vol%		0.554		0.005	
Fe	0.001				
Si	0.893				
Mn	0.144				
Mg	0.656				
Cu	0.285				